THE UNIVERSITY OF CHICAGO

TOWARDS A MULTI-SCALE UNDERSTANDING OF DROSOPHILA 3D RETINAL MORPHOGENESIS

A DISSERTATION SUBMITTED TO

THE FACULTY OF THE DIVISION OF THE BIOLOGICAL SCIENCES

AND THE PRITZKER SCHOOL OF MEDICINE

IN CANDIDACY FOR THE DEGREE OF

DOCTOR OF PHILOSOPHY

COMMITTEE ON DEVELOPMENT, REGENERATION, AND STEM CELL BIOLOGY

BY

XIAO SUN

CHICAGO, ILLINOIS

JUNE 2023

TABLE OF CONTENTS

TABLE OF FIGURES

ACKNOWLEDGEMENTS

I would like to express my sincere gratitude to everyone who has supported and encouraged me throughout my PhD journey.

First and foremost, my advisor Ilaria, for going through ups and downs with me the entire journey with unwavering support. I appreciate the environment she created for me to explore my own interests and potential with an extreme level of freedom and confidence in me. Because of this, I have the full experience of going wherever science leads me, trial and error, building collaborations, refining questions and conceptualizing and making connections in biology independently and freely, which I enjoyed so much. I'm grateful that she never forced ideas, which would take away the fun part of doing science, so that I can feel the most fulfillment from my own discovery. Feeling this extreme freedom is really the most important factor that will decide whether I want to continue pursuing scientific career. It is not the easiest experience, but it would benefit me longer term.

I want to thank my committee also for freedom and confidence and keeping me disciplined. I'm extremely thankful for Ed for taking on extra responsibilities to help me so much to grow the project I'm interested in. Rick, Ellie, Heng-chi for a good rotation experience and engagement to make sure I'm on track for graduation. The small sparks from our discussions really last a long time.

I'm thankful to Rebay lab members Nicelio Sanchez-Luege, Saman Tabatabaee, Jacob Decker, Julio Miranda Alban, Suzy Hur, Matt Hope, Catherine Wu, Juana Delao, Jemma Webber, Trevor Davis, Christine Cao for friendship and support at different stages of the journey. Also, I want to thank Will, Jiajie, Hitoshi, Sherzod, Audrey, Yupu, and Allison for their support.

I'm thankful for Thomas and the Lecuit lab, for hosting me as a visiting fellow. Bringing new insights in different aspects of my project and beyond. In an institute and lab environment that specializes in morphogenesis, I had the opportunity to continuously grow intellectually and in technique on a daily basis.

Finally, I want to thank my family for unconditional love and support. Beyond words!

ABSTRACT

Diverse shapes and patterns observed in nature are the optimal representation for fulfilling an organism's physiological needs and function, and they follow a shared set of design principles. Understanding how an organ acquires its functional form requires the reconstruction of its developmental trajectory, which bridges macroscopic tissue geometry to cellular behaviors. However, the inherent complexity on both scales presents challenges for 3D characterization. The field is in search of a 3D model organ that connects the complex morphogenetic and regulatory processes on different scales while reducing the complexity to draw general principles.

In this thesis, I use Drosophila pupal retina as the simplest complex 3D model to explore basic rules of organ morphogenesis. To establish a comprehensive framework, I develop three assays to characterize developmental trajectories on three different scales. On the macroscopic tissue scale, I use microCT to quantitatively describe retinal 3D geometrical changes that establish the precise optical alignment. The tissue analysis revealed two distinct phases of retinal geometrical transformation and suggested that retina establishes the proper optical alignment prior to the significant growth phase. On the mesoscale, considering each ommatidium as a multicellular unit, I develop a machine-learning based pipeline that provides a coarse-grained description of ommatidial packing across the retinal epithelium. The initial coordination of the apical and basal patterning affects the subsequent growth pattern and the final tissue morphology. On the cellular scale, I use confocal microscopy and 3D reconstruction to examine the cellular basis underlying the tissue growth pattern. I uncover a feedback mechanism between the pigment cells and photoreceptors that spatially coordinates the morphogenetic processes during retinal growth.

Together, this thesis provides a multiscale framework to study 3D retinal morphogenesis. I suggest that the basic principles identified in the retinal context will be at the core of other complex 3D morphogenetic programs.

Chapter 1. Introduction - macroscopic organ morphology

Overview

Diverse shapes and patterns in nature have been the source of inspiration for scientists across different disciplines. The appreciation for the beauty of an organism, as epitomized in D'Arcy Thompson's book "On Growth and Form", is not merely aesthetic but also the recognition of the efficiency of the physical rules organisms as "a diagram of forces" conform to, and the mathematical elegance of their final form as "an optimal representation" of the forces at work (Thompson, 1917). This understanding has led to the modern concepts of emergence and self-organization, which now pervade in developmental biology as well as in other fields. Throughout my PhD, I became increasingly intrigued by questions of how diverse shapes and patterns arise, how the form interacts with the specific functions it serves, and how complex and diverse natural phenomena can be reduced to simple, unifying rules and logic.

Understanding how organ form develops requires bridging macroscopic organ geometry to physical forces and molecular information spanning multitudes of scales. An ideal complete framework to characterize any morphogenetic process includes 1) a morphometric analysis to quantitatively describe the geometry and the developmental "transformation" or trajectory that lead to the final form; 2) developing a theoretical model using a minimal set of relevant physical or mechanical parameters to describe the shape and transformation; and 3) understanding both the genetic/molecular and mechanical basis that generates each parameter (which could then feed new rules into the model to refine the description, thus 1-3 only represent three different domains but not a step sequence). Although significant progress has been made to characterize morphogenesis in each domain, only few organ models, if any, fulfill the complete framework.

This thesis is organized following the above framework to understand different aspects of morphogenesis on different scales. For the introduction chapter, **section 1** will focus on the macroscopic characterization of tissue forms, and the general theoretical model and design principles shared by different model systems. First), I will summarize the history of paradigm shifts and the foundational work that led to the modern theory of "self-organization". Part of the history is reminiscent of my PhD journey that shifted from the traditional genetic framework and functional studies focusing primarily on local cell regulations to the current multi-scale characterization and interdisciplinary thinking of morphogenetic questions.

In the second part, as complex organ forms arise from different spatiotemporal combinations of basic shape transformations (building blocks such as curving, branching and growth/lengthening), I will summarize recent advances in understanding curving patterns with emphasis on the underlying mechanical and geometrical rules to better understand how nature plays origami!!

1.1 Paradigm shifts in history

Although it is now intuited that both genetic control and the mechanical consideration of forces and tissue property are two sides of the same coin to understand tissue morphogenesis, these two paradigms remained separated throughout the 20th century, "once an awkward confrontation between disciplines" as William Bialek puts it, and only became an integrated framework in recent decades.

In the early 1900s, biologists such as Stéphane Leduc and D'Arcy Thompson introduced rigorous physical theory and mathematical approaches to explain biological forms. This happened in the

context where epigenesis (development as a gradual elaboration of form) lacked a theoretical basis to explain embryogenesis while the prevailing Vitalism provided a convenient answer, attributing a vital force "*vis essentialis*" (C. F. Wolff, 1759) that could not be reduced to non-living physical or chemical factors. Leduc challenged Vitalism by using physical principles of diffusion and osmosis growth to mimic life-like forms and developmental processes (e.g. branching, karyokinesis of cells, fungi, plants etc.) and argued the same "power of physical forces and interactions" that organize non-living forms are also important to produce forms in living organisms (Leduc, 1911, 1912). In 1917, D'Arcy Thompson's book "On Growth and Form" was the first to use a rigorous mathematical approach of Cartesian coordinates to compare different forms in evolution, like birds' beaks or adult horse skulls of related species, as well as compare forms generated during development, such as the growing primates' skulls and plant leaves. He proposed the "theory of transformation" - that diverse biological forms can be related through simple mathematical transformation, which reveals the "law of growth" - that it is physical forces and internal growth parameters that affect shape and form (Thompson, 1917).

Both Leduc and Thompson's theoretical frameworks soon fell into obscurity during the genetic era in 20th century. The ecstasy of the discovery of genes and decoding gene function led to a "gene-centric" deterministic view of life form - that genes and genetic programs encode the development information and direct morphogenesis as a hard-wire programme. This view was exemplified by 1957 Waddington's "cell automaton" that development is seen as a sequence of cell decisions follows a hilly slope of "genetic landscape", ~1960 discovery of "morphogen" where molecule concentrations determine positional information and specify downstream patterning; 1995 Nobel Prize on genes control embryo development (Nüsslein-Volhard and Wieschaus, 1984); and the discovery of master genes like *eyeless*, that one single gene is sufficient to induce a gene network

that give rise to an ectopic eye, etc (Halder et al., 1792, 1995). Significant as these contributions are, genes and the determinism associated with it dominate for a century and overshadow the physical nature of the tissue that is carrying out the shape changes and patterning. Later in the 21st century, it was realized that pure molecular and genetic approaches to deplete a gene and characterizing phenotype is a useful tool to infer (also based on physical theory) how processes are formed and regulated, but cannot provide direct mechanistic explanation of the phenotype larger than molecular length scale, such as how cells move and change shape, how tissue curves, elongate etc. without incorporating mechanics and geometry information.

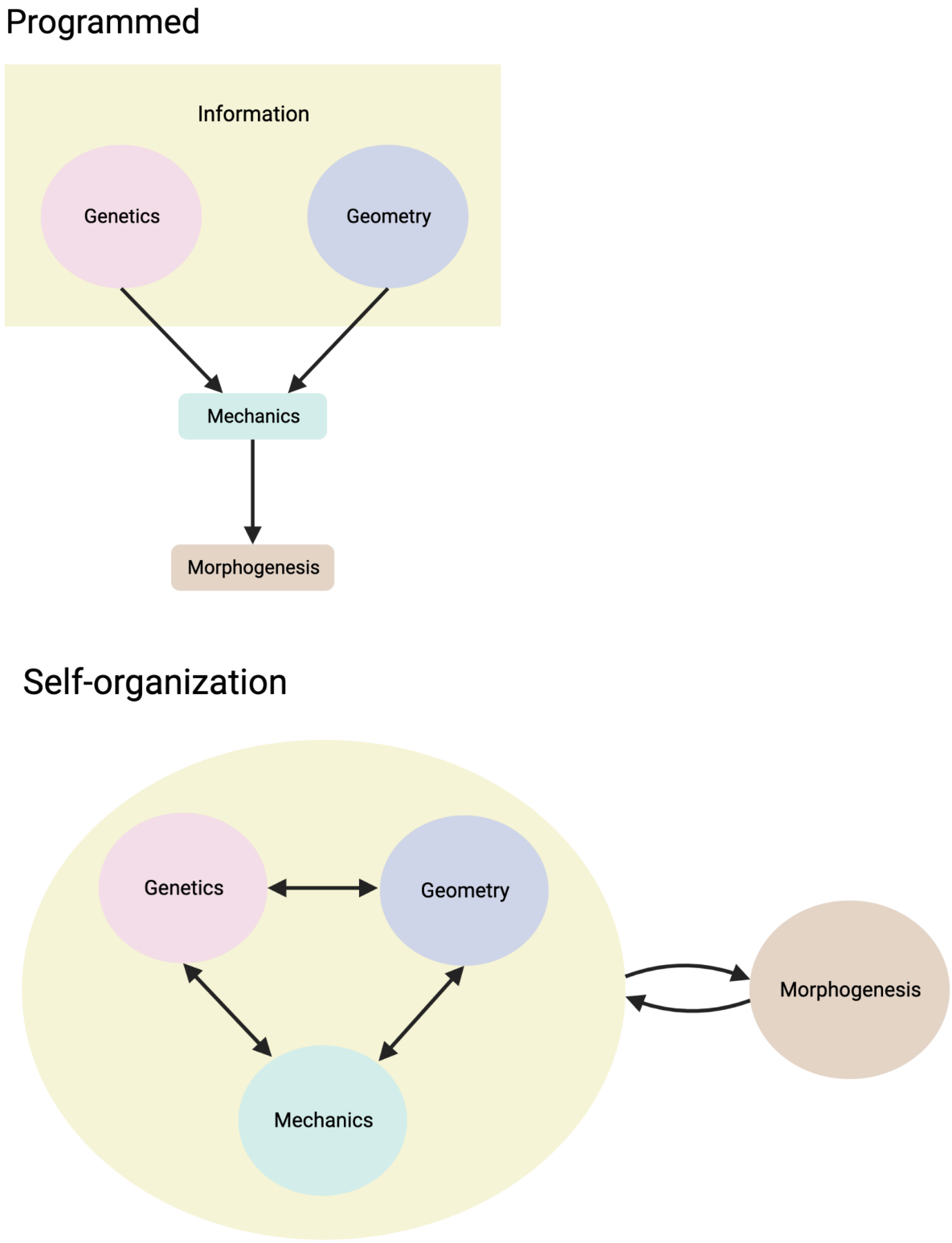

Figure 1.1 Information flow in the programmed vs. self-organization model.

1.2 Self-organization

Last ~15 years saw an increasing interest to revisit and revive D'Arcy Thompson's foundational work by integrating genetic information into a unified physical framework. The regained emphasis on the physical nature of the tissue and modeling approach to explain developmental patterning led to the view of "self-organization", which suggests that the emergence of form and order is a dynamic steady state that follows stochastic local interaction of the component. This is an alternative model to the "programmed" deterministic view, and both complement each other and work together in different fashions to modulate developmental processes (reviewed by Collinet and Lecuit, 2021; Newman, 2022). The features that distinguish the two models are a) the initial condition; b) flow of information (Figure 1.1); c) rules of interactions and d) final output. Programmed models start with initial conditions and pre-patterning that foretells and drives the rest of the developmental process, the information flow is hierarchical and relies on deterministic rules for interaction. Whereas in self-organization system, tissue starts with a homogenous state with no external driver to orchestrate the process, the information flow is non-hierarchical between genetic, mechanical and geometrical module. Each component does not communicate to the overall output of the process, instead follows the local interactions and statistic rules. Amplification of the initial local fluctuations through feedback and spatial coupling produces the ordered, precise and robust patterns.

Self-organization is evident in diverse patterning processes across different scales. It was first theorized by Turing (later extended to Turing-like mechano-chemical model) (Turing, 1952), that spontaneous symmetry breaking in embryos can occur by local activation and long-range inhibition that amplify the instabilities or fluctuations in the initial homogenous state to a

heterogeneous pattern, like regular arrays of stripes and dots, or oscillations and traveling waves (Pourquié, 2003; Economou and Ohazama, 2012; Cotterell et al., 2015). Heavily criticized at first, Turing model was later recognized when adapting mathematical modeling to recapitulate developmental patterning, and now serves as the mechanistic model to explain diverse morphogenetic processes, including the patterning of vertebrate digits in growing limb (Sheth, et al.,2012), somitogenesis (Cotterell et al., 2015, Tsiairis and Aulehla, 2016; Uriu et al., 2009), hair and feather primordia (Janoueix-Lerosey et a;., 2008; Sick et al., 2006), animal coat patterns (Meinhardt, 1982), Drosphila corneal nanocoating (Kryuchkov et al., 2020), etc. Self-organization is also a universal property to any physical phenomena regardless of scales or contexts, so it is easy to draw analogies to the physical world such as rippled patterns of sand dunes, orders in flocking birds or fish, ants colony etc, to understand the unifying rules that underlying diverse phenomena. In 1.3, I will use examples in morphogenesis to discuss how self-organization is employed to produce organ form.

1.3 On the growth and form of building blocks- curving

Diverse and complex tissue forms arise from the different spatio-temporal combinations of the basic shape changes, such as curving, branching, growth/extension. I will focus on curving with different examples to illustrate how geometrical and mechanical characterization help to build a reduced theoretical model, and how general principles of self-organization are employed in "Nature's origami".

One common shape deformation during organ morphogenesis is curving or folding, from large-scale tissue characteristics such as cortical convolution and gut looping, mesoscale patterns that

span hundreds of cells like gastrulation, to small buckling events that occur within a single cell like microvilli formation. Despite that the mechanisms or the origin of mechanical forces differ, these different scale patterns can be reduced to the one basic framework - that folding is driven by self-organization of stress-induced mechanical instabilities (reviewed by Collinet and Lecuit, 2021). In this framework, several factors come into play: first, tissue is under stress, which includes internal stress induced by inhomogeneous growth or cellular contractility and external stress imposed by physical constraints or boundary conditions; second, the sum of all stresses cause the mechanical instabilities that drives the tissue away from equilibrium; third, the tissue then rely on statistic rules and local interactions to self-organize into a new steady state, in a manner similar to an elastic material put under compressive forces that folds to relax stresses above threshold. Note that this basic framework could be predominantly working by itself in many contexts or working with programmed/deterministic model in different fashion. (For example the initiation of invagination in the embryonic stage during gastrulation is known to be governed by a deterministic program of a signaling cascade, GPCRs activating fog ligands which activate RhoA and myosin. The programmed initiation is followed by self-organized mechanical induction of myosin to further propagate the wave) (Sweeton et al., 1991; Costa et al., 1994; Bailles et al., 2019). Here I will summarize the theoretical framework of two classic examples: cortical convolution and gut looping. Each example below is organized in the sequence of a) summary of the theoretical framework or mechanical model; b) characterization of geometrical parameters and tissue mechanics that lead to the model; c) discussion of the efficiency of the design principle in serving the organ functions.

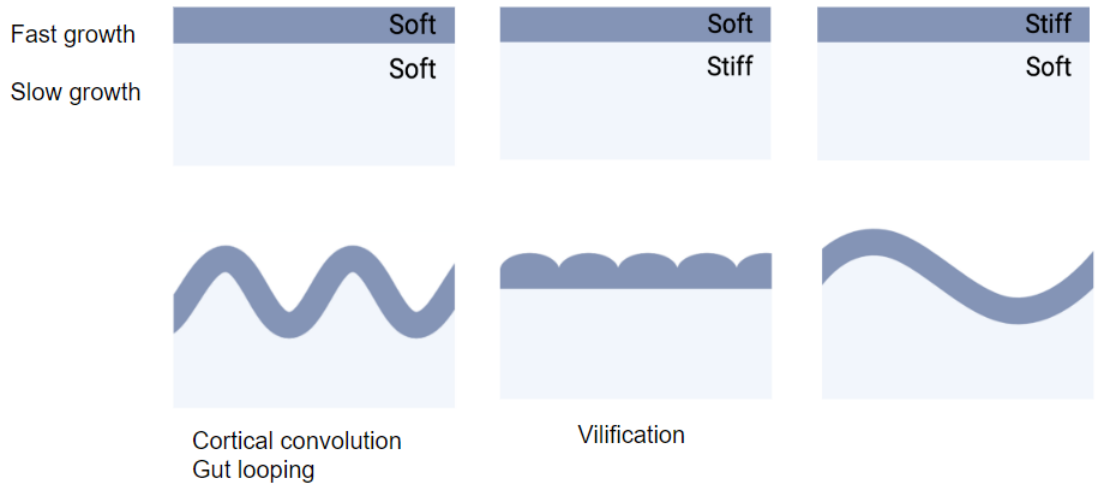

Figure 1.2 Differential growth leads to tissue curving.
Faster growing outer layer (dark) and slow growing inner layer (light), generate different curving patterns depending on tissue stiffness.

Cortical convolution

Vertebrate brain develops a highly complex, precise and reproducible folding pattern during development that serves its complex neural processing capacity. Intriguingly, the folds (or use term major gyri) are not positioned by the deterministic rules from upstream pre-pattern. Instead, brain folding during development is an emergent process that arises from mechanical instability induced by differential growth of different brain layers, and modulated by early tissue geometry (Figure 1.2) (Tallinen et al., 2014, 2016). This minimal model is based on a series of thorough characterization of geometrical changes and tissue mechanics. Brain comprises outer gray matter, the cerebral cortex wrapping the white matter, the inner subcortex which includes the brainstem that connects to the spinal cord. Both layers are organized in sheet-like structures that grow at different rates, folded into convoluted shapes and form characteristic gyri patterns (Vasung et al.,

2016; Lohmann et al., 2008). To describe the folding pattern of the whole brain, gyrification index GI, which is quantified by the ratio of total cortical surface to exposed surface area, is mapped on the reconstructed MRI scanned developing brain with millimeter scale. Comparing the simulated stress field and folding pattern showed that in highly curved regions, formation of gyri, as indicated by high convex curvature, favor their alignment perpendicular to the largest compressive stress. Physics model and theory suggested that the differential growth of gray matter relative to white matter are the sources of compressive stress- that tangential expansion of the gray matter is constrained by the inner white matter. This mechanical model was further consolidated by a biomimetic experiment using 3D printing of gel mini-brain with faster swelling of outer layer than inner to recapitulate the course of gyrification similar to real brain in space and time. This study also found the geometrical constraint of the initial brain could impact the folding pattern by modulating the stress distribution at each step (Tallinen et al., 2014, 2016).

It is still not fully understood how brain form and function are interacting with each other. Geometrical measurement of the mature brain across a wide range of species identified a universal scaling rule that describes the folding pattern in the adult brain as a function of the cortical surface area and cortical thickness. This scaling rule follows the principle of energy minimization, which might govern how the brain adopts its final optimal form (Mota and Herculano-Houzel, 2015). Evolutionary studies suggest that the adoption of a convoluted sheet-like structure is a selective adaptation to increase surface area within a limited head space. Maximizing surface area and minimizing distance between brain regions through folding allows efficient communication between neurons and optimize processing capacity to achieve higher cognitive function (Striedter, 2005; Lui et al., 2011)

Gut looping

Similar to brain convolution, gut shows a stereotyped looping pattern, which also arises from mechanical instability due to the differential growth of the gut and the attached mesentery membrane (Figure 1.2). Mechanical dissociation of these two layers results in gut decoiling and mesentery relaxation, suggesting that in vivo, the gut that grows at faster rate is normally compressed while mesentery that grows slower is stretched.

This model is supported by a simple biomimetic experiment, using a rubber tube and elastic sheet with different strains to mimic differential growth of the gut and mesentery membrane. To develop an elastic model to simulate the looping pattern, geometry is measured by the diameter of the gut tube and mesentery thickness. Tissue elastic properties are measured by the response curve after applying force with a magnetic steel ball. The elastic model predicts looping patterns (amplitude and wavelengths) in both bird species and mouse simply by tuning these measurable parameters of tissue geometry, elasticity and differential growth rate. This suggests that differential growth of elastic tissue might serve as the mechanical basis underlying diverse gut looping patterns in evolution (Savin et al., 2011).

REFERENCES

AM TURING, F. R. S. "The chemical basis of morphogenesis." Sciences-cecm. usp. br (1952).

Bailles, Anais, Claudio Collinet, Jean-Marc Philippe, Pierre-François Lenne, Edwin Munro, and Thomas Lecuit. "Genetic induction and mechanochemical propagation of a morphogenetic wave." Nature 572, no. 7770 (2019): 467-473.

Collinet, Claudio, and Thomas Lecuit. "Programmed and self-organized flow of information during morphogenesis." Nature Reviews Molecular Cell Biology 22, no. 4 (2021): 245-265.

Costa, Michael, Ellen T. Wilson, and Eric Wieschaus. "A putative cell signal encoded by the folded gastrulation gene coordinates cell shape changes during Drosophila gastrulation." Cell 76, no. 6 (1994): 1075-1089.

Cotterell, James, Alexandre Robert-Moreno, and James Sharpe. "A local, self-organizing reaction-diffusion model can explain somite patterning in embryos." Cell systems 1, no. 4 (2015): 257-269.

Economou, Andrew D., Atsushi Ohazama, Thantrira Porntaveetus, Paul T. Sharpe, Shigeru Kondo, M. Albert Basson, Amel Gritli-Linde, Martyn T. Cobourne, and Jeremy BA Green. "Periodic stripe formation by a Turing mechanism operating at growth zones in the mammalian palate." Nature genetics 44, no. 3 (2012): 348-351.

Halder, Georg, Patrick Callaerts, and Walter J. Gehring. "Induction of ectopic eyes by targeted expression of the eyeless gene in Drosophila." Science 267, no. 5205 (1995): 1788-1792.

Halder, Georg, Patrick Callaerts, and Walter J. Gehring. "New perspectives on eye evolution." Current opinion in genetics & development 5, no. 5 (1995): 602-609.

Janoueix-Lerosey, Isabelle, Delphine Lequin, Laurence Brugieres, Agnes Ribeiro, Loïc De Pontual, Valérie Combaret, Virginie Raynal et al. "Somatic and germline activating mutations of the ALK kinase receptor in neuroblastoma." Nature 455, no. 7215 (2008): 967-970.

Kryuchkov, Mikhail, Oleksii Bilousov, Jannis Lehmann, Manfred Fiebig, and Vladimir L. Katanaev. "Reverse and forward engineering of Drosophila corneal nanocoatings." Nature 585, no. 7825 (2020): 383-389.

Leduc, Stéphane. "The mechanism of life." (1911): 30-31.

Leduc, Stéphane. La biologie synthétique. Vol. 2. A. Poinat, 1912.

Lohmann, Gabriele, D. Yves Von Cramon, and Alan CF Colchester. "Deep sulcal landmarks provide an organizing framework for human cortical folding." Cerebral Cortex 18, no. 6 (2008): 1415-1420.

Lui, Jan H., David V. Hansen, and Arnold R. Kriegstein. "Development and evolution of the human neocortex." Cell 146, no. 1 (2011): 18-36.

Meinhardt, Hans. "Models of biological pattern formation." New York 118 (1982).

Mota, Bruno, and Suzana Herculano-Houzel. "Cortical folding scales universally with surface area and thickness, not number of neurons." Science 349, no. 6243 (2015): 74-77.

Newman, Stuart A. "Self-organization in embryonic development: myth and reality." In Self-Organization as a New Paradigm in Evolutionary Biology: From Theory to Applied Cases in the Tree of Life, pp. 195-222. Cham: Springer International Publishing, 2022.

Pourquié, Olivier. "The segmentation clock: converting embryonic time into spatial pattern." Science 301, no. 5631 (2003): 328-330.

Savin, Thierry, Natasza A. Kurpios, Amy E. Shyer, Patricia Florescu, Haiyi Liang, L. Mahadevan, and Clifford J. Tabin. "On the growth and form of the gut." Nature 476, no. 7358 (2011): 57-62.

Sheth, Rushikesh, Luciano Marcon, M. Félix Bastida, Marisa Junco, Laura Quintana, Randall Dahn, Marie Kmita, James Sharpe, and Maria A. Ros. "Hox genes regulate digit patterning by controlling the wavelength of a Turing-type mechanism." Science 338, no. 6113 (2012): 1476-1480.

Sick, Stefanie, Stefan Reinker, Jens Timmer, and Thomas Schlake. "WNT and DKK determine hair follicle spacing through a reaction-diffusion mechanism." Science 314, no. 5804 (2006): 1447-1450.

Striedter, George F. Principles of brain evolution. Sinauer associates, 2005.

Sweeton, D. A. R. I., S. U. K. I. Parks, Michael Costa, and E. R. I. C. Wieschaus. "Gastrulation in Drosophila: the formation of the ventral furrow and posterior midgut invaginations." Development 112, no. 3 (1991): 775-789.

Tallinen, Tuomas, Jun Young Chung, John S. Biggins, and L. Mahadevan. "Gyrification from constrained cortical expansion." Proceedings of the National Academy of Sciences 111, no. 35 (2014): 12667-12672.

Tallinen, Tuomas, Jun Young Chung, François Rousseau, Nadine Girard, Julien Lefèvre, and Lakshminarayanan Mahadevan. "On the growth and form of cortical convolutions." Nature Physics 12, no. 6 (2016): 588-593.

Thompson d'Arcy, W. "On growth and form." Cambridge: Cambridge University Press 16 (1917): 794.

Tsiairis, Charisios D., and Alexander Aulehla. "Self-organization of embryonic genetic oscillators into spatiotemporal wave patterns." Cell 164, no. 4 (2016): 656-667.

Uriu, Koichiro, Yoshihiro Morishita, and Yoh Iwasa. "Traveling wave formation in vertebrate segmentation." Journal of theoretical biology 257, no. 3 (2009): 385-396.

Vasung, Lana, Claude Lepage, Milan Radoš, Mihovil Pletikos, Jennifer S. Goldman, Jonas Richiardi, Marina Raguž et al. "Quantitative and qualitative analysis of transient fetal compartments during prenatal human brain development." Frontiers in neuroanatomy 10 (2016): 11.

Waddington, Conrad Hal. The strategy of the genes. Routledge, 2014 (first published in 1957).

Wieschaus, E., Ch Nüsslein-Volhard, and Gerd Jürgens. "Mutations affecting the pattern of the larval cuticle in Drosophila melanogaster: III. Zygotic loci on the X-chromosome and fourth chromosome." Wilhelm Roux's archives of developmental biology 193 (1984): 296-307.

Wolff, C. F. ", Theoria Generationis, Halle." (1759).

Chapter 2. Introduction- Drosophila pupal retina

2.1 Summary

Challenges to characterize 3D morphogenesis across scales

Previous studies have examined macroscopic morphometric and microscopic cellular processes. However, very few organs examined on both scales. Multiscale analyses on tissue surfaces and local regions are just emerging, with study of 3D whole organs even rarer. This is partly due to the challenges of imaging and analyzing not only the static tissue form but also the process or trajectory that leads to the form.

The ideal setup to characterize organ morphogenesis would be to perform long-term in toto live imaging of the 3D organ and its physical environment with cellular-level dynamics, and then to develop computational analyses that segment, map and quantify the entire developmental trajectory of both individual cells and the organ in 3D. This ideal setup would allow direct causal relations to be drawn from events that span orders of magnitudes in space and time. However, this type of approach is still almost infeasible for most cases. For example, if a tissue is located deep in the organism and migrates far from the original position as it develops, or if a tissue undergoes drastic deformations, it is difficult to directly image and map corresponding landmarks without extensive statistical shape analysis. Increasing the challenge, basic questions about how to describe 3D forms still need to be resolved. How does one quantitatively describe 3D topology and geometry of cells and organs? How does one set arbitrary axes for complex shapes? How does one identify the correct landmarks to map trajectories in 3D space across time?

The field is still in search of a 3D model system that connects the complex morphogenetic processes on different scales while reducing the dimensionality and complexity of describing the

morphogenetic processes and shape. The goal is to draw rules from simple models first and then expand the parameter space to more complex model systems. Throughout my PhD, I came to realize and increasingly appreciate the Drosophila pupal retina as a unique 3D model that fits this vision. However, when I started, there was very limited theoretical work done to establish it specifically as a 3D morphogenesis model. I focused my PhD on developing such a framework and used it to integrate and guide experiments.

Drosophila pupal retina as the simplest complex model to study 3D morphogenesis

The Drosophila pupal retina offers a unique and tractable 3D context in which the reiterative patterning of the ommatidial unit of the compound retina naturally defines two scales of questions. First, considering each ommatidial array as an optical unit, how are different ommatidia geometrically arranged to transform the thin flat epithelium into a hemispherical organ that achieves visual precision? Second, zooming in on each optical unit, how do the specialized functional domains of different retinal cells achieve proper organization within each ommatidium? By breaking down the complex 3D morphology into macroscopic retina, mesoscale multicellular ommatidium, and microscale individual cell and its subcellular machinery, it would be easy to bridge the morphogenetic processes with comparable length scales. Then integrate multiple scales to understand complex, dynamic retinal morphogenesis.

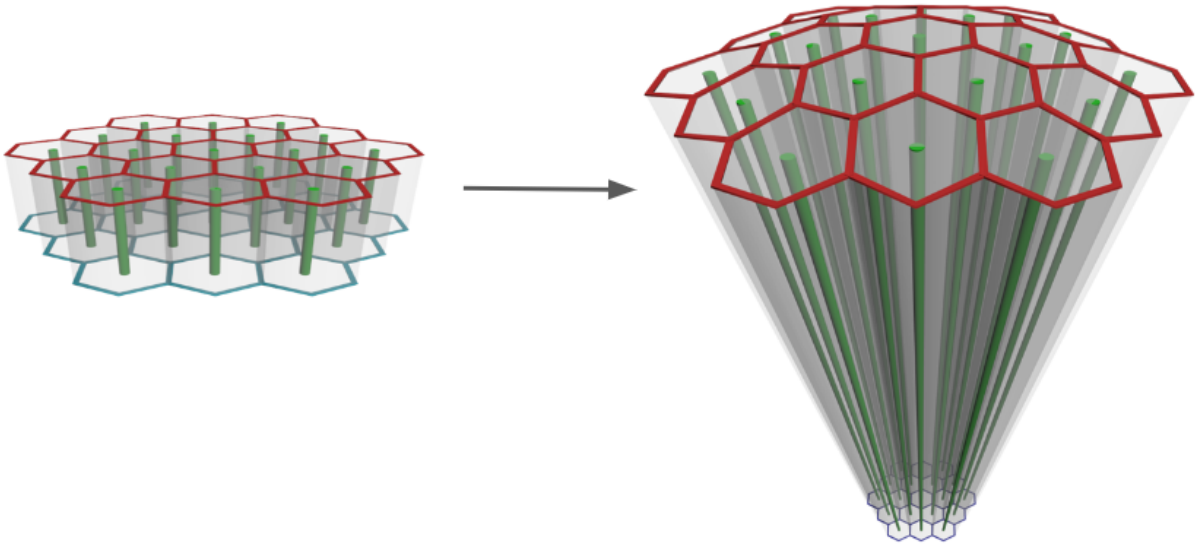

Figure 2.1 Ommatidial packing of the compound retina

Apical surface boundary (red), Basal surface boundary (blue), Optical axis and its structural basis Rhabdomere (green). The compound retina transforms from a thin flat epithelium with columnar ommatidial units into a hemispherical organ with elongated tapering hexagonal arrays.

Between the macro- and mesoscale: The compound retina is packed with ~750 ommatidial arrays, each organized around the central optical axis along which light is collected and transmitted. During pupal morphogenesis, as the retina transforms from a thin flat epithelium with columnar units into a hemispherical organ with elongated tapering hexagonal arrays, the tissue is also establishing an organized field of optical axes with precise outward angle (i.e. interommatidial angle). This evolving field/network of optical axes generates a natural axial coordinate system that connects the hexagonal grids that pattern the apical and basal curved surfaces. This arrangement can address the aforementioned challenges as it is relatively easy to acquire spatial information and find landmarks to map macroscopic shape changes, to describe the geometrical packing within the whole tissue and to define and measure growth rates along different axes.

Between the meso- and microscale: The functional specialization of different retinal cells results in a stereotyped 3D network of cytoskeletal domains and cell-cell/ECM contacts, which forms the structural basis of the optical axial network. In the center of each ommatidium, specialized rhabdomere structure of photoreceptors orients along the optical axis and anchors to the two ends of cone cells embedded in the apical and basal surfaces of the epithelium. The apical and basal domain of the pigment cells set up the boundary of each ommatidium and forms the hexagonal pattern that places the cone cells at the centroid. The stereotyped cellular processes that establish and maintain these contacts have been studied, which provides a good foundation to integrate and build a 3D view to understand how different processes are coordinated during morphogenesis.

History and well-studied areas using retina as model system

Early studies (~1800 to ~1980) of compound retina focused on zoological and functional characterization and used comparative methods to examine adult retinas of Drosophila and other Dipteran flies (Barlow, 1952; Miller et al., 1968; Nilsson, 1989). Developmental characterization of the retina really started with the Ready, Hansen and Benzer 1976 classic paper, where they used DIC (Differential interference contrast) optical microscopy of serial thin sections to characterize the neurocrystalline structure of the adult retina and the emergence of order in photoreceptor arrays at the larval stage (Ready et al., 1976). This study was followed by a series of papers by Ready and others to further characterize the cellular composition, behavior and organization during larval and early pupal stages. The complete developmental reconstruction during larval and early pupal stage were the foundation for all later studies, including those focused on signaling-controlled differentiation, planar polarity establishment of photoreceptor arrays, and the cell elimination and rearrangement of accessory cells (Ready et al., 1976; Thomlinson and Ready, 1987; Cagan and

Ready, 1989; Wolff and Ready, 1991; Longley and Ready, 1995; Kumar and Ready, 1995; Fan and Ready, 1997; Chang and Ready, 2000).

The first quantitative characterization of 3D geometrical change in the retina came from the Longley and Ready 1995 paper documenting integrin function during late pupal retinal morphogenesis! They used transmission EM of thin sections along basal and longitudinal planes to measure respective changes of the basal floor area and tissue depth. This study also provided evidence of the mechanical role of the basal floor and of integrin-mediated cell-ECM junctions to "support" retinal morphogenesis and elongation. The study was the first to consider different planes as an integral structure of the compound eye. As described in Chapter 3 of this thesis, my own studies show that this "support" derives from the mechanical feedback between basal contraction and longitudinal elongation that allows key structural features of the retina to match and achieve concomitancy in their developmental progress.

Don Ready, in his insightful "informal, speculative essay" (his own words) "Drosophila Compound Eye Morphogenesis: Blind Mechanical Engineers?" summarizes knowledge gained by the field from 1976 to ~2000. This book chapter was inspired by D'Arcy Thompson considering "the form of an object is a diagram of forces" and discussed specifically the source of forces and mechanisms that shape the pupal to adult retina.

Ready's book chapter was foundational to the ideas I brought to my PhD work. However, Ready's book chapter and his insights on retinal morphogenesis, which could have immediately served as a good framework to guide the field's interpretation of later experiments, was overlooked in the molecular genetic era (dominated by the discovery of master regulators in the eye in 1995 and the following two decades frenzy of research on retinal determination gene networks that control

photoreceptor neuronal fate). Because these events occurred in the larval eye disc, with a few exceptions (signaling control of pigment cell elimination and rhabdomere growth as examples) the field largely ignored pupal stages and directly credited the adult regularity of pattern mostly to the larval stage emergence of order.

In the following sections, I will review recent work on genetic, mechanical and geometrical characterization of different morphogenetic events during pupal development, following the sequence of macroscopic geometry/visual function, rhabdomere morphogenesis, planar patterning and lens secretion. The ultimate goal is to piece together the genetic and mechanical regulatory mechanisms of every event as a component, to integrate them all into an updated physical framework and eventually build an integrated force diagram of the pupal retina that describes 3D retinal morphogenesis.

2.2 Visual function and adult retinal morphology

Geometrical relations and acuity-sensitivity tradeoff

The main considerations in the design of the compound eye are the simple laws of optics and achieving visual perfection. The Drosophila compound retina is packed with ~750 ommatidia arrays with an outward angle that forms a hemispherical shape. Each ommatidial array samples light along the optical axis that contributes to one pixel in the visual image. In this way the hemispherical shaped eye provides panoramic vision. The interommatidial angle between the neighboring optical axes determines the sampling density or pixel resolution, which inversely describes the spatial acuity of the retina (Nielsson, 1989; Land & Nilsson, 2012).

Contrast sensitivity or sharpness is another visual property determined by the lens diameter, labeled D. The trade-off between spatial acuity and light sensitivity is demonstrated by the eye's geometry, such that when keeping the overall eye size constant, decreasing interommatidial angle, which increases spatial acuity, necessarily decreases lens size, which decreases light sensitivity, and vice versa (Land & Nilsson, 2012). As a result, the optimal lens diameter is expected when these two limits nearly meet.

Interommatidial angle is robust despite variations in eye sizes

Compound eyes have diversified during evolution to serve specific functions and demands such as hunting prey and navigating in complex surroundings under varying light conditions. This diversity is reflected in features such as the compound eye size, ommatidium number and size, interommatidial angle, rhabdomere length and diameter and neural circuits. Anatomical studies show that within a given species, interommatidial angle is a robust feature regardless of gender difference and retinal size variations (Lau et al., 2007; Gonzalez-Bellido et al., 2011; Currea et al., 2018). Recent experiments with lab-reared Drosophila showed that varying body size by limiting feeding during larval stages results in proportionally smaller eyes. Smaller eyes have substantially fewer and smaller ommatidia which results in loss of contrast sensitivity. This loss is compensated by increasing neural processing time, while maintaining interommatidial angle. These findings suggest that spatial acuity, determined by the interommatidial angle, is the priority in eye design, and that small eyes maintain spatial acuity by sacrificing contrast sensitivity at the optical level, but recover contrast sensitivity almost completely by sacrificing temporal acuity at the neural level (Currea et al., 2018).

The Drosophila compound eye, with a surface area of~0.15mm^2, in general shows no obvious regional specializations. On average, the interommatidial angle is $\Delta\varphi = 4.8°$ (Götz, 1964; Land, 1997; Gonzalez-Bellido et al., 2011), which means that the fly retina resolves image details 10cm apart at a distance of 1.4m. In other words, a fly needs to be closer than 30mm to see an object as more than a single spot. The smallest angle (acute zone, high acuity) was found in the central region of the eye ($\Delta\varphi = 4.5° \pm 0.08$SEM) with the smallest $\Delta\varphi$ is 3.38° (Gonzalez-Bellido et al., 2011).

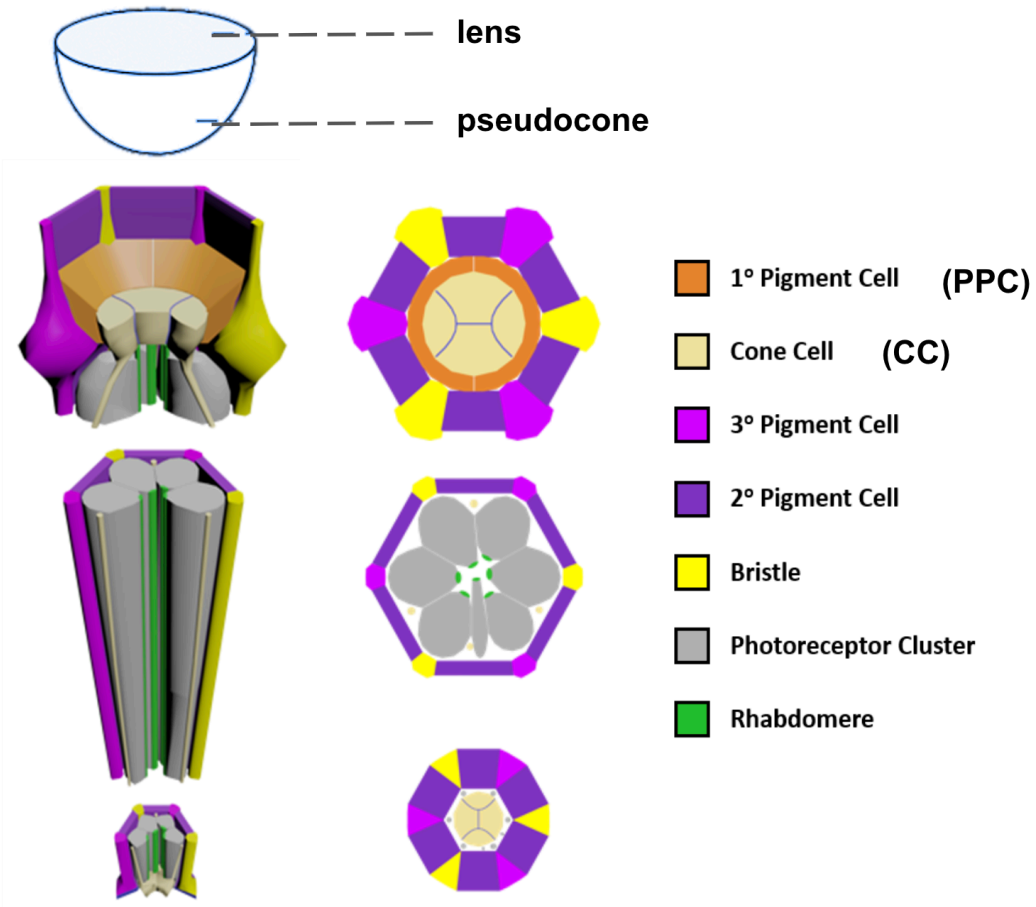

Figure 2.2 Cellular organization in each ommatidium

Functionally specialized structures in each optical unit

Each ommatidium features a light-focusing structure formed by the exoskeletal corneal lens and the crystalline pseudocone, and a light-sensing structure provided by the rhabdomeres that transduces signals for visual processing in the brain. The biconvex corneal lens collects light from a small angle and focuses it through a vitreous-like pseudocone onto the photoreceptor rhabdomeres (Franceschini 1972; Stahl, 2017). The size of the lens (measured by lens diameter = 16.85μm±0.21 SEM) (Gonzalez-Bellido et al., 2011) determines light intensity. The crystalline cone and the primary pigment cells (PPCs) form an aperture that dynamically changes its size under dark/light conditions, thus modulating the amount of light that reaches the photoreceptive layer (Nilsson 1982, 1983). The function for both pseudocone and the surrounding PCs is to seal the ommatidial space to optically isolate each ommatidium. The high refractive index of the pseudocone ensures that each ommatidium only receives light from its own lens, while PCs have dense curtains of screening pigment that prevent light from scattering to the neighboring ommatidia.

Drosophila photoreceptors have 8 subtypes, each carrying different rhodopsins that absorb light with different wavelengths. R1-R6 are outer photoreceptors, and R7 and R8 are centrally located and arranged in tandem with R7 above R8. In fact, R1-R6 photoreceptors in the same ommatidium rhabdomere each have their own optical axis, but the optical axis of each ommatidium is structurally defined by the rhabdomere of tandem R7/R8. Thus, the interommatidial angle $\Delta\varphi$ is defined as the angular difference between optical axes of R7/R8 in the neighboring ommatidia (Land, 1997; Katz and Minke, 2009; Lunau, 2014).

Improve vision - superposition (dark) and microsaccade (moving target)

The compound eyes in Drosophila and other dipteran flies are apposition eyes, in which each ommatidium is an individual optical unit that contributes to a single spot of the final composite image. The disadvantage of an apposition eye is the small size of lenses, that allows little light to reach the rhabdomeres. Vision is improved by the photoreceptors extending axons to the optical lobe of the brain for visual processing. Drosophila uses a superposition neural wiring mechanism, in which R1, R2, R3, R4, R5 and R6, one each from the six neighboring ommatidium, share the same optical axis that point to the same spot. By pooling their synaptic output to one cartridge in the laminar layer of the retina, the signal-to-noise ratio of the processed image could improve by √6 (de Ruyter van Steveninck and Laughlin, 1996; Zheng et al., 2006). Note that the neural superposition differs from the optical superposition, in which a compound eye forms a single image using optical, rather than neural-level processing. The advantage of neural superposition is to increase sensitivity by summing signals from six different optical units. This way, Drosophila eyes could adapt to dark and operate at lower light intensities.

Historically, because the compound eye has a rigid lens system extending from the rigid head cuticle and supported by rigid rhabdomeres, it was long assumed that the inner structures of the eye were also static, and that vision solely depended on the geometrical parameters of ommatidial structures and packing (interommatidial angles, lens area, rhabdomere area, length etc.). Remarkably, recent studies suggest that internal structures, such as rhabdomere length and orientation dynamically change in response to light change. Atomic force microscopy revealed that flies naturally have microsaccades, and that light can induce global intraocular muscle contractions, which could stretch and recoil rhabdomeres and induce lateral movements of

rhabdomeres about its width ~1400 nm. These microsaccades are initiated when photons are absorbed by rhodopsin, which induces PIP2 cleavage in the microvillar membrane that causes a change in membrane tension and photoreceptor contraction, which leads to the activation of dTRP channels that convert to electrical signals for phototransduction. These dynamic adjustments further sharpen light input in time and further provide dynamic hyperacute vision on moving objects (~ 1.16°) beyond the static optical resolution (~4.8°). Together these findings have replaced the old stationary view with a new morphodynamic active view of 3D organ structure and function (Hardie and Franze, 2012; Juusola et al., 2017; Kemppainen et al., 2022; Fenk et al., 2022)

2.3 Longitudinal axis

2.3.1 Photoreceptor apical domain (future rhabdomere) involution

A functionally important step during retinal morphogenesis is the involution and alignment of photoreceptor rhabdomeres along the optical axis. This process is achieved by a series of conserved local change of cell contacts between different retinal cell types. At the end of larval stage/the start of pupal morphogenesis, all retinal cells occupy the full depth of the epithelium although the cell bodies are positioned at different depths to accommodate each other as they rearrange apically or basally. Thus, at this stage the retina is a stratified epithelium although the cells are not fully columnar in shape, and the cone cell and pigment cells have not yet adopted their distinct shapes. Photoreceptors adopt spindle shapes, (shorter tip towards apical surface and tapered to the basal) with apical dots of adherens junctions clustered at the tip of the photoreceptors. As cone cells push through the photoreceptor clusters and rise to the apical surface to generate a tight quartet cap at the top of the ommatidium, photoreceptor cell membranes involute and the apical domains (future

rhabdomeres) expand from just below cone cell quartet to the retinal floor. The monolayer/stratified epithelium becomes pseudostratified, as the cone cell body and feet close above and below the photoreceptors cell bodies (Figure 2.3).

Photoreceptor involution was studied as a cell-autonomous polarity establishment process where classic transmembrane molecules such as Crumbs and Bazooka provide polarity cues, which further recruit structural molecules to the involuting domain (Izaddoost et al.,2002; Pellikka et al.,2002). Genetic studies show that the Par complex (Par6-aPKC-Baz) acts upstream of the Crumbs complex (Crb-Stardust-Patj) and provides a structural and signaling hub important for the extension of the domain (Hong et al.,2003; Nam and Choi,2003, 2006. Kumar and Ready, 1995; Longley and Ready,1995; Gibson and Perrimon, 2003; Tepass and Harris, 2007). F-actin and microtubules were also found at the involuting domains (centrosomin, major MT-organizing center) (Chen et al., 2011). Although we understand the molecular components that mediate the formation and extension of rhabdomeres, the organization of the cytoskeletal structure, assembly kinematics etc. have not been examined. It would be interesting for future studies to examine the mechanical machinery of the rhabdomere involution by drawing comparison with other well-characterized cellular processes like the ingression during cellularization or invagination formed during cytokinesis.

Considered from the whole tissue scale, ~750 units must initiate the same involution process around the same time and complete it in near synchrony. To achieve this, the tissue might iteratively employ simple intrinsic mechanical or geometrical rules to efficiently organize the process. These rules could in turn organize or works in parallel with the signaling molecules mentioned above. Don Ready in his “speculative essay” considered the physical environment “a

conserved mesh of cell-cell contacts" and the described the photoreceptor apical domain expansion far outstripping the growth of the basolateral cell surface. He proposed the differential growth within a confined space that reorients the rhabdomere expansion to be a plausible cause for involution. It would also be interesting to observe these processes on tissue scales, e.g. the temporal sequence (initiation and timing) and spatial differences (center vs. periphery) of the rhabdomere involution, and explore how the involution pattern affects tissue mechanics and generates tissue forms such as thinning and curving.

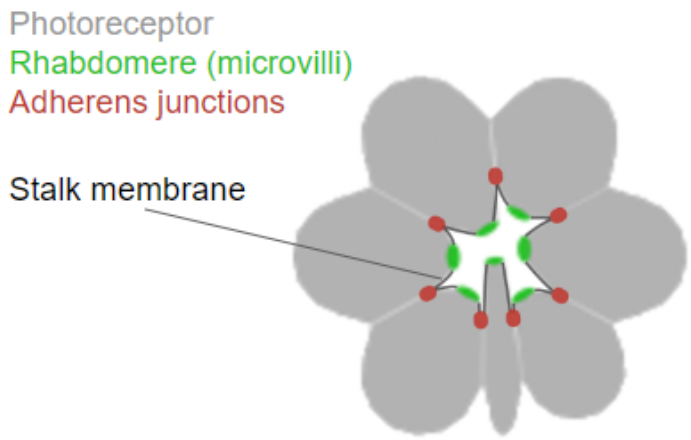

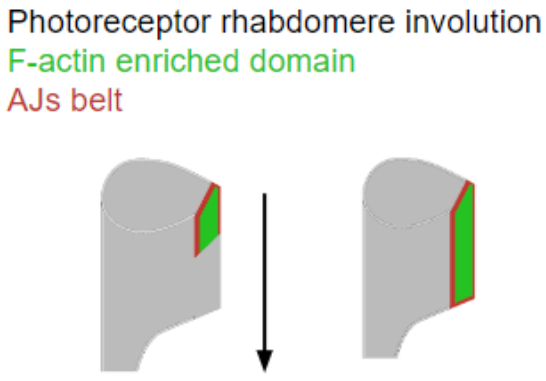

Figure 2.3 Composition of the photoreceptor specialized domain and rhabdomere involution

2.3.2 Rhabdomere morphogenesis

Compared to embryonic or other simple epithelia where the longitudinal axis is defined by a viscoelastic/rather relaxed lateral membrane or by transient cytoskeletal machinery, a unique feature of pupal-adult retinal epithelium is that the longitudinal axis is defined by a distinct rigid rod-like rhabdomere that is constantly growing and elaborating. This rhabdomere domain forms anchorage to both ends of the cone cell and maintains these connections to span the entire depth as the retina elongates.

Starting around 50% p.d., the highly specialized structure can be subdivided into different compartments, each comprising a different pool of structural molecules assembled in different organizations that serve distinct roles (Figure 2.3). The most apical part is the rhabdomere, which is the light-sensing organelle tightly packed with ~60,000 microvilli. Each microvillus is ~50 nm in diameter and 1-2 μm in length. This highly pleated array requires tremendous membrane deposition and increase in surface area to house tens of millions of rhodopsin molecules and other signaling molecules responsible for the detection of light (Zelhof, 2003; Knust, 2007). This is the compartment mostly observed when staining with phalloidin for F-actin.

The region on the plasma membrane directly adjacent to the microvilli-enriched compartment is the stalk membrane, which connects the rhabdomere to the zonula junctions, i.e. adherens junctions belt. The stalk provides a key constraint on plasma membrane that positions the elongating AJs to the sub-apical domain of the rhabdomere that marks the boundary of apical and basolateral membrane. Stalk membrane is enriched with apical determinants such as Crumbs, and serves the supporting role to both maintain AJs organization and rhabdomere elongation (Pellikka et al., 2002; Izaddoost et al., 2002). The photoreceptor cluster faces towards a luminal space called the inter-

rhabdomeral space (IRS), which physically separates and optically insolates the rhabdomeres from each other. Proteoglycan Eys shut (Eys) is the crucial component of the IRS luminal matrix and was found to be secreted through the stalk membrane.

The cytoplasm at the base of the rhabdomere is defined by the rhabdomere terminal web (RTW), a striking specialization of cortical actin cytoskeleton assembled into microfilaments. The structure of the rhabdomere terminal web is designed to provide sub-apical constraints to resist the protrusion of the expanding rhabdomere into the basal lateral cytoplasm, and thus the microfilaments are arranged in a way that resembles a paintbrush pressing upon a boundary surface (Arikawa, 1990; Chang, 2000). This structure is normally overlooked as the phalloidin signal in rhabdomeres is overwhelmingly strong, but two distinct stripes of myosin were detected along the full length of rhabdomere base/RTW, which might play a mechanical role and provide sub-apical contraction to consolidate the boundary (Baumann, 2004). Besides provide mechanical constraints, the RTW is also important for Rab-mediated biosynthetic trafficking that builds the rhabdomere during development. The vesicle-transport motor, Myosin V, is enriched in the RTW and used to directionally transport cargoes from the plasma membrane to construct the rhabdomeres along the longitudinal axes. Notable cargoes such as Rhodopsin 1 (Rh1), Crumbs (Crb), and Eyes shut (Eys) important to the functional and structural specialization of the rhabdomere relies on this vesicle trafficking machinery to the apical membrane (Li et al. 2007; Knust, 2007; Laffafian and Tepass, 2019)

In sum, these specialized compartments within the apical domain contribute to rhabdomere morphogenesis along two different directions: radially (apico-basal when referring to photoreceptor polarity) to resist microvilli protrusion; and also axially to stiffen and expand along

the longitudinal axes (distal-proximal depth of retinal epithelium). These two processes work in conjunction to transform the crescent-shaped short early rhabdomere to the final long cylinder in the adult retina, and to ensure proper physiological function.

2.4. Planar patterning

2.4.1 Cell behaviors during early phase of pattern formation- cell sorting/rearrangement, cell elimination, and fate specification

The Drosophila compound retina is best known for its precise hexagonal pattern and thus serves as a classic 2D model system to study tissue patterning. Pattern formation during early pupal stage (0-50% p.d. ~2 days) is orchestrated by different cell behaviors including cell fate specification, cell sorting/rearrangement, elimination, and shape changes. It involves three different cell populations- cone cells, primary pigment cells and interommatidial pigment cells. Interactions between these cells have been primarily examined on the apical surface.

By the end of larval stage, the cellular organization of an ommatidium is crudely formed, with cone cells rising on top of the photoreceptor cluster and forming the core in the center, while uncommitted cells surround the central assembly and fill in the interommatidial space. Although these retinal cells in the interommatidial space are born around the second mitotic wave during larval stage, their fates are not specified until the early and mid-pupal stage of development (Ready et al.,1976; Cagan and Ready, 1989a). Two primary pigment cells (PPCs) are specified first and join the central assembly. They adopt the enlarged kidney shape that holds the cone cell quartet and release their basal processes from the retinal floor. They are the only retinal cells that do not

maintain contact with the basal floor and only have apical appearance. It has been proposed that PPCs are through Delta-Notch signaling, where high level of Delta in cone cells activates Notch on the uncommitted neighbors to become PPC cells (Nagaraj and Banerjee, 2007). Interestingly, the two surrounding PPCs directly adhere to the anterior-posterior pair of cone cells, which coincides with non-uniform higher Delta expression in this A-P CC pair (Wolff and Ready, 1993, Nicelio thesis).

The process of secondary and tertiary PCs adopting their final fate, position and shape has also been well-characterized. The unspecified interommatidial cells are sorted from the initial arrangement of double or triple rows between the ommatidial cores into a single row. During this process, interommatidial cells actively rearrange and exchange neighbors in a manner similar to T1 transitions during embryonic germ band extension that converges into one row. They assume fluid-like behavior within the interommatidial space with no strictly defined spacing. CC-PPC centers take position but dynamically change shape and move locally to accommodate the dynamic cell rearrangement process happening in the interommatidial space, with gradually increasing order. This process is driven by heterophilic interaction between Nephrin-like adhesion receptors Hibris and Roughest along interommatidial PC (unspecified IOPCs)- PPC contacts, which favors the contacts between them while minimizing IOPC-IOPC contacts. The differential expression of Hibris and Roughest, and the differential adhesion is controlled by Notch (Bao et al., 2010; Bao, 2014; Shellenbarger and Mohler, 1975, Cagan and Ready, 1989b). Around 25-30% p.d, the IOPC who establishes contacts with three PPC becomes a tertiary PC, and the remaining ones contacting two PPCs assumes secondary PC fate. Around the same time, PCs undergo several rounds of apoptosis until ~40% p.d (Cagan and Ready,1989a; Wolff and Ready,1991b; Larson et al., 2008). It has been proposed that the pigment cell death is regulated in a position-dependent manner, and

through cell competition for the limited survival factor (Dos-Santos et al., 2008). Laser ablation of cone/PP cells results in ectopic apoptosis. This effect can be blocked if IOPCs receive a constitutive EGFR signal, indicating that cone/PP cells send a survival signal to IPCs via the EGFR signal transduction pathway (Miller and Cagan, 1998). The EGFR survival signal is counterbalanced by antagonistic signals, such as Argos diffusing from the cone cells, and Notch. However, whether cone cells of photoreceptors provide the signaling source for Notch activation is unknown. Mutations in the Notch gene result in extra PCs occupying the niche, but without severely interfering with regular spacing. The combined effect of EGFR survival signals coming from cone cells/PPCs and the antagonistic Notch signal from unknown source control this process (Cagan and Ready, 1989; Yu et al., 2002; Carthew, 2005).

2.4.2 Cell mechanics for the last phase of hexagonal patterning

By ~40% p.d, the retinal epithelium finishes the initial round of rearrangement and elimination. Interommatidial PCs have adopted their stereotyped position, and further refine their shape and organization into a hexagonal pattern with increasing precision. Occasional cell death might still happen, or the final ommatidium might still has few extra PCs, but the extra cells will squeeze and fit in a niche that is normally occupied by one cell and do not significantly affect hexagon order. During this last phase of patterning (~40-50% p.d), secondary PCs change from a relative relaxed round shape to a thin elongated shape that confines the six sides of the hexagonal "frame", and the tertiary PCs and bristles alternating at the vertices of the "frame". During this time the cone cell quartet finalizes its organization which resembles the configuration of soap bubble. Both the "frame" and internal organization has been well-characterized by a combination of genetics,

mechanical, live imaging approach and numerical modeling in a set of studies. I will summarize the cell mechanics that modulate each process below.

Cone cells quartet organization in the center of the "frame" is strikingly similar to the configuration of soap bubbles, which follows the rules to minimize surface area and free energy, as described in D'Arcy Thompson's book and even earlier developed by Joseph Plateau (Thompson, 1917; Plateau, 1873). Cells, however, differ from bubbles, in their composition and mechanics that determine the surface tension. The first model, a "preferential adhesion" model, was proposed only accounting the cell-cell adhesion for interfacial tension. Two cadherins types, E-cadherin (E-cad) and N-cadherin (N-cad) are expressed in different retinal cells. The four cone cells' interface between themselves are dominated by N-cad with very low E-cad, while the interface between cone cell and primary PC and other PCs only contains E-cad without any N-cad (Hayashi and Carthew, 2004). Misexpression or depletion of the adhesion molecule in specific cells always end up in a configuration as Plateau proposed in the energy minimization model in the bubble. However, their interpretation did not take into consideration other machinery associated with E-cad, like contractile cortical actomyosin, that could also be affected in the misexpression or depletion experiment. In 2007, Lecuit and Lenne reviewed a large number of experiments and showed that a cell's surface tension results from the counterbalance of adhesion and cytoskeletal contraction (Lecuit and Lenne, 2007). The "preferential adhesion" was soon corrected by considering both cell-cell adhesion and contractility into the energy equation. Indeed, in silico predictions based on energy minimization reproduce well the cone cell shapes (Käfer et al., 2007; Hilgenfeldt et al., 2008). Later, more experiments that examined the molecular and mechanical nature of the interfacial tension consolidated the model. In particular, mechanical measurement and modeling found that myosin localization and intensity is dependent on N-cad, with myosin contractility

yielding two-fold stronger force than N-cad bonds, further emphasizing the interplay between cadherins and actomyosin networks in the cell patterning (Chan et al., 2017; Blackie et al., 2020).

In the case of the ommatidial hexagonal “frame”, the balance of contractility and adhesion also applies at the PC-PC interface. Beautiful apical live imaging from ~25-40% p.d. shows an oscillatory expansion and constriction of secondary PC-tertiary PC contacts, as the secondary PC becomes slender and gradually shortens the contact to the tertiary PC. Each expansion or contraction of LC-LC contact lasts 14.2 ± 3.0 min on average, with the amplitudes of ~15% junctional length. The study also shows that Arp2/3-mediated growth of branched actin network drives the lengthening, and actomyosin mediates the contraction (Signore et al., 2017). Although the study did not examine the maintenance of pattern after 50% p.d., or the dynamics on the basal PC contractile feet, similar mechanisms and dynamics might also apply.

When considering the ommatidial apical profiles together, modeling revealed that the PCs forming the ommatidial “frame” are under greater tension than those cells inside the frame (primary PCs and cone cells). Within the internal organization, the cone cells cluster is under significantly higher tension than the primary pigment cells. Thus, the primary PCs provide an easily deformable "buffer" between the stiffer frame and central core. This finding suggested a buffer mechanism which ensures robust hexagonal patterns even though the internal organization might not be completely error-free (Kim et al., 2016).

2.4.3 Basal patterning

Compared to the extensive characterization on the apical patterning, the ommatidial basal patterns has been an unexplored territory due to several factors. 1. It is difficult to image. The existing characterization of the basal pattern is based on the valuable early electron micrographs (Cagan and Ready, 1989). Due to the deepening and pigmentation of the tissue, confocal light microscopy can live image basal pattern only up until ~55% p.d; recent two-photon imaging extends the live imaging window to ~80% p.d (my preliminary observation) 2. Although confocal imaging of dissected fixed tissue is possible at any stage, it is difficult to characterize the basal pattern, as the early basal floor has no distinct pattern to distinguish different cell types up till 40% p.d. The petal pattern formed after 40% p.d. is not visually intuitive to associate with the hexagonal ommatidial boundary.

From the EM reconstruction of the ommatidial cell organization at ~25%-30% p.d, it was observed and assumed that the early patterning of interommatidial PCs begins at the apical surface, and "zippers down" basally to rearrange the remainder of the cells into new position (Cagan and Ready, 1989). This observation justifies studying the early patterning as a 2D context. However, the EM reconstruction is only based on static images at different planes at fixed time points, and with limited sample size. Emerging studies start to emphasize the role of the basolateral membrane to lead the cell rearrangement. For example, live 3D imaging during germ band extension found that basolateral protrusions initiate the movement prior to the apical domain movement (Sun et al., 2017). Applying modern imaging techniques to examine the 3D rearrangement of PCs during the patterning phase is needed to update the previous model based on static imaging.

Relatively more studies of basal pattern have focused on the later half of pupal development, during which the cell contacts are maintained as the ommatidial field undergoes ~fourfold contraction. The Drosophila basal plane is known as the retinal floor with PC feet opposing an underlying ECM. PC feet radiate from the central ring and connect to the neighboring six grommets. Each PC foot organizes planar arrays of actomyosin stress fibers which anchor to the grommet in the integrin-dependent focal adhesion point (Longley and Ready, 1995; Ready, 2002; Baumann, 2004). Grommets are distinctive, laminin-containing rings that allows each photoreceptor axon to exit the retina through a tiny port. Cone cell feet (~3-4 μm depth, based on my anecdotal measurement) plug the central grommet, leaving a small port just the right size for axons, and form stable Ecad-mediated contacts with PC feet at the most basal plane. These contacts are reinforced with septate junctions like Neurexin slightly above (Banerjee et al., 2008). Interestingly, cone cell feet are not standing on an ECM, suggesting that the adhesion between PC and CC feet are sufficient for cone cells to lock in the position and to withhold the expanding rhabdomeres anchored on them. With this arrangement, as the basal floor contracts isotropically within one ommatidium, and between the neighboring ommatidia, the same forces are transmitted through the connecting PC feet resulting in a uniform petal-like pattern across the floor. Recent studies suggested that a calcium wave might coordinate the tissue-scale basal contraction through inositol 1,4,5-triphosphate receptor (IP3R) signaling (Ready and Chang, 2021). However, this study has the caveat that the Calcium imaging is only characterized on the apical surface of the compound eye, not basal. It would be interesting to image (maybe at a slightly earlier light accessible stage) simultaneously the PC contraction dynamics and the Calcium waves, and then characterize the exact correspondence of Calcium wave and the contractile activities to make sense of how the tissue interprets the intriguing Calcium wave pattern.

REFERENCES

Bao, Sujin. "Two themes on the assembly of the Drosophila eye." Current topics in developmental biology 93 (2010): 85-127.

Banerjee, Swati, Kevin Blauth, Kimberly Peters, Stephen L. Rogers, Alan S. Fanning, and Manzoor A. Bhat. "Drosophila neurexin IV interacts with Roundabout and is required for repulsive midline axon guidance." Journal of Neuroscience 30, no. 16 (2010): 5653-5667.

Bao, Sujin, and Ross Cagan. "Preferential adhesion mediated by Hibris and Roughest regulates morphogenesis and patterning in the Drosophila eye." Developmental cell 8, no. 6 (2005): 925-935.

Bao, Sujin, et al. "Preferential adhesion maintains separation of ommatidia in the Drosophila eye." Developmental biology 344.2 (2010): 948-956.

Bao, Sujin. "Notch controls cell adhesion in the Drosophila eye." PLoS genetics 10, no. 1 (2014): e1004087.

Barlow, Horace B. "The size of ommatidia in apposition eyes." Journal of experimental Biology 29, no. 4 (1952): 667-674.

Blackie, Laura, Melda Tozluoglu, Mateusz Trylinski, Rhian F. Walther, François Schweisguth, Yanlan Mao, and Franck Pichaud. "A combination of Notch signaling, preferential adhesion and endocytosis induces a slow mode of cell intercalation in the Drosophila retina." Development 148, no. 10 (2021): dev197301.

Blackie, Laura, Rhian F. Walther, Michael F. Staddon, Shiladitya Banerjee, and Franck Pichaud. "Cell-type-specific mechanical response and myosin dynamics during retinal lens development in Drosophila." Molecular Biology of the Cell 31, no. 13 (2020): 1355-1369.

Bonini, Nancy M. "Surviving Drosophila eye development." Cell Death & Differentiation 4, no. 1 (1997): 4-11.

Cagan, Ross L., and Donald F. Ready. "The emergence of order in the Drosophila pupal retina." Developmental biology 136, no. 2 (1989): 346-362.

Cagan, Ross. "Principles of Drosophila eye differentiation." Current topics in developmental biology 89 (2009): 115-135.

Carthew, Richard W. "Pattern formation in the Drosophila eye." Current opinion in genetics & development 17, no. 4 (2007): 309-313.

Chan, Eunice HoYee, Pruthvi Chavadimane Shivakumar, Raphael Clement, Edith Laugier, and Pierre-François Lenne. "Patterned cortical tension mediated by N-cadherin controls cell geometric order in the Drosophila eye." Elife 6 (2017): e22796.

Chang, Hui-Yun, and Donald F. Ready. "Rescue of photoreceptor degeneration in rhodopsin-null Drosophila mutants by activated Rac1." Science 290, no. 5498 (2000): 1978-1980.

Currea, John P., Joshua L. Smith, and Jamie C. Theobald. "Small fruit flies sacrifice temporal acuity to maintain contrast sensitivity." Vision research 149 (2018): 1-8.

De Ruyter van Steveninck, R. R., and S. B. Laughlin. "The rate of information transfer at graded-potential synapses." Nature 379, no. 6566 (1996): 642-645.

Del Signore, Steven J., Rodrigo Cilla, and Victor Hatini. "The WAVE regulatory complex and branched F-actin counterbalance contractile force to control cell shape and packing in the Drosophila eye." Developmental cell 44, no. 4 (2018): 471-483.

Fan, Seng-Sheen, and Donald F. Ready. "Glued participates in distinct microtubule-based activities in Drosophila eye development." Development 124, no. 8 (1997): 1497-1507.

Fenk, Lisa M., Sofia C. Avritzer, Jazz L. Weisman, Aditya Nair, Lucas D. Randt, Thomas L. Mohren, Igor Siwanowicz, and Gaby Maimon. "Muscles that move the retina augment compound eye vision in Drosophila." Nature (2022): 1-7.

Gonzalez-Bellido, Paloma T., Trevor J. Wardill, and Mikko Juusola. "Compound eyes and retinal information processing in miniature dipteran species match their specific ecological demands." Proceedings of the National Academy of Sciences 108, no. 10 (2011): 4224-4229.

Hardie, Roger C., and Kristian Franze. "Photomechanical responses in Drosophila photoreceptors." Science 338, no. 6104 (2012): 260-263.

Hayashi, Takashi, and Richard W. Carthew. "Surface mechanics mediate pattern formation in the developing retina." Nature 431, no. 7009 (2004): 647-652.

Hilgenfeldt, Sascha, Sinem Erisken, and Richard W. Carthew. "Physical modeling of cell geometric order in an epithelial tissue." Proceedings of the National Academy of Sciences 105, no. 3 (2008): 907-911.

Juusola, Mikko, An Dau, Zhuoyi Song, Narendra Solanki, Diana Rien, David Jaciuch, Sidhartha Anil Dongre et al. "Microsaccadic sampling of moving image information provides Drosophila hyperacute vision." Elife 6 (2017): e26117.

Käfer, Jos, Takashi Hayashi, Athanasius FM Marée, Richard W. Carthew, and François Graner. "Cell adhesion and cortex contractility determine cell patterning in the Drosophila retina." Proceedings of the National Academy of Sciences 104, no. 47 (2007): 18549-18554.

Katz, Ben, and Baruch Minke. "Drosophila photoreceptors and signaling mechanisms." Frontiers in cellular neuroscience (2009): 2.

Kemppainen, Joni, Ben Scales, Keivan Razban Haghighi, Jouni Takalo, Neveen Mansour, James McManus, Gabor Leko et al. "Binocular mirror–symmetric microsaccadic sampling enables

Drosophila hyperacute 3D vision." Proceedings of the National Academy of Sciences 119, no. 12 (2022): e2109717119.

Kim, Sangwoo, Justin J. Cassidy, Boyuan Yang, Richard W. Carthew, and Sascha Hilgenfeldt. "Hexagonal patterning of the insect compound eye: Facet area variation, defects, and disorder." Biophysical journal 111, no. 12 (2016): 2735-2746.

Kumar JP, Bowman J, Otousa JE, Ready DF (1997) Rhodopsin replacement rescues photoreceptor structure during a critical developmental window.

Kumar, Justin P., and Donald F. Ready. "Rhodopsin plays an essential structural role in Drosophila photoreceptor development." Development 121, no. 12 (1995): 4359-4370.

Land, Michael F. "Visual acuity in insects." Annual review of entomology 42, no. 1 (1997): 147-177.

Larson, David E., Zoe Liberman, and Ross L. Cagan. "Cellular behavior in the developing Drosophila pupal retina." Mechanisms of development 125, no. 3-4 (2008): 223-232.

Lau, Ting Fan Stanley, Elisabeth Gross, and Victor Benno Meyer-Rochow. "Sexual dimorphism and light/dark adaptation in the compound eyes of male and female Acentria ephemerella (Lepidoptera: Pyraloidea: Crambidae)." European Journal of Entomology 104, no. 3 (2007): 459-470.

Lecuit, Thomas, and Pierre-Francois Lenne. "Cell surface mechanics and the control of cell shape, tissue patterns and morphogenesis." Nature reviews Molecular cell biology 8, no. 8 (2007): 633-644.

Longley Jr, Robert L., and Donald F. Ready. "Integrins and the development of three-dimensional structure in the Drosophila compound eye." Developmental biology 171, no. 2 (1995): 415-433.

Lunau, Klaus. "Visual ecology of flies with particular reference to colour vision and colour preferences." Journal of Comparative Physiology A 200 (2014): 497-512.

Nilsson, Dan-Eric. "Optics and evolution of the compound eye." In Facets of vision, pp. 30-73. Springer Berlin Heidelberg, 1989.

Plateau, Joseph Antoine Ferdinand. Statique expérimentale et théorique des liquides soumis aux seules forces moléculaires. Vol. 2. Gauthier-Villars, 1873.

Ready, Donald F. "Drosophila compound eye morphogenesis: blind mechanical engineers?." Drosophila Eye Development (2002): 191-204.

Ready, Donald F., Thomas E. Hanson, and Seymour Benzer. "Development of the Drosophila retina, a neurocrystalline lattice." Developmental biology 53, no. 2 (1976): 217-240.

Stahl, Aaron L., Mark Charlton-Perkins, Elke K. Buschbeck, and Tiffany A. Cook. "The cuticular nature of corneal lenses in Drosophila melanogaster." Development genes and evolution 227 (2017): 271-278.

Stavenga, Doekele G., and Roger C. Hardie, eds. Facets of vision. Springer Science & Business Media, 2012.

Sun, Zijun, Christopher Amourda, Murat Shagirov, Yusuke Hara, Timothy E. Saunders, and Yusuke Toyama. "Basolateral protrusion and apical contraction cooperatively drive Drosophila germ-band extension." Nature cell biology 19, no. 4 (2017): 375-383.

Tomlinson, Andrew, and Donald F. Ready. "Neuronal differentiation in the Drosophila ommatidium." Developmental biology 120, no. 2 (1987): 366-376.

Wolff, T. A. N. Y. A., and DONALD F. Ready. "The beginning of pattern formation in the Drosophila compound eye: the morphogenetic furrow and the second mitotic wave." Development 113, no. 3 (1991): 841-850.

Zheng, Lei, Gonzalo G. de Polavieja, Verena Wolfram, Musa H. Asyali, Roger C. Hardie, and Mikko Juusola. "Feedback network controls photoreceptor output at the layer of first visual synapses in Drosophila." The Journal of general physiology 127, no. 5 (2006): 495-510.

Chapter 3. Orthogonal coupling of a 3D cytoskeletal scaffold coordinates cell morphogenesis and maintains tissue organization in the Drosophila pupal retina

Xiao Sun[1], Jacob Decker[1], Nicelio Sanchez-Luege[1], Ilaria Rebay[1,2,3]

[1]Committee on Development, Regeneration and Stem Cell Biology

[2]Ben May Department for Cancer Research

University of Chicago, Chicago, IL 60637 USA

[3]Corresponding Author

Key words: Abelson; Drosophila eye development; morphogenesis; 3D cytoskeletal network; apical-basal polarity; actin cytoskeleton; epithelial patterning; cell-cell interactions; feedback mechanism; photoreceptor; pigment cell

ABSTRACT

How complex three-dimensional (3D) organs coordinate cellular morphogenetic events to achieve the correct final form is a central question in development. The question is uniquely tractable in the late *Drosophila* pupal retina where cells maintain stereotyped contacts as they elaborate the specialized cytoskeletal structures that pattern the apical, basal and longitudinal planes of the epithelium. In this study, we combined cell typespecific genetic manipulation of the cytoskeletal regulator Abelson (Abl) with 3D imaging to explore how the distinct cellular morphogenetic programs of photoreceptors and interommatidial pigment cells coordinately organize tissue pattern to support retinal integrity. Our experiments revealed an unanticipated intercellular feedback

mechanism whereby correct cellular differentiation of either cell type can non-autonomously induce cytoskeletal remodeling in the other *Abl* mutant cell type, restoring retinal pattern and integrity. We propose that genetic regulation of specialized cellular differentiation programs combined with inter-plane mechanical feedback confers spatial coordination to achieve robust 3D tissue morphogenesis.

Introduction

The spatial arrangement of cells within an epithelium is critical to the final form and function of the tissue. During development, genetically controlled terminal differentiation programs produce the specialized cytoskeletal structures, cell-cell junctional adhesions and cell-extracellular matrix (ECM) contacts unique to each cell type. In turn, the resulting cell shapes, structures and connections introduce specific packing constraints that influence final organ form. While progress has been made in describing the acquisition of tissue form in simple epithelia with relatively homogeneous cell composition, how complex tissues with diverse cell fates, shapes, and physical properties spatially coordinate dramatic morphogenetic remodeling to maintain robust organization remains poorly understood (Collinet and Lecuit, 2021).

Previous studies have shown that coordinated cell shape changes driven by subcellular cytoskeletal and junction remodeling produce tissue-level morphology. The best-studied process is apical constriction, where supracellular networks physically couple cell

apices across a tissue plane to drive numerous morphogenetic processes including epithelial folding, bending, invagination and closure (Martin and Goldstein, 2014; PerezVale and Peifer, 2020). Subsequent consideration of cells as 3D units has emphasized how remodeling of cellular structure along basal or lateral planes or of the ECM can also promote morphogenetic change (Daley and Yamada, 2013; Gracia et al., 2019; Harmansa et al., 2022; Roellig et al., 2022; Sui et al., 2018). Temporal sequences of independent planar changes also coordinate 3D change. Notable examples include the sequential activation of actomyosin contractility along different planes to organize the successive patterns of apical and lateral contraction required for endoderm invagination in the ascidian embryo (Sherrard et al., 2010) and lumen morphogenesis in the C. elegans vulva (Yang et al., 2017). In all these examples, the apical-lateral-basal organization inherent to polarized epithelial tissues provides an intuitive physical conduit for driving 3D cellular and tissue-level morphogenetic change. Despite the established importance of supracellular networks in providing mechanical coupling within individual planes, whether and how remodeling processes interact across different planes to produce specific 3D cellular and tissue scale morphologies remains to be explored.

The stereotyped pseudostratified epithelial architecture of the Drosophila compound eye makes it an attractive model to approach this question. The fly retina is a complex epithelial organ whose form and function depends on the precise organization of highly specialized and uniquely shaped cell types (Figure 3.1A and 3.1B; (Charlton-Perkins and Cook, 2010; Ready et al., 1976a; Wolff and Ready, 1993). Clusters of eight photoreceptor neurons occupy the central core of each ommatidial unit, with their photosensitive rhabdomeres defining the longitudinal optical axis of the epithelium. Directly above each cluster, an apical assembly of four cone and two primary

pigment cells produces the lens that will focus incoming light onto the underlying photoreceptors. A hexagonal lattice of secondary and tertiary interommatidial pigment cells (IOPCs) surrounds each photoreceptor cluster. Through their cortical cytoskeletal-enriched junctional domains and basal cell-cell/ECM junctional contacts, the IOPCs provide inplane connections across the apical and basal planes of the retinal field.

Pupal retinal development can be separated into two phases, a pattern establishment phase and a tissue elongation phase during which pattern is maintained (Figure 3.1A) (Cagan and Ready, 1989; Johnson, 2021; Ready et al., 1976b). During the patterning phase, cone cell and IOPC rearrangements produce the precise hexagonal lattice pattern while photoreceptor apical domain involution and anchorage to the cone cells aligns the optical axis relative to the apical and basal surfaces. During the elongation phase, cell-cell contacts and overall tissue organization are maintained while the photoreceptor and IOPC terminal differentiation programs elaborate functional specialized structures and the epithelium elongates four-fold. Although the emergence of two-dimensional (2D) planar pattern and the individual morphogenetic events in different retinal cell types during the early patterning phase have been well-described (Bao and Cagan, 2005; Baumann, 2004; Cagan and Ready, 1989; Hayashi and Carthew, 2004; Hilgenfeldt et al., 2008; Johnson, 2021; Kafer et al., 2007; Longley and Ready, 1995; Pellikka et al., 2002; Pham et al., 2008; Ready, 2002; Ready and Chang, 2021; Signore et al., 2018), how the subsequent cellular morphogenetic changes are regulated, coordinated and integrated across different tissue planes to maintain 3D retinal organization and integrity during retinal elongation has not been explored.

We chose the cytoplasmic tyrosine kinase and cytoskeletal regulator Abelson (Abl) as a tool to examine the impact of modulating retinal cell shapes and structures on tissue organization. Prior phenotypic analyses showed that Abl is required for multiple aspects of the photoreceptor terminal differentiation program and that its loss perturbs ommatidial organization and retinal pattern (Bennett and Hoffmann, 1992; Henkemeyer et al., 1987; Henkemeyer et al., 1990; Kannan et al., 2014; Singh et al., 2010; Xiong and Rebay, 2011; Xiong et al., 2013). Mechanistic studies have shown how Abl modulates cytoskeletal remodeling and junctional dynamics that control cell morphology in a wide range of epithelial tissues. For example, in the early embryonic epithelium Abl helps to coordinate apical constriction during mesoderm invagination and to produce the cell shape changes that drive convergent extension during germband elongation (Fox and Peifer, 2007; Jodoin and Martin, 2016; Tamada et al., 2012; Yu and Zallen, 2020). Inhibition of Enabled (Ena)-mediated linear F-actin assembly is a key aspect of Abl function in many contexts (Comer et al., 1998; Forsthoefel et al., 2005; Fox and Peifer, 2007; Gates et al., 2007; Gertler et al., 1995; Grevengoed et al., 2001; Kannan et al., 2014; Kannan et al., 2017; Lin et al., 2009; Rogers et al., 2021). Best studied is the embryonic central nervous system, where in response to different axon guidance cues, Abl modulates the balance between linear and branched F-actin by regulating the activity not only of Enabled, but also of the WAVE/SCAR complex (Forsthoefel et al., 2005; Gertler et al., 1995; Kannan et al., 2017; Liebl et al., 2000; Wills et al., 1999).

In this study, we investigated how cellular morphogenetic events are individually controlled and effectively communicated between two different retinal cell types as the late pupal retina elaborates and maintains its precise 3D organization. Our approach was to combine genetic perturbation of Abl function with single-cell resolution fixed and live time-lapse imaging to

examine retinal cell shapes and tissue-scale patterns. First, we used global depletion of Abl to characterize its contributions to the cytoskeletal specializations each cell type elaborates. In contrast to a wildtype retina where correctly elaborated and aligned photoreceptor and IOPC cytoskeletal domains confine cell shape and organization, loss of Abl disrupted photoreceptor and IOPC terminal differentiation, resulting in a tissue whose heterogenous cellular shapes, structures and intercellular connections were insufficient to maintain retinal integrity. Second, we probed how IOPCs and photoreceptors interact by restoring Abl to each individual cell type in an otherwise *abl* mutant background. Strikingly, these experiments uncovered a feedback interaction between the two cell types that enabled rescue of either photoreceptor or IOPC cellular differentiation to induce morphogenetic remodeling of the other cell type and thus restore retinal 3D organization and tissue integrity. Together our results suggest that the cytoskeletal and junctional adhesions of the photoreceptors and IOPCs provide a mechanically coupled structural scaffold that coordinates cellular differentiation to ensure the robust tissue-level architecture needed for vision.

Results

Loss of *abl* results in photoreceptors "falling" out of the retinal epithelium. Prior work showed that in *abl* mutant retinas, photoreceptors are specified correctly but then fail to carry out their normal terminal differentiation program (Henkemeyer et al., 1987; Henkemeyer et al., 1990; Singh et al., 2010; Xiong and Rebay, 2011; Xiong et al., 2013). We were interested in how retinal cell terminal differentiation impacts the elaboration of cell and tissue morphology. As a framework for exploring this, we briefly summarize how the apical, basal and longitudinal networks of actin-based cytoskeletal structures and junctional adhesions established during the patterning phase are subsequently remodeled to produce the specialized structures of a mature wildtype retina (Longley and Ready, 1995; Ready, 2002).

First, the apical network is defined by the hexagonally arranged IOPC apical junctional domains. After its establishment by 50% p.d., the apical network is stably maintained with minimal change (Bao and Cagan, 2005; Cagan and Ready, 1989; Hayashi and Carthew, 2004; Signore et al., 2018). Second, at the basal epithelial plane, IOPCs refine their cell-ECM contacts by anchoring to integrin-reinforced rings, or grommets, at the center of each ommatidium, and by tiling the entire retinal floor with a radial pattern of contractile actomyosin "feet"; during the elongation phase, coordinated contraction of this basal network compacts the retinal floor (Baumann, 2004; Longley and Ready, 1995; Ready and Chang, 2021). Referred to as the "fenestrated membrane", this specialized contractile network supports and separates the retina from the brain. Third, the longitudinal network is defined by rhabdomeric precursors consisting of the photoreceptor involuted apical membranes which bridge the apical and basal tissue planes at the centerpoint of

each ommatidium through junctional connections with the cone cell apical caps and basal feet; for simplicity, we refer to these specialized domains as rhabdomeres, regardless of stage. This unique coupling is established by 50% p.d. and then maintained as the rhabdomeres mature and expand during the elongation phase (Cagan and Ready, 1989). Because rhabdomeres anchor to the cone cell feet, which like the IOPC feet are anchored to the grommets, these rings mark a hub of junctional attachments that physically connect the longitudinal and basal networks and that couple the basal network to the ECM (Figure 3.1B and 3.1F).

Photoreceptors do not contribute directly to the 2D apical and basal patterns because their longitudinal anchor points are located below and above the apical network plane and basal network plane, respectively. Conversely, IOPCs contribute minimally to the longitudinal network because their thin cellular projections occupy minimal tissue space and do not make junctional connections with photoreceptors along the longitudinal axis.

Using this framework, we first examined final retinal organization by comparing photoreceptor position in wildtype and abl^{null} 100% p.d. retina-brain complexes (Figure 3.1C-3.1E; Figure S1A and S1B). In wildtype, the photoreceptor nuclei clustered in a tight row just below the retinal surface (Figure 3.1D; Figure S1C and S1D). In contrast, in abl^{null}, photoreceptor nuclei were scattered throughout the longitudinal length of the retina and were also found fallen beneath the retinal floor in the space between retina and lamina, a phenotype we refer to as loss of retinal integrity. (Figure 3.1E). Despite the aberrant position of these cells, lineage tracing confirmed their photoreceptor origin and identity (Figure S1E and S1F). Retinal depth was noticeably reduced relative to wildtype (Figure 3.1E vs. 3.1D). Thus, Abl is required for photoreceptors to maintain their proper position and for the retina to maintain structural integrity and elongate.

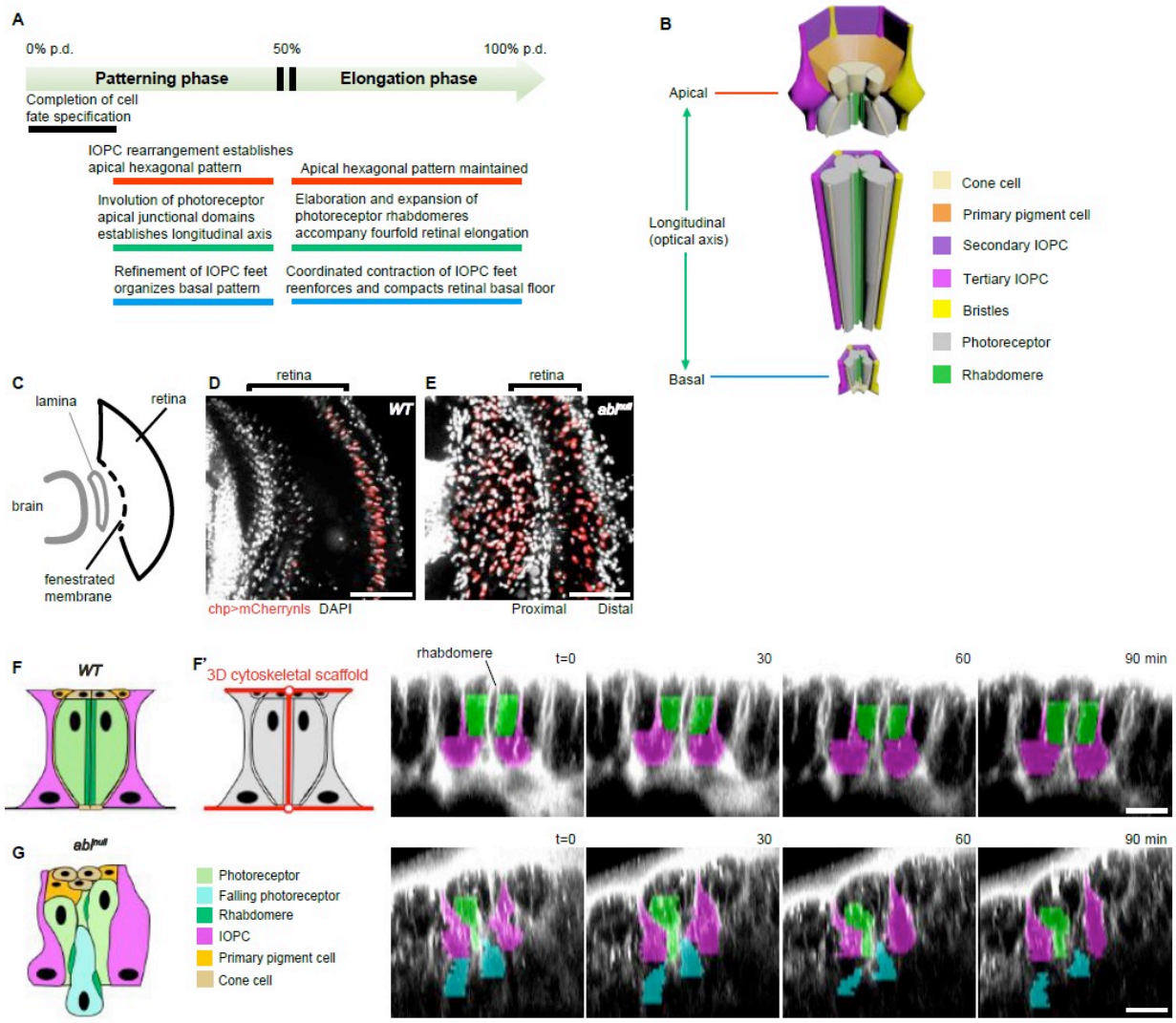

Figure 3.1. Loss of abl results in photoreceptors "falling" out of the retinal epithelium.

(A) Timeline summarizing the sequence of key morphogenetic events that pattern the apical, longitudinal and basal planes of the pupal retinal epithelium. IOPC, interommatidial pigment cell; p.d., pupal development.
(B) Schematic summarizing the 3D organization of a 100% p.d. ommatidium.
(C) Schematic of the adult visual system. The retinal fenestrated membrane (dashed line) separates it from the underlying lamina, the distal-most ganglion of the brain optic lobe.
(D,E) Comparison of photoreceptor nuclear position (red) in 100% p.d. retinal-brain complexes. DAPI (white) marks all nuclei. Scale bar = 50 µm.
(F, G.) Schematics and stills from time-lapse movies of 50% p.d retinas injected with CellMask (white). False color shows photoreceptors (green), fallen photoreceptors (cyan) and secondary IOPCs (magenta) in a representative ommatidium. Scale bars = 10µm. See also Figure S2A-S2D. F' depicts the 3D scaffold.

To examine the changes in retinal cell shapes and relative positions during the falling process, we labeled cell membranes and performed time-lapse live imaging (Figure 3.1F and 3.1G; Figure S2A-S2D). In wildtype, completion of the early patterning phase resulted in stereotyped cell shapes, positions and contacts that did not appreciably change (Figure 3.1F; Figure S2A and S2B). Although the intensity of the injected dye precluded examination of apical network relationships, lateral views highlighted the distinctive interlocking shapes of the photoreceptors and IOPCs (Figure 3.1F). Photoreceptor cell bodies surround the central rhabdomere-defined longitudinal axis of each ommatidium, occupying the bulk of the tissue space except toward the basal plane, where they narrow to accommodate the IOPC bodies and basal feet. IOPCs maintain connection with the apical plane via thin processes that separate neighboring photoreceptor clusters and fill up the inter-ommatidial space. Despite the lack of junctional connections between photoreceptors and IOPCs, each appears to support and constrain the other's shape and position through their 3D spatial relationships.

In contrast, the shapes, positions and contacts of abl^{null} retinal cells were aberrant, showed heterogeneity within the same cell type and changed over the 90min course (Figure 3.1G; Figure S2C and S2D). Most photoreceptor cell bodies had dropped basally and rhabdomeres appeared disorganized. Occasional photoreceptors were detected breaching the fenestrated membrane (Figure 3.1G, cyan cells) leaving uneven spacing between neighboring ommatidia. The surrounding IOPCs rearranged their position and shape to accommodate the falling photoreceptors, thereby keeping the remaining epithelial sheet intact (Figure 3.1G). The resulting irregular apical and basal contacts impacted pattern along both surfaces (Figure S2C and S2D). Together, these

observations suggest that the distinct shapes and spatial arrangement of the photoreceptors and IOPCs is critical to the tissue's ability to withstand morphogenetic change and maintain integrity.

Abl is required to elaborate the specialized cytoskeletal domains of both photoreceptors and IOPCs that together organize 3D tissue pattern

To study how morphogenetic remodeling in photoreceptors and IOPCs collectively maintains retinal 3D organization, we examined the consequences of Abl loss to each cell type and to tissue patterning along the different epithelial planes (Figure 3.2). To bridge cellular and tissue scale analyses, we further conceptualized the specialized cytoskeletal domains that organize the apical, basal and longitudinal planes as a 3D structural scaffold (Figure 3.1F'). IOPC apical and basal domains provide hexagonally patterned in-plane connections while the photoreceptor rhabdomeres mediate out-ofplane coupling, physically bridging the apical and basal surfaces through anchorage to the cone cell caps and feet embedded in each plane. Scaffold alignment and connections are maintained throughout the elongation phase despite extensive remodeling of the cellular structures. We hypothesized that structural integrity and correct organization of the 3D scaffold is crucial to maintain retinal integrity. Therefore, defects in the terminal differentiation programs that establish the cellular structures and connections that define the scaffold should contribute to the collapse of abl^{null} photoreceptors. As they fall, the photoreceptors may further perturb scaffold structures and connections.

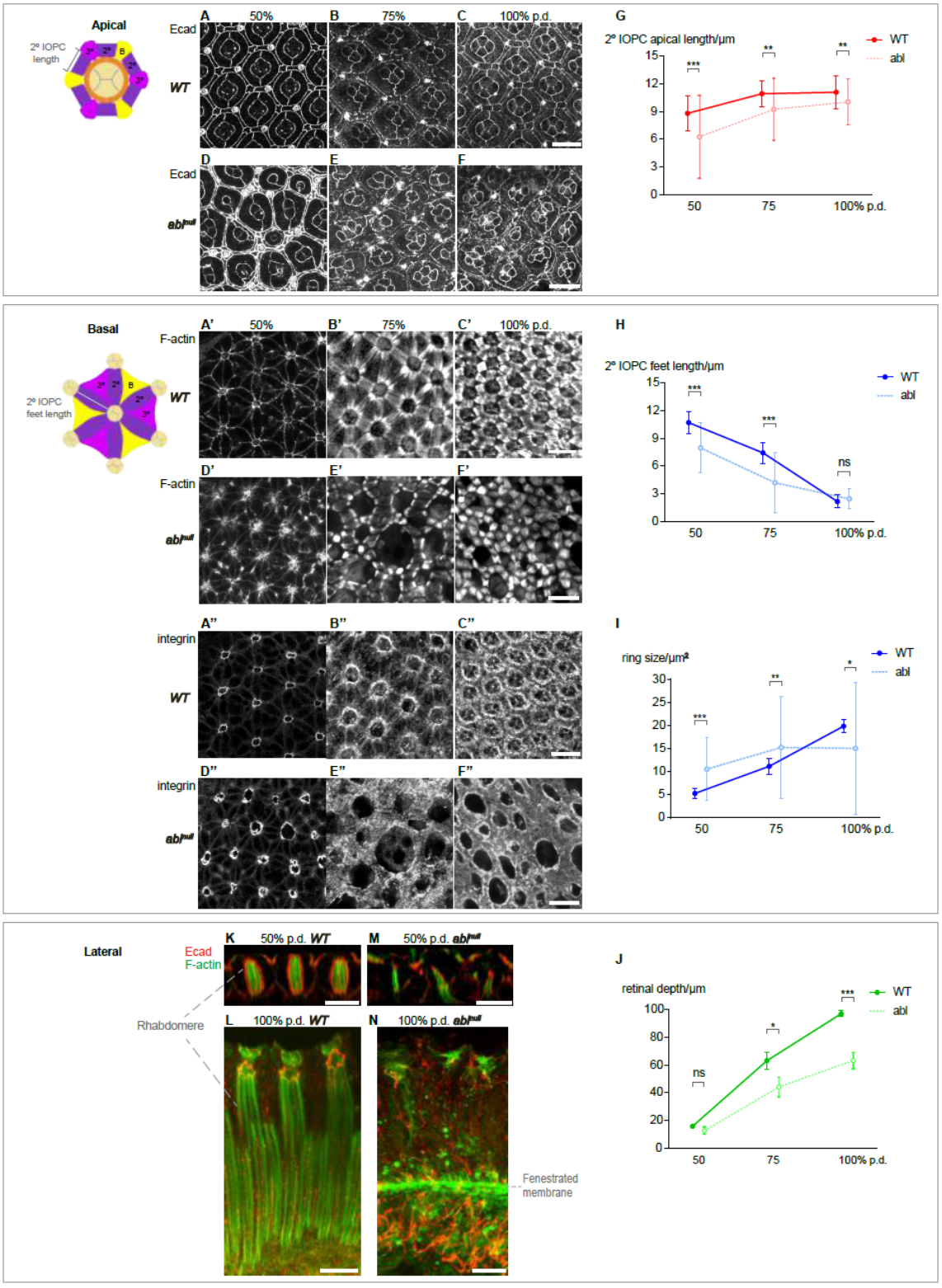

Figure 3.2. Abl-mediated terminal differentiation specializes the cytoskeletal and junctional structures of the apical, basal and longitudinal networks.

Figure 3.2 continued
(A-C) The stereotyped hexagonal pattern of the WT apical network, with single ommatidium schematic color-coded as in Figure 3.1B.
(D-F) Abl loss disrupts the apical network, although pattern improves over time.
(A'-C') Elaboration and isotropic contraction of the WT basal network, with schematic.
(D'-F') Abl loss disrupts the basal network, precluding its isotropic contraction.
(A"-C") Attachment points of the basal network to the central rings are reenforced by anchorage to the underlying ECM.
(D"-F") Abl loss disrupts basal network-ECM connections, contributing to loss of pattern and integrity. Note that in (**A-F"**), for each time point and genotype, the same disc, and the same set of ommatidia, were imaged at apical vs. basal planes. Scale bars = 10μm.
(G-I) Plots of mean ± SEM of secondary IOPC apical domain length, secondary IOPC basal foot length and basal ring area. For each time point and genotype, measurements were made in 30 ommatidia/retina, n= minimum of 4 retinas.
(J) Plot of mean ± SEM of retinal depth. For each time point and genotype, measurements were made in the central-most 10 ommatidia/retina, n= 3 retinas. **(K,L)** Lateral reconstructions of WT retinas showing the establishment and elaboration/elongation of the longitudinal network of rhabdomere bundles.
(M,N) Lateral reconstructions of abl^{null} retinas show the collapse of the longitudinal network, and the associated defects in retinal elongation and integrity. Scale bars = 10μm.

To identify the cellular defects that disrupt tissue-level pattern, we compared wildtype and *abl*^{null} retinas along each plane from 50% p.d. when photoreceptor falling begins to 100% p.d. when the final adult form is achieved. We used F-actin to highlight the specialized cytoskeletal structures that give retinal cells their distinct shapes and Ecadherin (Ecad) to mark the adherens junction connections that organize them into ommatidial units. Focusing first on the apical network, in *abl* mutant retinas, variable apical cell shapes, sizes and cell-cell contacts at 50% p.d. precluded regular hexagonal packing and suggested an anisotropic tension distribution (Figure 3.2D vs. 3.2A). For example, multiple rows of IOPCs, rather than a single secondary IOPC, separated adjacent ommatidia while some cone cells dropped sub-apically, disrupting the stereotyped quartet-pattern of apical contacts (Figure 3.2D). By 100% p.d., apical network pattern was improved, as indicated by the more regular ommatidial shapes and IOPC and cone cell apical profiles (Figure 3.2E and 3.2F vs, 3.2B and 3.2C). Measurements of secondary IOPC length as a proxy for the regularity of hexagonal pattern confirmed these observations (Figure 3.2G). The gradual improvement in regularity of ommatidial hexagonal packing suggested that IOPCs continuously optimize their contacts within the apical network, allowing them to recover a more uniform tension distribution after the disturbance of the falling photoreceptors moved away from the apical toward the basal side.

An opposite temporal progression was observed in the basal network (Figure 3.2A'-3.2F''). At 50%. p.d., F-actin localization outlined a recognizable radial pattern of IOPC feet in *abl*^{null} retinas (Figure 3.2D' vs. 3.2A') although heterogeneity in the central rings suggested tension was unevenly distributed across the plane (Figure 3.2D" vs. 3.2A"). Over time, although the IOPC footprints contracted as in wildtype (Figure 3.2H), the radial alignment of their F-actin bundles,

their connections to the central rings, and the underlying ECM all appeared increasingly disorganized and variable (Figure 3.2E'-3.2F" vs. 3.2B'-3.2C"; 3.2I). The increasing severity of basal network disruption over time paralleled the temporal progression of photoreceptor collapse and loss (Figure 3.1), suggesting that in response to the physical damage caused by the falling photoreceptors, the IOPC feet rearranged their cell-cell and cell-ECM contacts to fill the tissue space and minimize loss of integrity.

The disorganization and heterogeneity within the apical and basal networks predicted the two tissue planes would be out of register. We examined the longitudinal cytoskeletal network that normally provides this alignment. The disruptions of the photoreceptor rhabdomeres caused by *abl* loss were striking (Figure 3.2H and 3.2K-3.2N). At 50% p.d., wildtype rhabdomere clusters align perfectly along the longitudinal axis, span the full tissue depth with anchor points at the apical cone cell caps and basal feet, and their cytoskeletal domains are surrounded by an adherens junction belt that connects neighboring photoreceptors within each ommatidium (Figure 3.2K). In contrast, in *abl* mutant retinas, cytoskeletal domains and adhesions were fragmented and were no longer oriented orthogonal to the apical and basal surfaces. Junctional connections to the overlying cone cells appeared disrupted and basal collapse was evident (Figure 3.2M). By 100% p.d., the fragmentation and misalignment of *abl* mutant rhabdomeres (Figure 3.2N) was in sharp contrast to the intact well-aligned rhabdomere bundles of wildtype (Figure 3.2L). Below the fenestrated membrane, a tangled mass of Ecad-marked apical membrane reported the collapse of *abl* mutant photoreceptors through the retinal floor (Figure 3.2N). Retinal depth was significantly reduced relative to wildtype (Figure 3.2N vs. 3.2L; Figure 3.2J). Together these phenotypes suggest Abl function is required at the cellular level to produce the specialized shapes, structures and

connections of the photoreceptors and IOPCs. At the tissue level, the structural integrity of the entire 3D scaffold relies on these cellular features; if they are disrupted, the retinal epithelium cannot complete the morphogenetic program.

Abl is enriched in the cytoskeletal specializations of both photoreceptors and IOPCs

To define the subcellular contexts for Abl function, we examined Abl protein localization using an endogenously GFP-tagged allele (Nagarkar-Jaiswal et al., 2015). Abl expression was detected in all retinal cell types, with enrichment in the IOPC and photoreceptor cytoskeletal and junctional domains that define the 3D structural scaffold (Figure 3.3 and Figure S3). For example, Abl overlapped with F-actin along the full length of the developing (Figure 3.3A-3.3D and Figure S3A and S3B) and mature rhabdomeres (Figure S3D and S3E). Abl was also detected in the IOPCs (Figure 3.3B, 3.3B' and 3.3D, 3.3D') where the overlap with F-actin was particularly striking in the basal feet (Figure 3.3D, 3.3D' and Figure S3). The expression and localization of Abl in both the photoreceptors and IOPCs position it in time and space to regulate the specialization of the F-actin based scaffold.

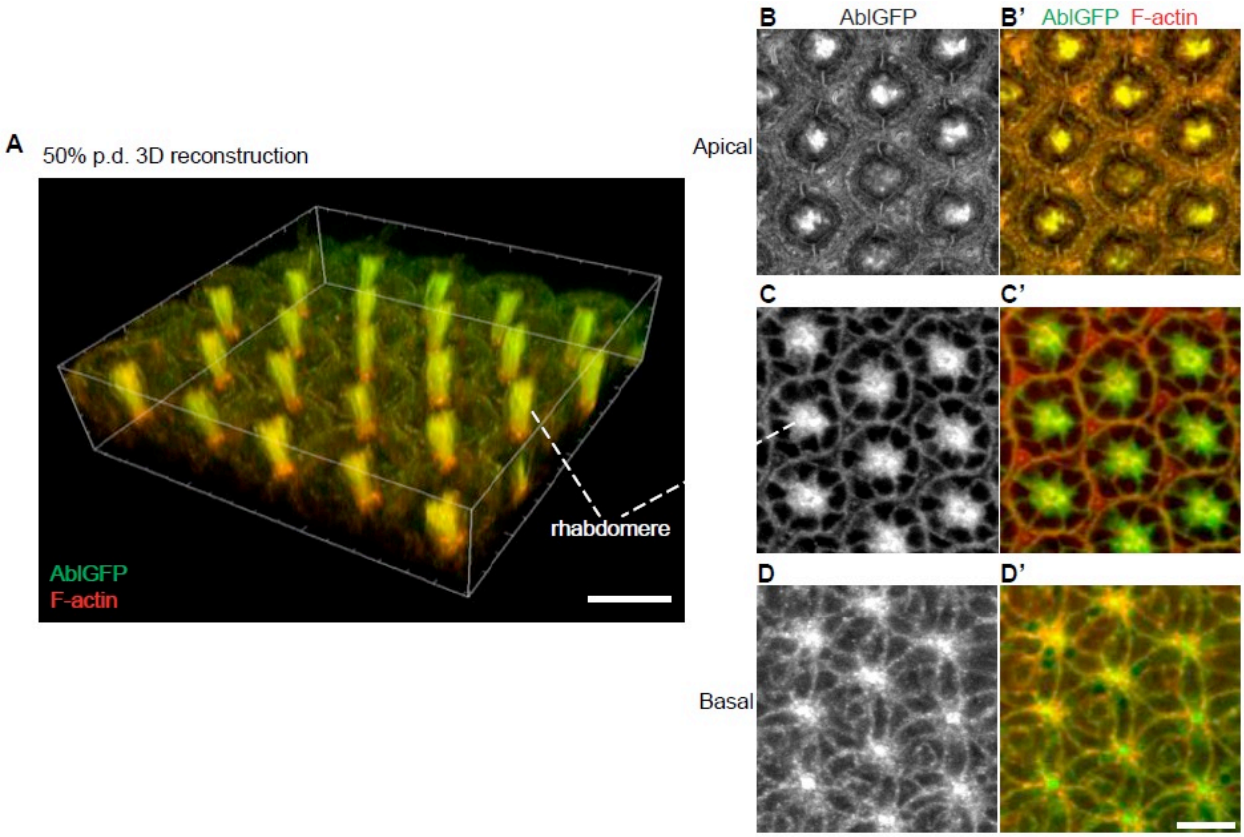

Figure 3.3. Abl is enriched in the photoreceptor and IOPC F-actin networks along all planes of the 3D scaffold.

(A) 3D reconstruction showing Abl^{mimicGFP} enrichment in the F-actin-rich longitudinal network of a WT 50% p.d. retina. Sections encompassing the most apical and basal planes shown in **B** and **D** were omitted for clarity.

(B,B') Apically, Abl^{mimicGFP} enrichment is strongest at the rhabdomere-cone cell anchor points in the center of each ommatidium, with lower levels detected in cone cells and IOPCs, but not in primary PCs.

(C,C') A subapical plane (dashed line) shows Abl^{mimicGFP} enrichment in rhabdomeres.

(D,D') Basally, Abl^{mimicGFP} overlaps F-actin at the rhabdomere-cone cell feet anchor points and outlines the basal network of IOPC feet. Scale bars = 10μm.

Abl has Ena-dependent functions in the photoreceptors and Ena-independent functions in the IOPCs

Assembly of branched F-actin networks supports the specialized structures in both photoreceptors and IOPCs (Galy et al., 2011; Signore et al., 2018). Given that a balance between linear and branched F-actin networks is required for a cell to build specific cytoskeletal structures (Burke et al., 2014; Kannan et al., 2017; Suarez and Kovar, 2016), and that Enabled (Ena) promotes linear F-actin assembly and is inhibited by Abl in a variety of cellular contexts (Comer et al., 1998; Forsthoefel et al., 2005; Fox and Peifer, 2007; Gates et al., 2007; Gertler et al., 1995; Grevengoed et al., 2001; Kannan et al., 2014; Kannan et al., 2017; Lin et al., 2009; Rogers et al., 2021), we asked if the mechanisms underlying Abl function in the photoreceptors and IOPCs involved negative regulation of Ena. Using rhabdomere organization (Figure 3.4A-3.4B') and photoreceptor nuclear position (Figure 3.4C-3.4D') at the subapical plane as readouts, we found that heterozygosity for *ena*, which on its own did not perturb retinal development, suppressed the *abl* mutant phenotype. This result could reflect Abl inhibition of Ena in the photoreceptors, in the IOPCs or in both cell types. We examined Ena expression to distinguish between these possibilities. Overlap with F-actin was detected in wildtype photoreceptor rhabdomeres (Figure 3.4E and 3.4E') whereas in abl^{null} ommatidia Ena subcellular localization was disrupted and appeared more basally dispersed (Figure 3.4G and 3.4G'). Within the IOPCs, low Ena levels were detected in their apical domains (Figure 3.4E and 3.4E') but not in their basal feet (Figure 3.4F and 3.4F'). These expression differences predicted that Abl deploys Ena-dependent regulation in the photoreceptor rhabdomeres but acts via Ena-independent mechanisms in the IOPC contractile feet.

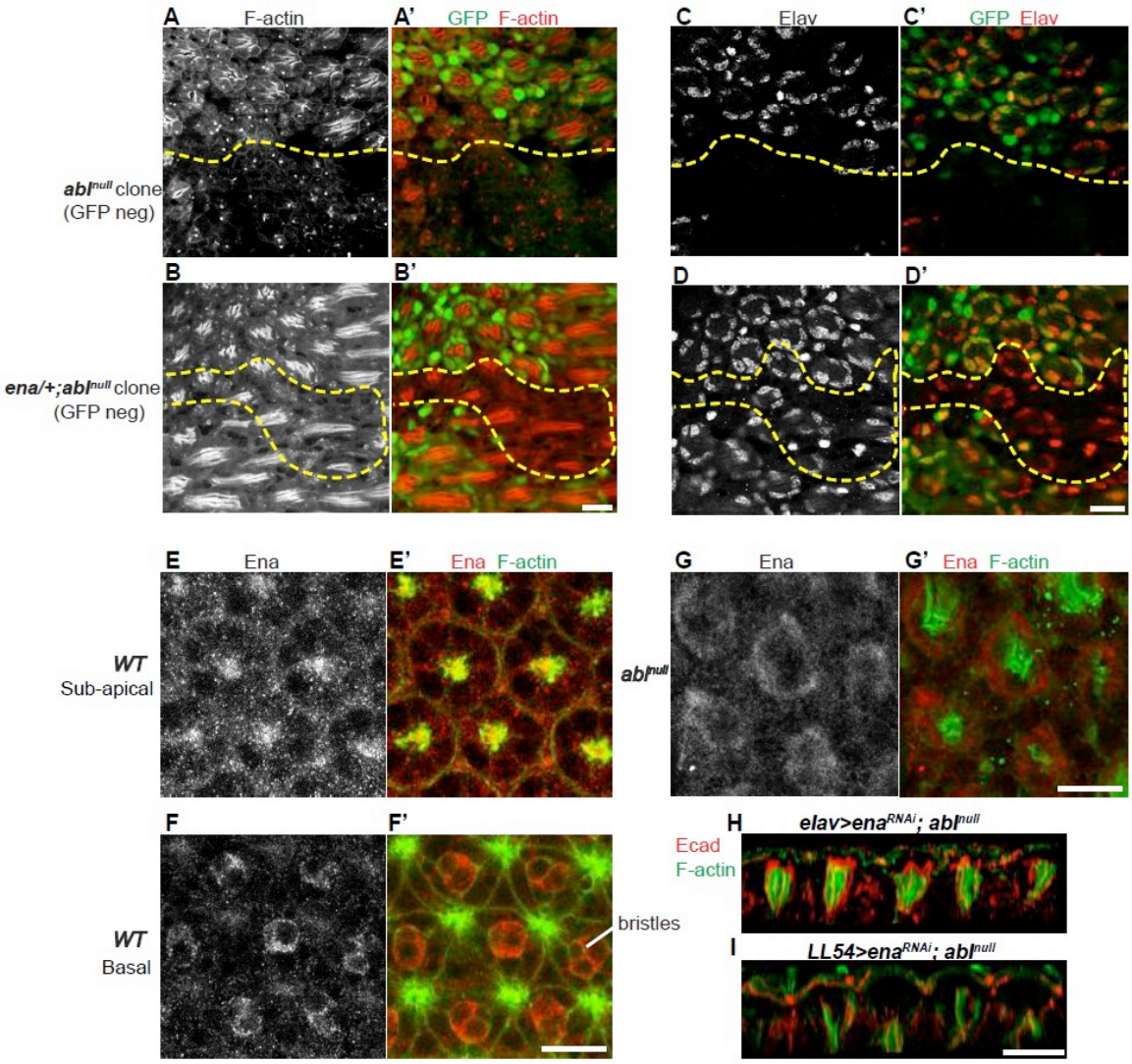

Figure 3.4. Abl uses Ena-dependent and independent mechanisms to regulate the cytoskeleton in photoreceptors vs. IOPCs

Figure 3.4 continued

(A-D') Subapical planes of 75% p.d. retinas with GFP-negative *abl*^{null} (*abl*^{2}) clones, with clonal boundaries marked by yellow dashed lines, show that reducing *ena* dose suppresses the terminal differentiation defects associated with photoreceptor "falling". **(E,E')** Subapical plane showing Ena localization to the rhabdomeres and photoreceptor cell bodies.
(F,F') Basal plane showing Ena enrichment in bristles, but not in the IOPC feet.
(G,G') Subapical plane showing loss of rhabdomeric Ena enrichment in *abl*^{null}.
(H,I.) Lateral plane reconstructions at 50% p.d. showing that photoreceptor-specific Ena knockdown, but not IOPC-specific Ena knockdown, improves rhabdomere structure, organization and spacing in *abl*^{null} retinas. Scale bars = 10µm.

To test this, we selectively expressed Ena dsRNA (Ena^{RNAi}) in either photoreceptors or IOPCs in an abl^{null} background. Photoreceptor-specific Ena^{RNAi} improved the orientation, regularity and organization of the rhabdomeres (Figure 3.4H) whereas IOPC-specific Ena^{RNAi} did not (Figure 3.4I). Restoring an organized rhabdomere core to each ommatidium (Figure 3.4H) also significantly improved surrounding IOPC planar pattern in a non-autonomous manner (Figure S4). These results suggest that the terminal differentiation programs of the photoreceptors and IOPCs rely on distinct Abl-mediated regulation to organize the specialized F-actin structures that underlie their unique cellular morphologies.

Local interactions between photoreceptors and IOPCs organize the 3D scaffold

Our results above suggested that the distinctive terminal differentiation programs of photoreceptors and IOPCs collectively elaborate a 3D scaffold that maintains tissue organization and integrity. The observation that proper rhabdomere organization could non-autonomously correct IOPC patterning defects (Figure 3.4H) raised the possibility that interactions between these two retinal cell types coordinate this process. We considered two possibilities. First, one cell type might be the primary organizer, with their shape, position and connections imposing dynamic physical constraints that influence how the terminal differentiation program of the other unfolds. Alternatively, there might be redundancy, with local interactions between photoreceptors and IOPCs mutually constraining and influencing the structures and contacts they each contribute to the scaffold.

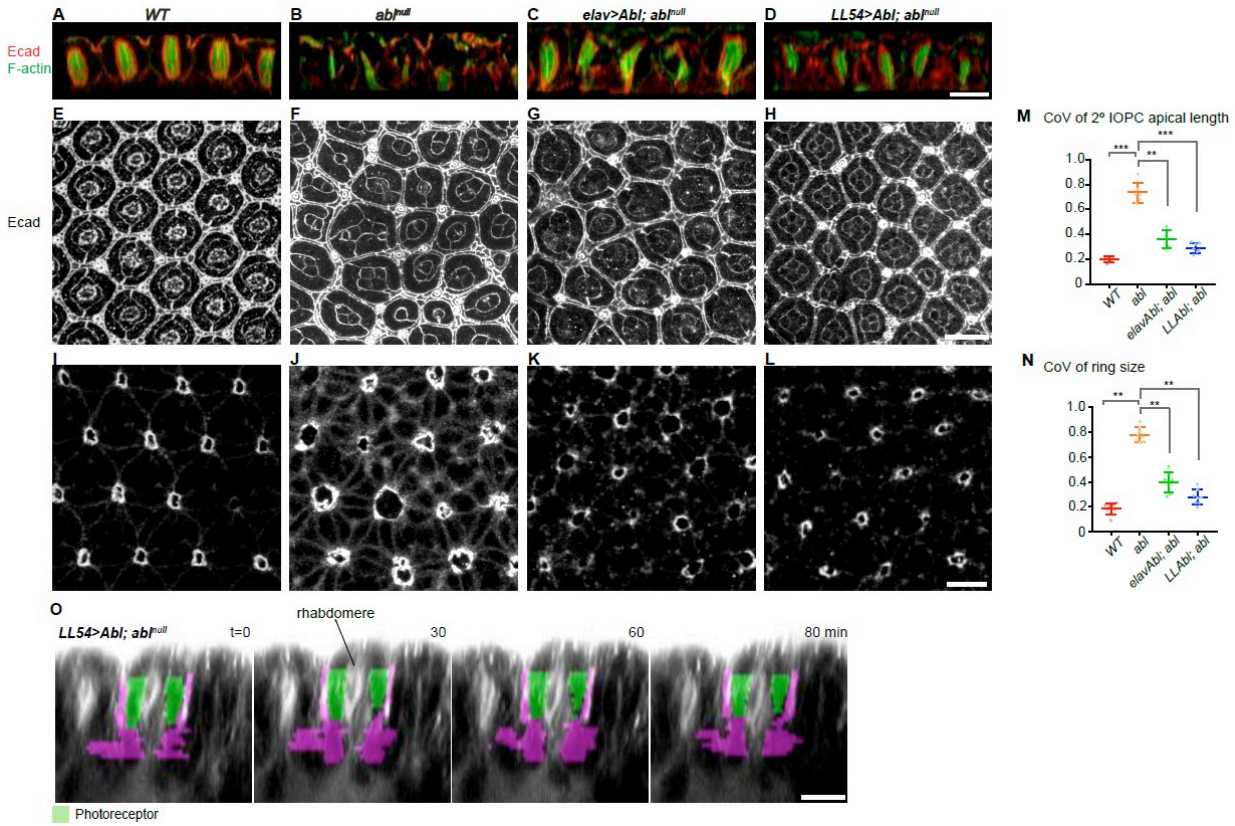

Figure 3.5. Cell-type specific rescue experiments reveal that local interactions between photoreceptors and IOPCs coordinate 3D scaffold organization

(A-D) Lateral, **(E-H)** apical and **(I-L)** basal views of 50% p.d. retinas highlight the sufficiency of restoring Abl function either to the photoreceptors or to the IOPCs in an otherwise *abl*^{null} retina to organize the apical, longitudinal and basal network cytoskeletal structures and junctional connections into an intact 3D scaffold. Scale bars = 10µm.
(M,N) Plots of the CoV of apical secondary IOPC length and of basal ring size. For each genotype, and for each data point, measurements were made in at least 30 ommatidia/retina, n= minimum of 4 retinas.
(O) False colored stills from a time-lapse movie of a 50% p.d retina shows that selective restoration of Abl to the IOPCs rescues IOPC and photoreceptor cell shapes, rhabdomere integrity and 3D tissue organization. Scale bar = 10µm.

As we had shown that Abl is required for both photoreceptor and IOPC terminal differentiation, we tested these possibilities by restoring Abl function selectively to one cell type and then assessing the impact on the other *abl* mutant cell type and on overall retinal organization. We used the partial rescue strategy instead of a selective knockdown approach because abl^{RNAi} does not recapitulate abl^{null} phenotypes in the retina (Xiong et al., 2009). Control experiments confirmed the specificity of the genetic strategy, with the expected restriction of *elav-Gal4* and *LL54-Gal4* driven expression to photoreceptor and IOPCs, respectively (Figure S5A-S5F), and no leaky expression or rescue with *UAS-*Abl^{GFP} alone (Figure S5G-S5L).

Focusing on 50% p.d., the timepoint marking completion of scaffold establishment, we first asked how restoring Abl to the photoreceptors influenced IOPC shapes and apical and basal network patterns in an otherwise abl^{null} retina (elav>Abl, abl^{null}). As expected, expressing Abl specifically in the photoreceptors restored their morphology, with marked improvement in organization and alignment of the rhabdomere bundles that pattern the longitudinal network, and prevented their basal collapse (Figure 3.5A – 3.5C). When we examined the IOPC response along the apical plane, their apical profiles revealed significant improvement in the regularity of apical network pattern (Figure 3.5E-3.5G and 3.5M). Non-autonomous rescue of basal network pattern was also evident, with reduced variation in ring sizes indicating a more uniform distribution of tension (Figure 3.5I-3.5K and 3.5N). These results suggested that correct photoreceptor cell morphology, and by extension an intact longitudinal network, promotes correct IOPC morphology and pattern within the apical and basal networks.

Second, in the reciprocal experiment we examined the response of abl^{null} photoreceptors to IOPC-specific restoration of Abl (LL54>Abl, abl^{null}). As expected, expressing Abl in the IOPCs rescued

their cellular morphology and improved apical (Figure 3.5H and 3.5M) and basal (Figure 3.5L and 3.5N) network patterns. When we examined the photoreceptor response in the longitudinal plane, the organization, alignment and apical/basal junctional connections of the rhabdomere bundles were all improved, indicating suppression of their basal collapse (Figure 3.5D, compare to 3.5B and 5A). Timelapse imaging further emphasized how the improved overall 3D organization prevented the photoreceptor clusters from collapsing basally; overall, the characteristic shapes and relative positions of both cell types resembled those of a wildtype retina (Figure 3.5O, Figure S6A and S6B). Together, these partial rescue experiments suggested that interactions between these two major retinal cell types, with each nonautonomously influencing the morphology of the other, redundantly coordinate the organization, orientation and integrity of the 3D scaffold.

Mechanical feedback within the 3D scaffold coordinates terminal differentiation programs in different cells to maintain robust tissue organization

The non-autonomous influence of correct cellular morphology and pattern along an individual plane on cellular morphology and pattern along the orthogonal plane suggested that interactions between the IOPCs and the photoreceptors are an integral organizing feature of the 3D scaffold. These interactions could be primarily passive, with cell shapes adjusting to fill available tissue space, or more active, with morphogenetic change in each cell type promoting the terminal differentiation program of the other. Given the extensive deposition of cellular material and elaboration of structure that occurs within the longitudinal and basal networks during elongation, we predicted that active interactions would be needed to coordinate the completion of these two terminal differentiation programs.

To test this, we used the same cell-type specific partial rescue strategy and assessed rhabdomere expansion, fenestrated membrane contraction, tissue elongation and epithelial integrity in 100% p.d. retinas. We first asked whether selective restoration of Abl function to the photoreceptors (elav>Abl, abl^{null}), which supported the elaboration and elongation of a mature longitudinal network of rhabdomere bundles (Figure 3.6I), was sufficient to rescue the structure and function of the basal network of contractile IOPC feet. In contrast to the disorganized pattern seen in abl^{null} (Figure 3.6B), in elav>Abl, abl^{null} partial rescue retinas, the radial alignment of actin bundles in the IOPC feet and their connections to the central rings appeared more uniform (Figure 3.6C vs. 3.6A), suggesting successful elaboration of the cytoskeletal structures and connections

needed for isotropic contraction of the fenestrated membrane. Similar results were obtained by genetically suppressing the abl^{null} phenotype with photoreceptor-specific Ena knockdown (elav>Ena^{RNAi}, abl^{null}) while little or no suppression was obtained with IOPC-specific Ena knockdown (LL54>Ena^{RNAi}, abl^{null}), consistent with Abl using an Ena-dependent mechanism in the photoreceptors and an Ena-independent mechanism in the IOPC basal stress fibers (Figure 3.6E and 3.6F). Measurement of ring size, a metric that summarizes IOPC shape, radial actin alignment and regularity of tissue-level basal network pattern (Figure 3.6G and 3.6H) and of retinal depth (Figure 3.6K) confirmed rescue of the entire tissue-level morphogenetic program and maintenance of retinal integrity. These results suggested that photoreceptor-IOPC interactions actively induce morphogenetic remodeling in the IOPCs, and that at the tissue level, an intact longitudinal network can nonautonomously rescue the basal network, thereby reconstructing an intact scaffold capable of maintaining retinal integrity during elongation.

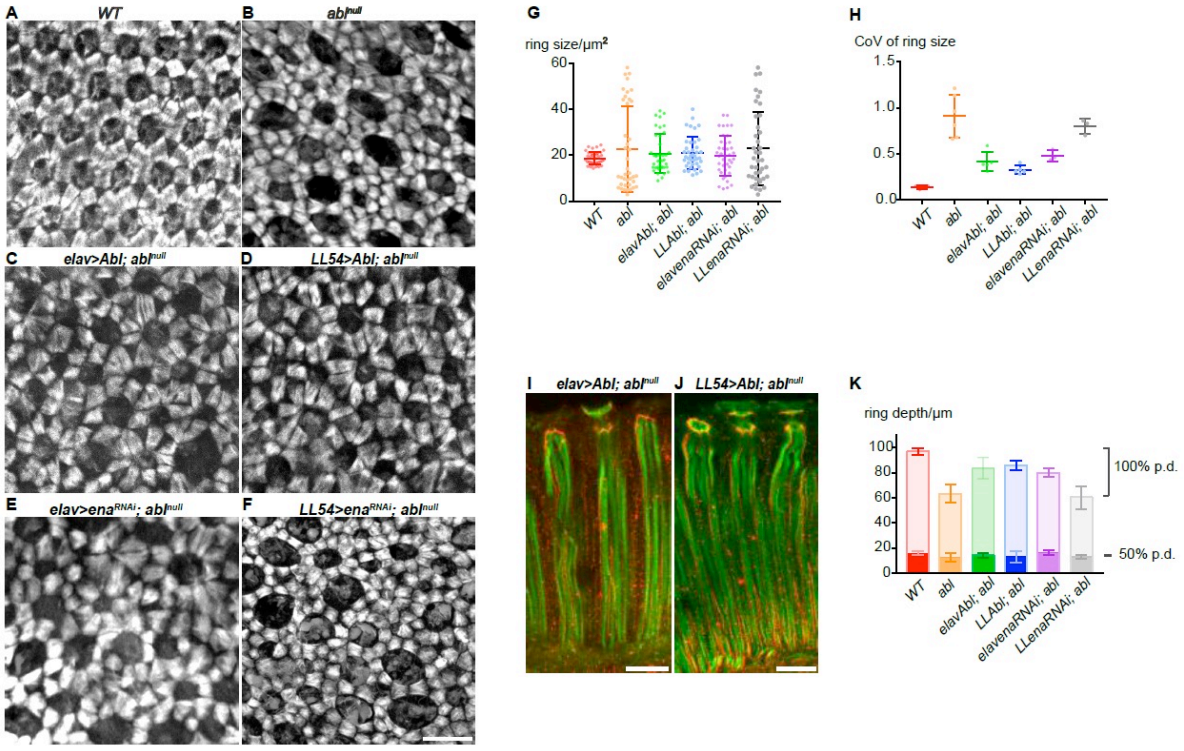

Figure 3.6. Feedback within the 3D scaffold coordinates photoreceptor and IOPC terminal differentiation programs to maintain tissue organization and integrity during retinal elongation

(A-F) Basal F-actin patterns in the IOPC feet of 100% p.d. retinas highlight the sufficiency of a correct photoreceptor terminal differentiation program to non- autonomously induce a basal network with proper radial orientation, symmetry and regularity of IOPC feet in an otherwise abl^{null} retina. Scale bars = 10 µm.
(G) Plot showing mean ± SEM of 100% p.d. ring size. For each genotype, data show measurements made in at least 30 ommatidia from a single retina.
(H) Plot of CoV of ring size. For each genotype, and for each data point, measurements were made in at least 30 ommatidia/retina, n= minimum of 4 retinas.
(I,J) Lateral views of 100% p.d. rhabdomeres highlight the sufficiency of IOPC-specific expression of Abl to non-autonomously induce active remodeling of photoreceptor rhabdomeres and tissue elongation in an otherwise abl^{null} retina. Scale bars = 10 µm.
K. Plot showing mean ± SEM of retinal depth at 50% (dark colored bars) and 100% (light colored bars) p.d.. For each time point and genotype, measurements were made in the central-most 10 ommatidia/retina, n= 3 retinas.

Finally, we examined the reciprocal partial rescue experiment to ask whether elaboration of correct apical/basal network pattern was sufficient to induce remodeling and elongation of the photoreceptor rhabdomeres (LL54>Abl, abl^{null}). As expected, restoring Abl function to the IOPCs resulted in correct elaboration of the basal network (Figure 3.6D, 3.6G and 3.6H). Remarkably, this non-autonomously rescued the terminal differentiation program of the abl^{null} photoreceptors such that they elaborated wellorganized and properly oriented rhabdomeres that spanned the full longitudinal axis of the epithelium (Figure 3.6J) and maintained junctional attachments to the apical cone cell caps (Figure 3.6J) and basal cone cell feet (Figure S6C-E). Not only were rhabdomere structures, junctional contacts and organization restored, but their elongation was also recovered (Figure 3.6K), indicating active remodeling of this highly specialized structure. We conclude that interactions between photoreceptors and IOPCs, mediated through the 3D scaffold structures and connections, actively coordinate their terminal differentiation programs, and that together this confers physical robustness to the tissue-level morphogenetic program.

Discussion

Organ form and function derives from the precise arrangement of different cell types with various sizes, shapes and specialized structures. In complex tissues, coordinating different cellular morphogenetic events in 3D to achieve the correct final form presents a major developmental challenge. Here we showed that the Drosophila pupal retina resolves this challenge by forming a physically coupled 3D cytoskeletal scaffold that integrates two modules of regulation: cell-type specific terminal differentiation programs mediated by Abl specialize the cytoskeletal domains that pattern the individual planes of the scaffold; and tissue-intrinsic feedback relays within the scaffold coordinate morphogenetic change between different retinal cell types. Both modules

together ensure the fidelity and integrity of retinal morphogenesis. We propose such 3D scaffolds might be a general feature of tissue morphogenesis, taking on context-specific forms but providing analogous cell and tissue-level coordination to the acquisition of 3D organ form.

Mechanical feedback matches developmental progress in different cells to coordinate 3D tissue morphogenesis

Late pupal retinal morphogenesis involves drastic shape changes at the cell and tissue level. In contrast to many epithelia where tissue elongation and growth involves changes of junctional contacts through cell intercalation, division and motility along the axes of elongation/growth (Aigouy et al., 2010; Baena-López et al., 2005; Blankenship et al., 2006; Clarke and Martin, 2021; Dye et al., 2017; Dye et al., 2021; Etournay et al., 2015; Glickman et al., 2003; Irvine and Wieschaus, 1994; Mao et al., 2013; Paré and Zallen, 2020; Shindo, 2018; Silva and Vincent, 2007; Warga and Kimmel, 1990; Wilson and Keller, 1991; Zallen and Wieschaus, 2004), the pupal retina relies on a persisting network of cell-cell contacts and cytoskeletal domains to generate and withstand the morphogenetic changes during elongation that produce adult organ form.

One significant finding in this study is that photoreceptors and IOPCs coordinate their morphogenetic programs in order to reenforce tissue organization during

morphogenesis (Figure 3.7A). First, consistent with previous studies (Baumann, 2004; Longley and Ready, 1995; Ready, 2002), our 3D reconstructions highlight the concomitant elaboration of photoreceptor rhabdomeres with the elaboration and contraction of IOPC feet. As both cytoskeletal

structures converge from different planes to anchor to the cone cell feet, the cellular coordination between photoreceptors and IOPCs stems from the physical coupling between their specialized cytoskeletal structures along orthogonal planes. Second, restoring Abl function in either the photoreceptors or IOPCs is sufficient to support the terminal differentiation program of the other *abl* mutant cell type. This result shows that the non-autonomous rescue is not merely a passive restoration of cell position and shape, but also induces active remodeling of the cytoskeletal domains and structural specializations through an Ablindependent mechanoresponse. Strikingly, when Abl was specifically restored to the IOPCs, the refined planar pattern not only provided physical support that kept the photoreceptors from falling out of the epithelium, but also induced elaboration and expansion of rhabdomeres in the absence of Abl. On the other hand, rescuing the organization of the central photoreceptor cell clusters by restoring Abl or reducing Ena dosage in photoreceptors was sufficient not only to correct the position and shape of the surrounding IOPCs, but also to direct the radial assembly of contractile IOPC feet. In both scenarios, the reiteration of local interactions between photoreceptors and IOPCs across the ommatidial field restored large-scale tissue order, implying an underlying tissue-level orthogonal coupling that coordinates diverse morphogenetic events in 3D space to achieve robust retinal morphogenesis.

Mechanical feedback through an orthogonally coupled 3D scaffold mediates cellular communication

One way to explain this tissue-level coordination is through feedback within the mechanically coupled 3D cytoskeletal adhesion network architecture. Previous studies described planar supracellular networks that span multiple cell apices as central to many morphogenetic processes including epithelial closure, elongation, invagination and folding (Kiehart et al., 2000; Martin et

al., 2009; Popkova et al., 2021; Yevick et al., 2019). Our study extends this concept to 3D. We suggest that the specialized cytoskeletal/junctional domains of the photoreceptors and IOPCs provide a mechanically coupled 3D scaffold that channels cell and tissue-scale feedback. Through these interactions, cytoskeletal structure and pattern in one cell type along one plane promotes cytoskeletal organization and pattern in the other cell type along the orthogonal plane. This positive feedback system allows dynamic communication between cells that ensures the concomitancy of their morphogenetic progress. Given the significant morphogenetic changes that accompany the final stages of retinal elongation, incorporating intrinsic feedback between different planes in the 3D scaffold may be critical for maintaining robust tissue organization.

Two general mechanisms could underlie a tissue's ability to communicate between orthogonal axes. One relies on the incompressibility of the cytoplasm, with competition for cell volume constraining cell shapes and coordinating 3D change (Bagnat et al., 2022; Gelbart et al., 2012; Harmansa et al., 2022; Stooke-Vaughan and Campàs, 2018). Alternatively, forces could be transmitted directly through the dedicated cytoskeletal scaffold, with the geometrical arrangement of the scaffold affecting interplane communication (Figure 3.7B). Our finding that restoring one plane of the 3D scaffold could induce remodeling and reorientation of the orthogonal plane suggests that the tissue simultaneously favors orthogonal organization for efficient morphogenesis and intrinsically corrects and minimizes off-axis pattern. If one axis is tilted, the component forces will be exchanged with the opposing plane, which triggers cytoskeletal remodeling or cellular level rearrangement in the opposing plane as in an adaptive planar supracellular network (Aigouy et al., 2010; Chanet et al., 2017; Coen and Rebocho, 2016; Huang et al., 2018; Khalilgharibi et al., 2019; Mao and Baum, 2015; Rebocho et al., 2017; Shyer et al., 2013; Wyatt et al., 2020; Yevick et al.,

2019). The component forces strictly coming from the orthogonal plane induce the constructive remodeling along the opposing plane, thereby mechanically coupling rhabdomere expansion and isotropic contraction of IOC feet.

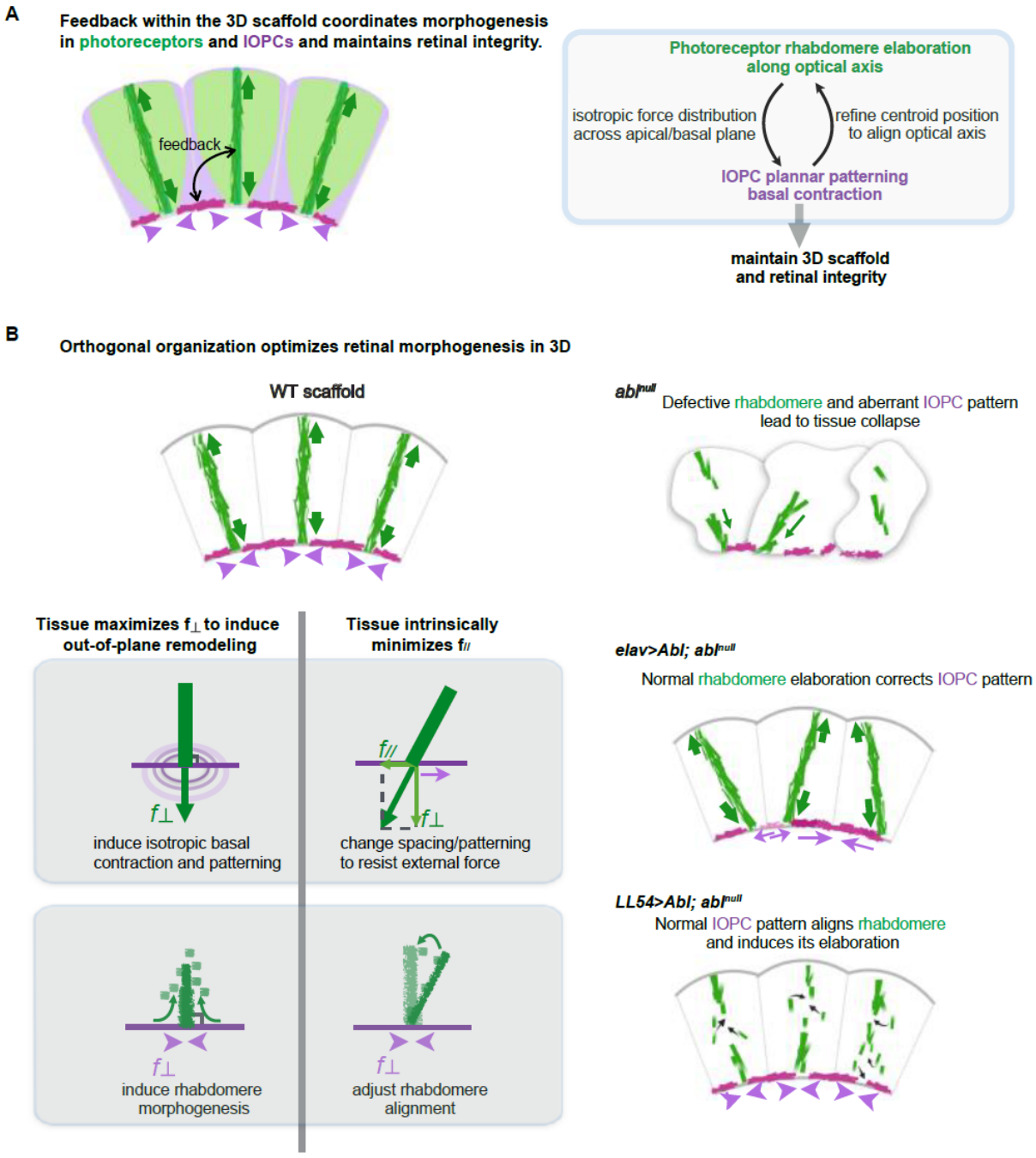

Figure 3.7. Model of feedback within the 3D scaffold

Figure 3.7 continued

(A) Schematic depicting the spatial organization of photoreceptors (light green) and IOPCs (light pink). Black arrow represents feedback between them as they elaborate their specialized cytoskeletal structures (dark green, elongating rhabdomeres; dark pink, contractile basal feet). Green arrows depict the force exerted by rhabdomere elongation along the optical axis. Pink arrowheads depict the isotropic contraction of the retinal floor in each ommatidium.
(B) Schematics showing how the orthogonal structure of the 3D scaffold actively communicates and coordinates concurrent morphogenetic changes in different cell types across different tissue axes. Pink arrows depict the response of the retinal floor to external forces exerted by the rhabdomeres.

In the wildtype retinal 3D scaffold, rhabdomeres maintain an almost orthogonal arrangement to the curved surfaces of the IOPC apical and basal domains throughout morphogenesis (Figure 3.7A and 3.7B). Given that elaboration of rhabdomere structure requires extensive membrane/cytoskeletal biogenesis and deposition (Raghu et al., 2009), in addition to being important for vision, maintaining the optimal orthogonal orientation has the advantage of minimizing biogenesis during elongation. In an *abl* mutant retina where coupling through the dedicated 3D scaffold collapses, the first mechanism (competition for volume) likely dominates but is insufficient to maintain the orthogonal organization that supports full tissue elongation. In the cell-type specific rescues, restoration of one plane exerts forces to the anchor point, triggering the opposing plane to minimize the component forces along the same orientation. Adjusting both axes relative to each other eventually restores the orthogonal organization of the scaffold, such that all in-plane stresses can be efficiently used for remodeling along the orthogonal axis and can support close to wildtype tissue elongation. We speculate that orthogonally coupled cytoskeletal configurations may represent a general strategy not only for communicating and resolving out of register geometries, but also for optimizing the use of in-plane stresses to direct out-of-plane remodeling and thus coordinate robust 3D morphogenetic change.

Remodeling of cytoskeleton, junctions and ECM all contribute to 3D scaffold structure and integrity

Our study highlights how the 3D scaffold couples orthogonally oriented morphogenetic events to maintain retinal organization. Although our characterization focused on interactions between photoreceptors and IOPCs, additional interactions, such as anchorage to the cone cells and to the basal ECM, contribute to the structural specialization of scaffold components and maintenance of scaffold integrity. The cone cell quartet provides a hub that physically connects both apical and

basal planar hexagonal patterns to the orthogonally oriented rhabdomeres. The cone cell feet also plug the central rings and complete the in-plane tiling of the basal floor by making septate junction connections with the IOPC feet (Banerjee et al., 2008). Thus, as the photoreceptor rhabdomeres mature and the IOPC feet elaborate contractile stress fibers, concomitant remodeling of cone cell shape and junctional connections with both cell types will further strengthen the scaffold. Consistent with this, in *abl* mutants, our observation of increased and irregular ring size implicates elaboration of correct cone cell feet shape and attachments as an integral component of scaffold elaboration. Identification of Neurexin IV, a septate junction component, and *DPax2,* a transcription factor that presumably regulates many aspects of cone cell terminal differentiation, as "photoreceptor falling" mutants (Banerjee et al., 2008; Charlton-Perkins et al., 2017), further supports our model.

The retinal floor is comprised not only of the IOPC basal contractile network but is also constrained by the underlying ECM; close coupling between these two components enables coordinated force transmission across the entire plane. IOPCs form integrin-mediated focal adhesions that anchor the contractile fibers to the underlying ECM. Concomitant with contraction of the IOPC basal network, the ECM shows signs of increasing collegen IV (Vkg-GFP) deposition and increased integrin intensity around the central rings (Figure S2E). This suggests that mechanical coupling between the elaborating ECM layer and the IOPC basal network matches their developmental progress during elaboration of the specialized retinal floor, thereby contributing to its integrity and coordination of cellular and tissue-scale events during elongation. Consistent with this, integrins have long been known to be essential to retinal integrity (Longley and Ready, 1995). The specific contributions of different ECM components remain to be explored.

In addition to the cone cell and ECM components, previous studies have identified several other cytoskeletal/junctional components or regulators whose loss compromises retinal integrity such that photoreceptors fall below the retinal floor. The list includes:

Arp2/3 and WAVE/SCAR components (Galy et al., 2011); Cofilin (Pham et al., 2008);

DRac1 (Chang and Ready, 2000); Pebbled/Hindsight (Pickup et al., 2002); and Afadin/Canoe (Matsuo et al., 1999). A few on the list have been implicated in Abl function in other developmental contexts (Grevengoed et al., 2003; Kannan and Giniger, 2017; Kannan et al., 2017; Yu and Zallen, 2020), and so could provide insight into mechanisms of Abl function in the retina. More broadly, based on our analysis and interpretation of the *abl* loss of phenotype together with the known function of these gene products in regulating actin cytoskeleton and cell-cell junctions, we suggest that this set of genes likely contributes via a variety of mechanisms to the connectivity and mechanosensitive remodeling of the scaffold structure.

In conclusion, we propose that the mechanical connectedness of the 3D scaffold underlies a feedback mechanism that ensures the concurrent remodeling of the different components and coordinates developmental progress across the tissue. Together these interactions maintain robust tissue organization. Future study of the cellular machineries and mechanics of the 3D scaffold coupled with characterization of tissue-level growth, geometry and developmental trajectories will provide further insight into how cell and tissue-scale processes collectively produce complex 3D organ form.

Acknowledgements

We thank Ed Munro, Ellie Heckscher and Rick Fehon for experimental advice and comments on the manuscript, Saman Tabatabaee for assistance with graphics, Christine Labno and Audrey Williams for live image processing advice, past and present Rebay lab members for helpful discussions and G. Bashaw, S.L. Zipursky, R.W.

Carthew and S. Horne-Badovinac for fly stocks. X.S. was supported by NIH R01 EY021459 to I.R., J.D. was supported by NIH T32 GM007183, and N.S.L. was supported by NIH T32 GM007281 and by NIH R01 EY021459 to I.R..

Methods

Drosophila genetics

All crosses were carried out at 25°C in standard laboratory conditions. w^{1118} (3605), abl^{1} (3554), abl^{2} (8565), $Abl^{mimicGFP}$ (59761), *LL54-Gal4* (5129), *Elav-Gal4* (8765), ena^{23} (8571), *G-TRACE* (2820) were from the Bloomington Stock Center. UAS-Abl-GFP (O'Donnell and Bashaw, 2013) was a gift from G. Bashaw. *UAS-ena*^{RNAi} (106484) was from the Vienna Drosophila Resource Center. *vkg-GFP* (CC00791) was from Flytrap (Buszczak et al., 2007). $Chp^{4.5}$*-Gal4* (Mishra et al., 2013) was a gift from S.L. Zipursky. GMR-wIR^{13D} (Lee and Carthew, 2003) was a gift from R. Carthew.

w^{1118} was used as wildtype in all experiments. To generate abl^{null} animals, abl^{2}*/TM6B* males were crossed to abl^{1}*/TM6B* virgins and abl^{1}/abl^{2} (non-Tubby) were selected. To generate abl^{2} clones, abl^{2}*,FRT80B/TM6B* males were crossed to *ey-FLP;* GFP^{nls}*,FRT80B* virgins. To reduce *ena* dose

in *abl*^{2} clones, *ena*^{23}*/CyO, abl*^{2} *FRT80B/TM6B* males were crossed to *ey-FLP; GFP*^{nls}*,FRT80B* virgins. For cell type specific rescue experiments, *abl*^{2} was recombined with the *UAS-Abl-GFP* transgenes inserted in 86Fb docking site (O'Donnell and Bashaw, 2013). *abl*^{2}*,UAS-Abl-GFP/TM6B* males were crossed to *LL54 (or Elav)-Gal4; abl*^{1}*/TM6B* virgins. To test Abl-Ena interactions in specific cell types, *UAS-ena*^{RNAi}*; abl*^{2}*/TM6B* males were crossed to *LL54 (or Elav)-Gal4; abl*^{1}*/TM6B* virgins. For lineage tracing, *w,GMR-w.IR*;*+/+;chaoptin-Gal4, abl*^{2}*/TM6B* females were crossed to *w; G-TRACE; abl*^{1}*/TM6B* males. GMR-w.IR reduced pigment deposition, improving imaging. *G-TRACE = P{w[+mC]=UASRedStinger}4, P{w[+mC]=UAS-FLP.D}JD1, P{w[+mC]=Ubip63E(FRT.STOP)Stinger}9F6/CyO*.

For developmental staging, white pre-pupae (0hr APF) were selected and aged at 25ºC.

50%, 75% and 100% p.d. animals for dissection were selected by time (48, 72 and 96hrs APF, respectively), confirmed by morphological landmarks prior to dissection (Bainbridge 1981) and by cellular features after dissection.

Immunostaining

50% p.d. pupal eye discs were dissected in PBS and fixed for 10 min in 4% paraformaldehyde in PBT (PBS with 0.1% Triton X-100). For 75% and 100% p.d.

dissections, pupal/adult heads were prefixed for 20 min, retina were dissected and fixed for 10 min, washed three times in PBT, blocked in PNT (PBT+3% normal goat serum) for 1 hr, incubated overnight at 4°C in primary antibodies diluted in PNT, washed three times in PBT, incubated in secondary antibodies diluted in PNT for 6 hours, washed three times in PBT and mounted in 90% glycerol in 0.1M Tris pH 8.0 with 0.5% n-propyl gallate.

In cell type specific rescue experiments in which *UAS-Abl-GFP* was ectopically expressed under the control of *LL54-Gal4* or *Elav-Gal4*, F-actin was stained with AlexaFluor-488 Phalloidin. Although GFP and AlexaFluor-488 are both excited by the same wavelength, the *UAS-Abl-GFP* signal faded during our standard staining protocol and was no longer detected with the confocal settings used to image F-actin. For Supplementary Figure 3, to preserve the UAS-Abl-GFP signal, discs were imaged after only a 2hr incubation with AlexaFluor-568 Phalloidin.

Antibodies were from the Developmental Studies Hybridoma Bank (DSHB): mouse antiElav (1:50); mouse anti-Ecad (1:500), mouse anti-βPS integrin (1:100), mouse anti-Ena (1:50). Cy3/Cy5/FITC-conjugated secondaries,1:2000 (Jackson ImmunoResearch). AlexaFluor-488 and AlexaFluor-568 Phalloidin,1:1000 (Fisher).

Fixed Microscopy and image analysis

Fluorescent images were obtained using a Zeiss LSM880 confocal microscope with Airyscan. Image processing and depth and ring size measurements were performed using Fiji. To obtain the image of different planes, multiple z-stack slices (0.4µm interval) that encompass the region of interest were averaged.

3D reconstructions and lateral views were made in Imaris (Bitplane). For views that include intact rhabdomeres, the 3D reconstructions were rotated and cropped to expose the lateral view of one line of aligned ommatidia. Graphing and statistical analyses were performed in Prism7 (GraphPad). For all graphs, data were plotted as mean ± SEM and statistical differences between conditions were determined with two-tailed unpaired t tests.

To measure retinal depth, we chose the central region of the retina for all genotypes to avoid regional variation. We generated multiple lateral views in Imaris and used the average length of 10 ommatidia in the central region as the retinal depth.

Live imaging

Staged 50% p.d. pupae were selected and the puparium was dissected away to expose the distal (apical) surface of the retina. After injecting ~0.5uL of CellMask Deep Red Plasma Membrane Stain (Thermo-Fisher) diluted 1:25 in Schneider's *Drosophila* medium into the head, the pupae were incubated in a humid chamber at 25ºC for 4 hours. Injected pupae were mounted in a cover-glass bottom dish such that the region of the head containing the developing retina was directly in contact with the cover-glass in a thin layer of Halocarbon 700 oil (Halocarbon Products). Pupae were oriented and immobilized using a log of petroleum jelly and the imaging vessel was kept humid with blotting paper soaked in Schneider's *Drosophila* medium (method adapted from (Hellerman et al., 2015)). Mounted retinas were immediately imaged on a Zeiss LSM

880 laser scanning confocal microscope using the 40x oil-immersion objective on AiryScan mode. Optical slices of 1um were acquired through the entire apical-basal depth of the tissue every 5 minutes. Although we cannot rule out the possibility that our protocol stalls development or negatively impacts the tissue, in a control experiment, injected animals continued to develop and 85% (n=20) eclosed with no obvious morphological defects. Because the dye injection resulted in a huge intensity difference between apical and basal planes, Fiji Top-Hat (Spot Radius = 0.75) was run on the entire 4D image stack to equalize signal and enhance cell outlines (Script by G. Landini, adapted for use on hyperstacks by C. Labno: https://blog.bham.ac.uk/intellimic/g-

landinisoftware/). The modified macro can be accessed on the University of Chicago Microscopy Core's GitHub (https://github.com/UChicago-Integrated-LightMicroscopy/ImageJ_macros).

Individual cells were annotated by hand in ImageJ using the xy-planes because of the ease in distinguishing cell outlines. After manually correcting drift, lateral projections of the resulting time-lapse images were made using ImageJ software.

Supplemental Figures

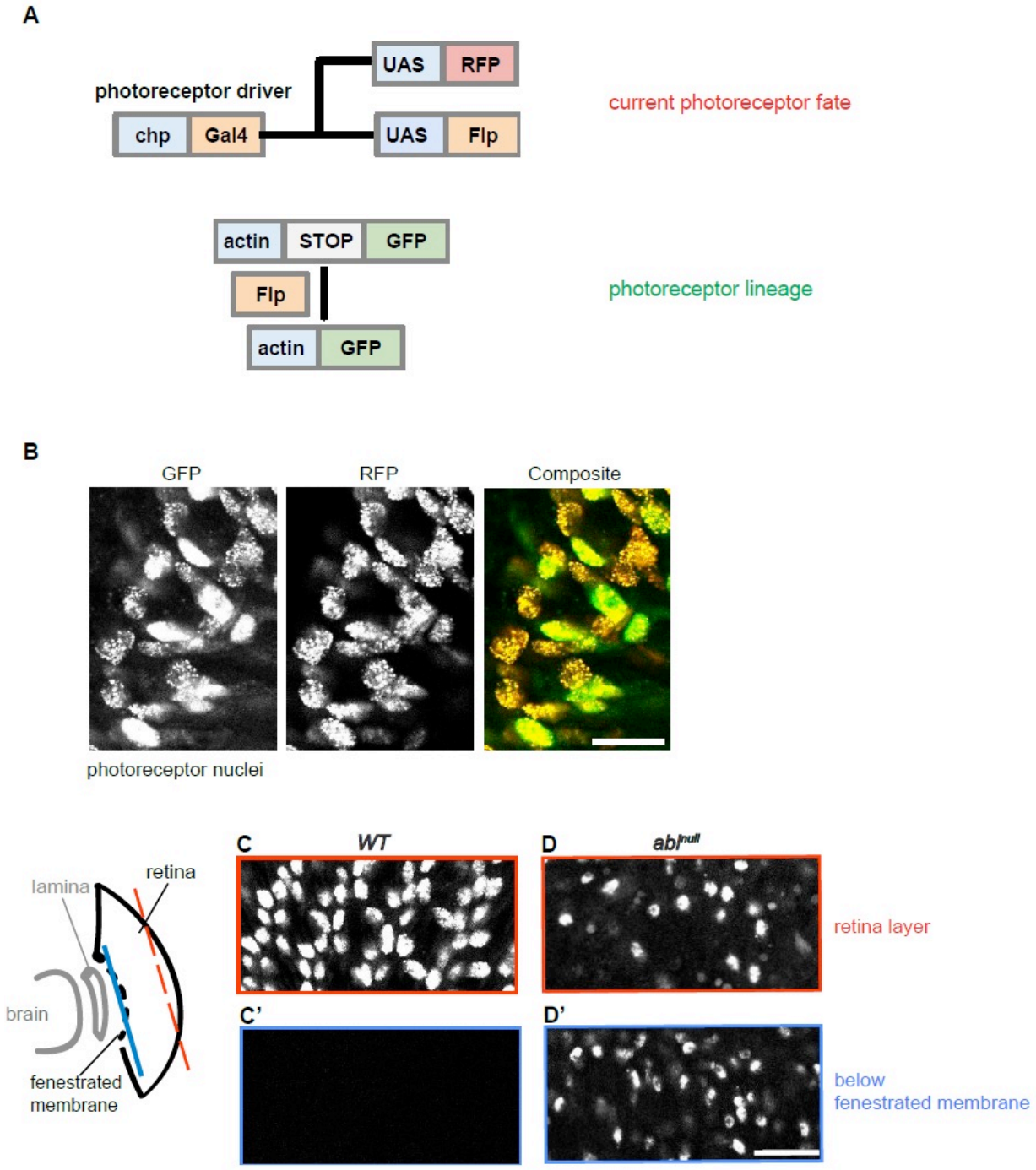

Figure S1. Lineage tracing to examine maintenance of photoreceptor cell fate and position in the retinal epithelium.

Figure S1 continued
(A,B) Genetic elements of the G-TRACE lineage trace system result in coexpression of GFP and RFP in photoreceptor nuclei: *chp-Gal4* drives photoreceptor-specific expression of RFP and FLP. FLP removes the stop in the actin-stop-GFP cassette, establishing a permanent lineage mark (GFP).
(C,D) Lineage-traced photoreceptor nuclei in a WT 100% p.d. retina reside apically and are never detected beneath the fenestrated membrane.
(E,F) Lineage-traced photoreceptor nuclei in an abl^{null} 100% p.d. retina suggest that even though cell position changes, with some nuclei found beneath the fenestrated membrane, cell fate is not changed. Schematic indicating apical (red) and basal (blue) planes imaged. Scale bars = 10µm.

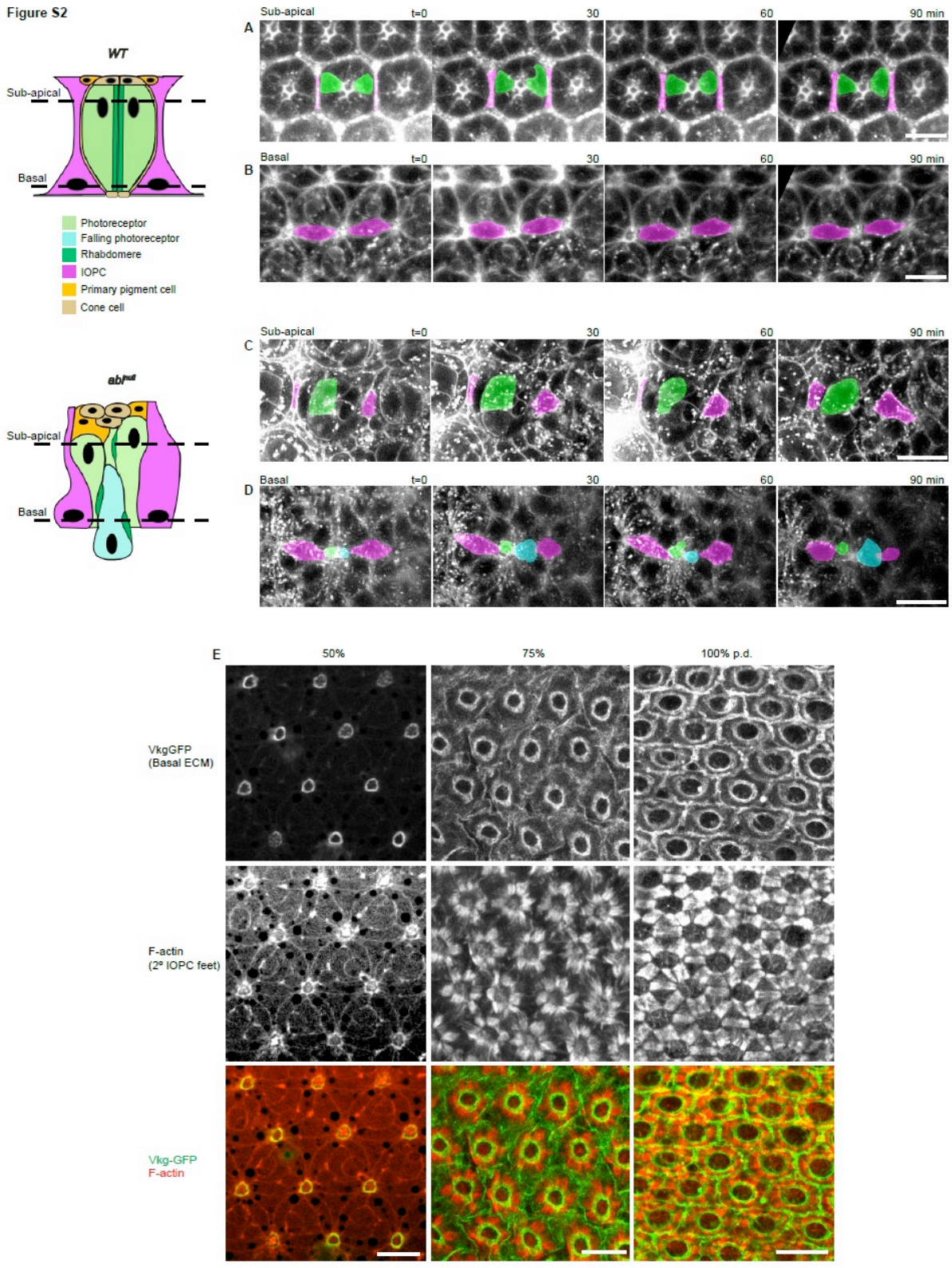

Figure S2. Time-lapse images and subsequent basal ECM elaboration to examine apical and basal network pattern.

Figure S2 continued
(A-D) Schematics and stills from time-lapse movies of 50% p.d retinas injected with CellMask (white). False color shows photoreceptors (green), fallen
photoreceptors (cyan) and secondary IOPCs (magenta) in a representative ommatidium. Abl loss results in irregular photoreceptor and secondary IOPC cell shapes and contacts that change over the time-course. Basally, photoreceptor "falling" is marked by the appearance of the cyan-marked cell between IOPC feet.
Scale bars = 10µm
(E) Progression of basal ECM deposition at 50, 75 and 100% p.d., visualized with Viking-GFP (collagen IV), occurs in sync with the contraction of the IOPC feet and expansion of the central rings in a WT retina. Scale bars = 10 um.

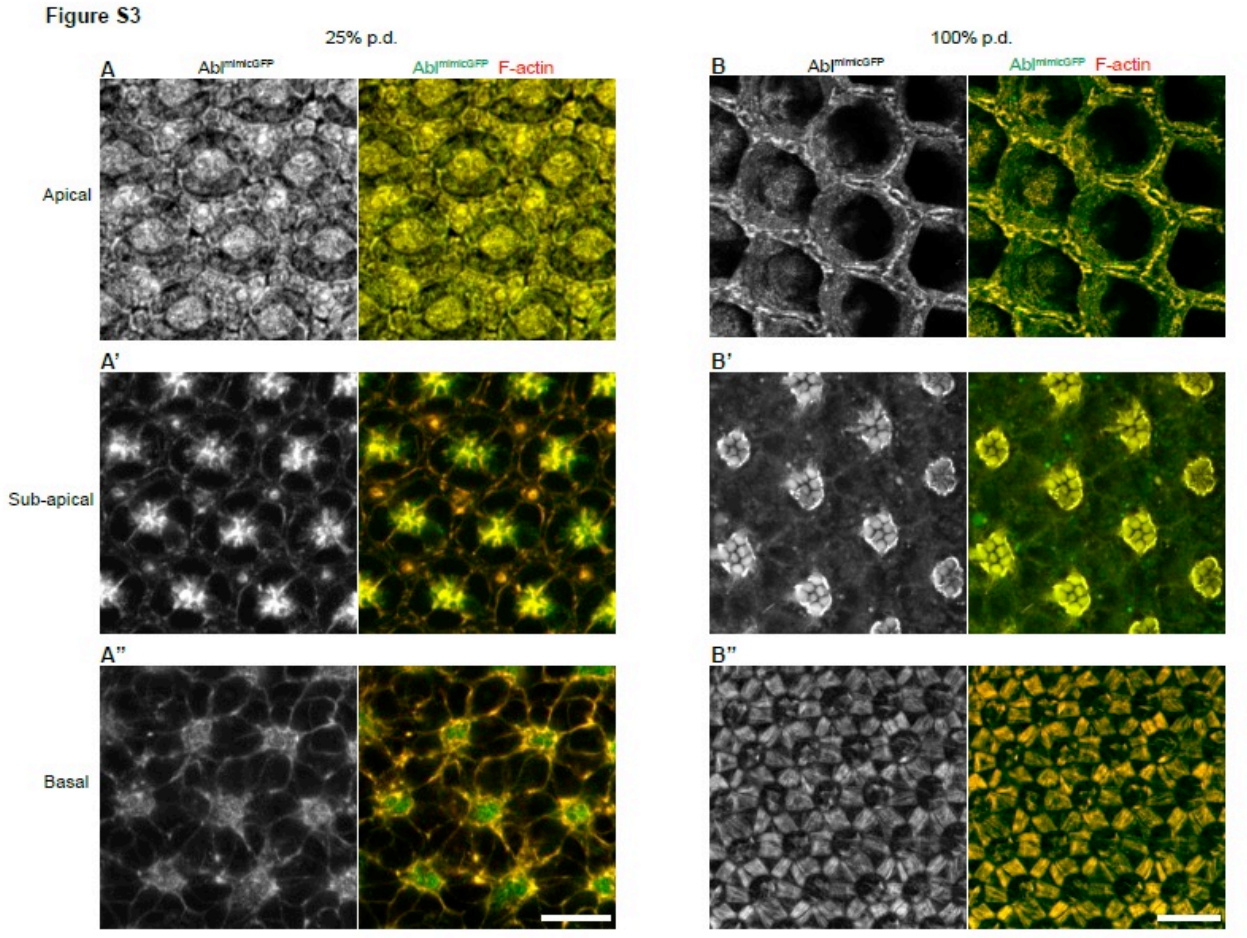

Figure S3. Abl is enriched in photoreceptor and IOPC F-actin structures at 25% and 100% p.d..

(A-F') Apical, subapical and basal planes showing the enrichment of Abl^{mimicGFP} and Factin in photoreceptors and IOPCs throughout retinal development, beginning prior to scaffold establishment and continuing in the adult scaffold. Scale bar = 10µm.

Figure S4

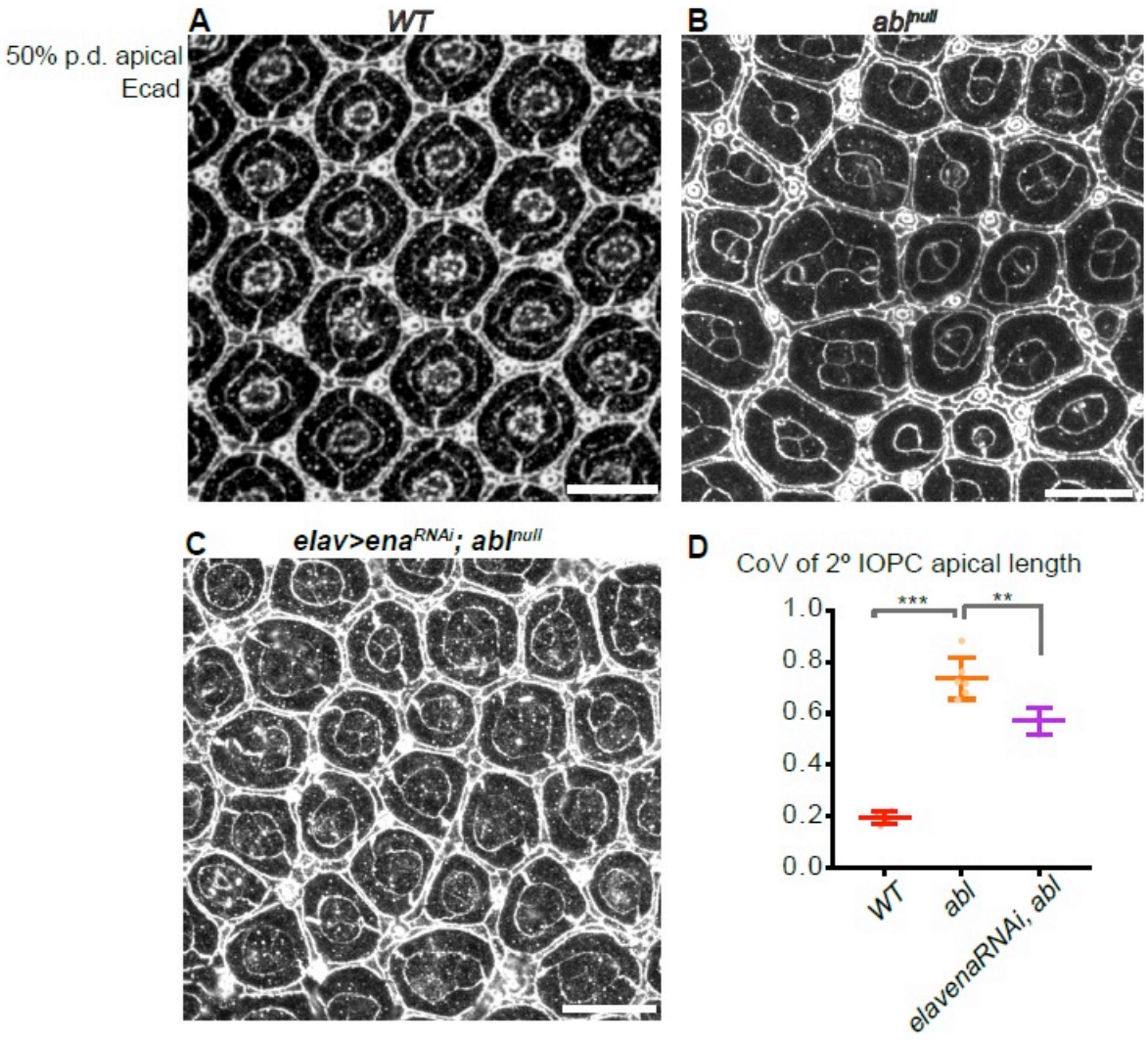

Figure S4. Abl-Ena genetic interactions show that photoreceptors nonautonomously affect IOPC apical network pattern.

(A-C) Apical network pattern of 50% p.d. retinas. Scale bars = 10µm.
(D) Plots of the CoV of apical secondary IOPC length. For each genotype, and for each data point, measurements were made in at least 30 ommatidia/retina, n= minimum of 4 retinas.

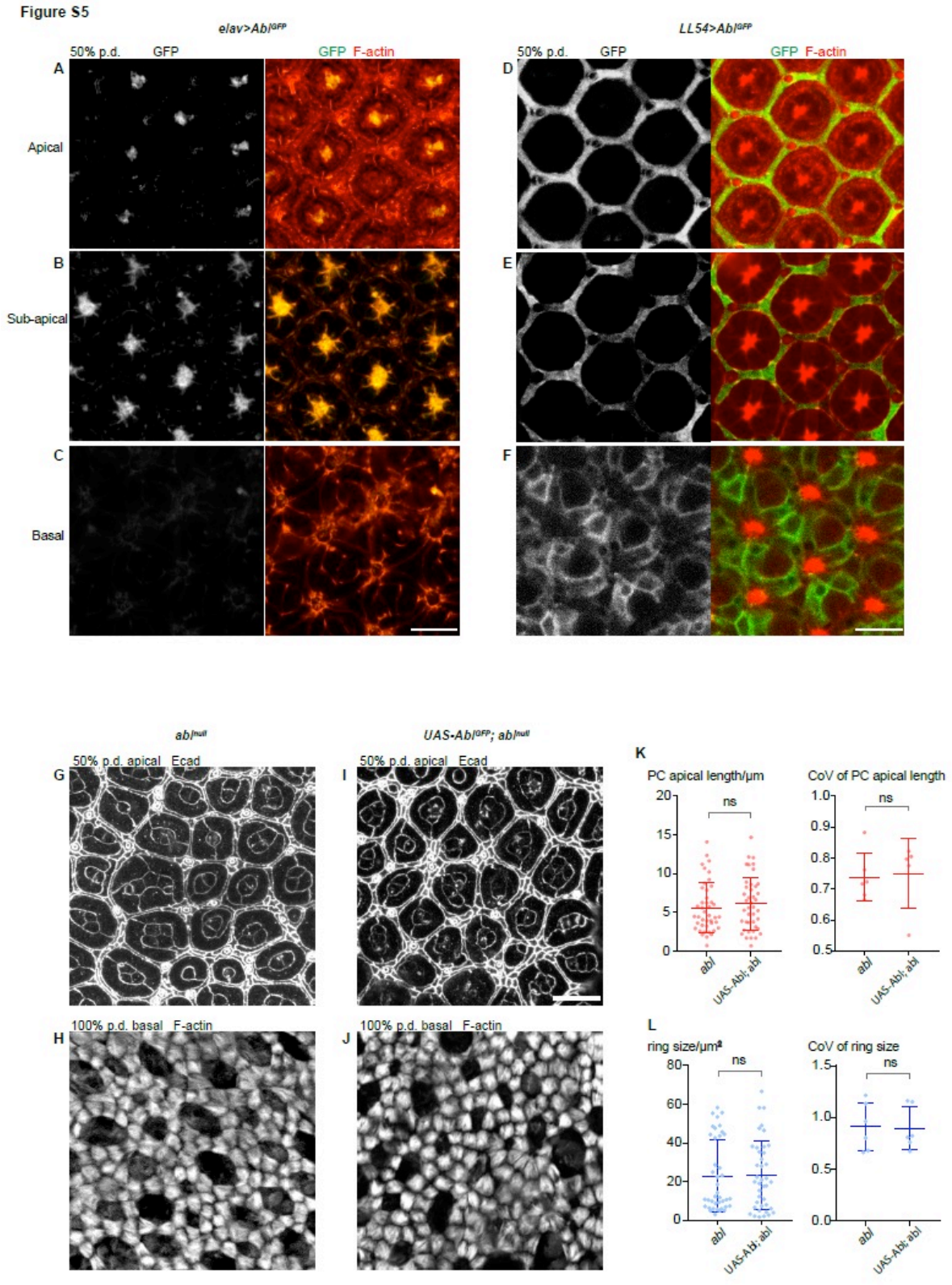

Figure S5. Specificity of Elav- and LL54-Gal4 expression and lack of rescue by UAS-Abl^{GFP} in the absence of a Gal4 driver.

Figure S5 continued
(A-C') Elav-Gal4 drives expression specifically in photoreceptors, with no leaky expression detected in IOPCs or cone cells.
(D-F') LL54-Gal4 drives expression specifically in IOPCs, with no leaky expression detected in photoreceptors or cone cells.
(G-J) Without a Gal4 driver, the UAS-Abl^{GFP} transgene does not rescue apical or basal network pattern. Scale bars = 10µm.
(K,L) Measurement and CoV of secondary IOPC apical length and basal ring size. Plots of secondary IOPC apical length show measurements made in at least 30 ommatidia in a single disc for each genotype. In the CoV plots, for each genotype, and for each data point, measurements were made in at least 30 ommatidia/retina, n= minimum of 4 retinas.

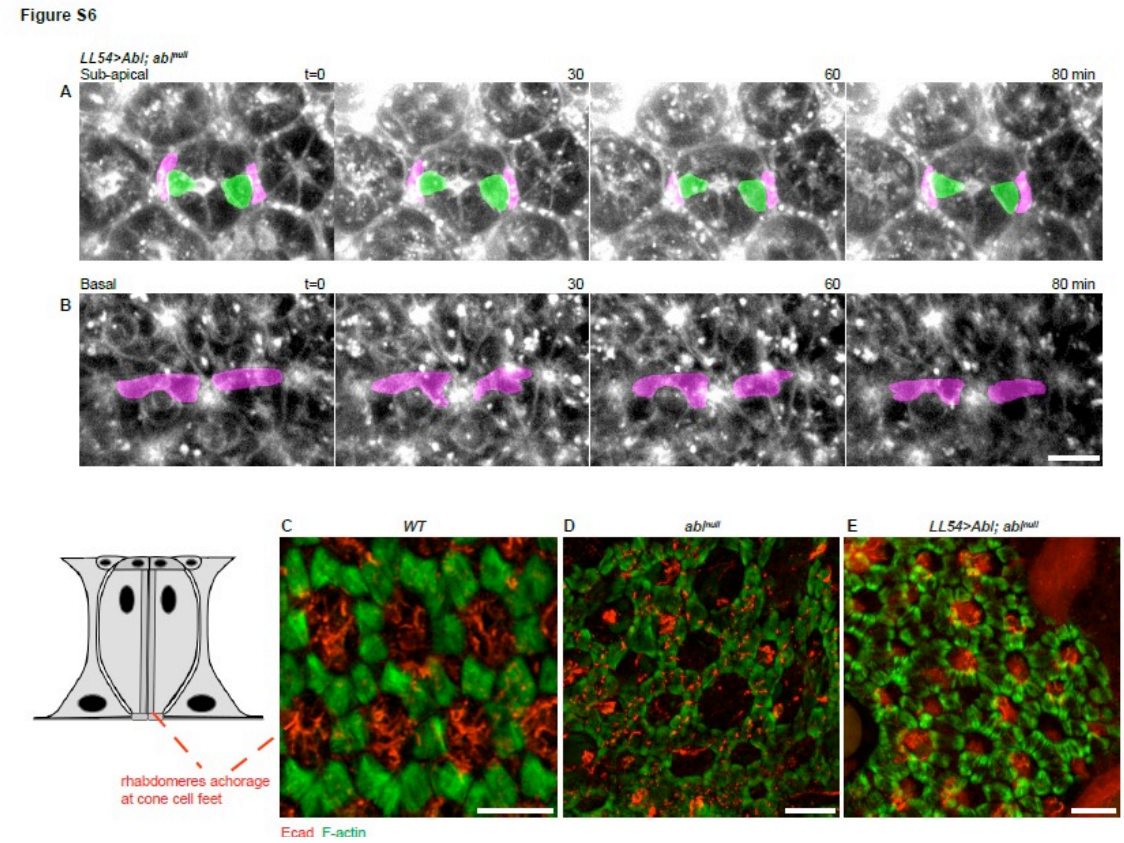

Figure S6. IOPC-specific expression of Abl in an otherwise *abl^{null}* retina restores correct cell-cell contacts within the scaffold.

(A,B) Schematics and stills from a time-lapse movie of a 50% p.d *LL54>Abl;abl^{null}* retina injected with CellMask (white) showing restoration of apical and basal pattern. False color shows photoreceptors (green) and secondary IOPCs (magenta) in a representative ommatidium. Compare to Figure S2A-D.
(C-E). Basal plane of 100% p.d. retinas, with schematic, shows how restoration of Abl to the IOPCs rescues the anchorage of the rhabdomeres to the cone cell feet, suggesting that non-autonomous induction of rhabdomere remodeling reconstructs the structural integrity of the 3D scaffold. Scale bars = 10 µm.

References

Aigouy, B., Farhadifar, R., Staple, D. B., Sagner, A., Röper, J.-C., Jülicher, F. and Eaton, S. (2010). Cell Flow Reorients the Axis of Planar Polarity in the Wing Epithelium of Drosophila. *Cell* 142, 773–786.

Baena-López, L. A., Baonza, A. and García-Bellido, A. (2005). The Orientation of Cell Divisions Determines the Shape of Drosophila Organs. *Curr Biol* 15, 1640–1644.

Bagnat, M., Daga, B. and Talia, S. D. (2022). Morphogenetic Roles of Hydrostatic Pressure in Animal Development. *Annu Rev Cell Dev Bi* 38, 375–394.

Banerjee, S., Bainton, R. J., Mayer, N., Beckstead, R. and Bhat, M. A. (2008). Septate junctions are required for ommatidial integrity and blood–eye barrier function in Drosophila. *Dev Biol* 317, 585–599.

Bao, S. and Cagan, R. (2005). Preferential Adhesion Mediated by Hibris and Roughest Regulates Morphogenesis and Patterning in the Drosophila Eye. *Dev Cell* 8, 925– 935.

Baumann, O. (2004). Spatial pattern of nonmuscle myosin-II distribution during the development of the Drosophila compound eye and implications for retinal morphogenesis. *Dev Biol* 269, 519–533.

Bennett, R. L. and Hoffmann, F. M. (1992). Increased levels of the Drosophila Abelson tyrosine kinase in nerves and muscles: subcellular localization and mutant phenotypes imply a role in cell-cell interactions. *Development* 116, 953–966.

Blankenship, J. T., Backovic, S. T., Sanny, J. S. P., Weitz, O. and Zallen, J. A. (2006).

Multicellular Rosette Formation Links Planar Cell Polarity to Tissue Morphogenesis. *Dev Cell* 11, 459–470.

Burke, T. A., Christensen, J. R., Barone, E., Suarez, C., Sirotkin, V. and Kovar, D. R. (2014). Homeostatic Actin Cytoskeleton Networks Are Regulated by Assembly Factor Competition for Monomers. *Curr Biol* 24, 579–585.

Buszczak, M., Paterno, S., Lighthouse, D., Bachman, J., Planck, J., Owen, S., Skora, A. D., Nystul, T. G., Ohlstein, B., Allen, A., et al. (2007). The Carnegie Protein Trap Library: A Versatile Tool for Drosophila Developmental Studies. *Genetics* 175, 1505– 1531.

Cagan, R. L. and Ready, D. F. (1989). The emergence of order in the Drosophila pupal retina. *Dev Biol* 136, 346–362.

Chanet, S., Miller, C. J., Vaishnav, E. D., Ermentrout, B., Davidson, L. A. and Martin, A. C. (2017). Actomyosin meshwork mechanosensing enables tissue shape to orient cell force. *Nat Commun* 8, 15014.

Chang, H.-Y. and Ready, D. F. (2000). Rescue of Photoreceptor Degeneration in Rhodopsin-Null Drosophila Mutants by Activated Rac1. *Science* 290, 1978–1980.

Charlton-Perkins, M. and Cook, T. A. (2010). Chapter Five Building a Fly Eye Terminal Differentiation Events of the Retina, Corneal Lens, and Pigmented Epithelia. *Curr Top Dev Biol* 93, 129–173.

Charlton-Perkins, M. A., Sendler, E. D., Buschbeck, E. K. and Cook, T. A. (2017). Multifunctional glial support by Semper cells in the Drosophila retina. *Plos Genet* 13, e1006782.

Clarke, D. N. and Martin, A. C. (2021). Actin-based force generation and cell adhesion in tissue morphogenesis. *Curr Biol* 31, R667–R680.

Coen, E. and Rebocho, A. B. (2016). Resolving Conflicts: Modeling Genetic Control of Plant Morphogenesis. *Dev Cell* 38, 579–583.

Collinet, C. and Lecuit, T. (2021). Programmed and self-organized flow of information during morphogenesis. *Nat Rev Mol Cell Bio* 22, 245–265.

Comer, A. R., Ahern-Djamali, S. M., Juang, J.-L., Jackson, P. D. and Hoffmann, F. M. (1998). Phosphorylation of Enabled by the Drosophila Abelson Tyrosine Kinase Regulates the In Vivo Function and Protein-Protein Interactions of Enabled. *Mol Cell Biol* 18, 152–160.

Daley, W. P. and Yamada, K. M. (2013). ECM-modulated cellular dynamics as a driving force for tissue morphogenesis. *Curr Opin Genet Dev* 23, 408–414.

Dye, N. A., Popović, M., Spannl, S., Etournay, R., Kainmüller, D., Ghosh, S., Myers, E. W., Jülicher, F. and Eaton, S. (2017). Cell dynamics underlying oriented growth of the Drosophila wing imaginal disc. *Development* 144, 4406–4421.

Dye, N. A., Popović, M., Iyer, K. V., Fuhrmann, J. F., Piscitello-Gómez, R., Eaton, S. and Jülicher, F. (2021). Self-organized patterning of cell morphology via mechanosensitive feedback. *Elife* 10, e57964.

Etournay, R., Popović, M., Merkel, M., Nandi, A., Blasse, C., Aigouy, B., Brandl, H., Myers, G., Salbreux, G., Jülicher, F., et al. (2015). Interplay of cell dynamics and epithelial tension during morphogenesis of the Drosophila pupal wing. *Elife* 4, e07090.

Forsthoefel, D. J., Liebl, E. C., Kolodziej, P. A. and Seeger, M. A. (2005). The Abelson tyrosine kinase, the Trio GEF and Enabled interact with the Netrin receptor Frazzled in Drosophila. *Development* 132, 1983–1994.

Fox, D. T. and Peifer, M. (2007). Abelson kinase (Abl) and RhoGEF2 regulate actin organization during cell constriction in Drosophila. *Development* 134, 567–578.

Galy, A., Schenck, A., Sahin, H. B., Qurashi, A., Sahel, J.-A., Diebold, C. and

Giangrande, A. (2011). CYFIP dependent Actin Remodeling controls specific aspects of Drosophila eye morphogenesis. *Dev Biol* 359, 37–46.

Gates, J., Mahaffey, J. P., Rogers, S. L., Emerson, M., Rogers, E. M., Sottile, S. L., Vactor, D. V., Gertler, F. B. and Peifer, M. (2007). Enabled plays key roles in embryonic epithelial morphogenesis in Drosophila. *Development* 134, 2027–2039.

Gelbart, M. A., He, B., Martin, A. C., Thiberge, S. Y., Wieschaus, E. F. and Kaschube, M. (2012). Volume conservation principle involved in cell lengthening and nucleus movement during tissue morphogenesis. *Proc National Acad Sci* 109, 19298–19303.

Gertler, F. B., Comer, A. R., Juang, J. L., Ahern, S. M., Clark, M. J., Liebl, E. C. and Hoffmann, F. M. (1995). enabled, a dosage-sensitive suppressor of mutations in the Drosophila Abl tyrosine kinase, encodes an Abl substrate with SH3 domain-binding properties. *Genes Dev* 9, 521–533.

Glickman, N. S., Kimmel, C. B., Jones, M. A. and Adams, R. J. (2003). Shaping the zebrafish notochord. *Development* 130, 873–887.

Gracia, M., Theis, S., Proag, A., Gay, G., Benassayag, C. and Suzanne, M. (2019). Mechanical impact of epithelial−mesenchymal transition on epithelial morphogenesis in Drosophila. *Nat Commun* 10, 2951.

Grevengoed, E. E., Loureiro, J. J., Jesse, T. L. and Peifer, M. (2001). Abelson kinase regulates epithelial morphogenesis in Drosophila. *J Cell Biol* 155, 1185–1198.

Grevengoed, E. E., Fox, D. T., Gates, J. and Peifer, M. (2003). Balancing different types of actin polymerization at distinct sites. *J Cell Biology* 163, 1267–1279.

Harmansa, S., Erlich, A., Eloy, C., Zurlo, G. and Lecuit, T. (2022). Growth anisotropy of the extracellular matrix drives mechanics in a developing organ. *Biorxiv* 2022.07.19.500615.

Hayashi, T. and Carthew, R. W. (2004). Surface mechanics mediate pattern formation in the developing retina. *Nature* 431, 647–652.

Hellerman, M. B., Choe, R. H. and Johnson, R. I. (2015). Live-imaging of the Drosophila Pupal Eye. *J Vis Exp* 52120.

Henkemeyer, M. J., Gertler, F. B., Goodman, W. and Hoffmann, F. M. (1987). The Drosophila abelson proto-oncogene homolog: Identification of mutant alleles that have pleiotropic effects late in development. *Cell* 51, 821–828.

Henkemeyer, M., West, S. R., Gertler, F. B. and Hoffmann, F. M. (1990). A novel tyrosine kinase-independent function of Drosophila abl correlates with proper subcellular localization. *Cell* 63, 949–960.

Hilgenfeldt, S., Erisken, S. and Carthew, R. W. (2008). Physical modeling of cell geometric order in an epithelial tissue. *Proc National Acad Sci* 105, 907–911.

Huang, C., Wang, Z., Quinn, D., Suresh, S. and Hsia, K. J. (2018). Differential growth and shape formation in plant organs. *Proc National Acad Sci* 115, 12359–12364.

Irvine, K. D. and Wieschaus, E. (1994). Cell intercalation during Drosophila germband extension and its regulation by pair-rule segmentation genes. *Development* 120, 827–841.

Jodoin, J. N. and Martin, A. C. (2016). Abl suppresses cell extrusion and intercalation during epithelium folding. *Mol Biol Cell* 27, 2822–2832.

Johnson, R. I. (2021). Hexagonal patterning of the Drosophila eye. *Dev Biol* 478, 173– 182.

Kafer, J., Hayashi, T., Maree, A. F., Carthew, R. W. and Graner, F. (2007). Cell adhesion and cortex contractility determine cell patterning in the Drosophila retina. *Proc Natl Acad Sci U S A* 104, 18549–18554.

Kannan, R. and Giniger, E. (2017). New perspectives on the roles of Abl tyrosine kinase in axon patterning. *Fly* 11, 260–270.

Kannan, R., Kuzina, I., Wincovitch, S., Nowotarski, S. H. and Giniger, E. (2014). The Abl/Enabled signaling pathway regulates Golgi architecture in Drosophila photoreceptor neurons. *Mol Biol Cell* 25, 2993–3005.

Kannan, R., Song, J.-K., Karpova, T., Clarke, A., Shivalkar, M., Wang, B., Kotlyanskaya, L., Kuzina, I., Gu, Q. and Giniger, E. (2017). The Abl pathway bifurcates to balance Enabled and Rac signaling in axon patterning in Drosophila. *Development* 144, 487– 498.

Khalilgharibi, N., Fouchard, J., Asadipour, N., Barrientos, R., Duda, M., Bonfanti, A., Yonis, A., Harris, A., Mosaffa, P., Fujita, Y., et al. (2019). Stress relaxation in epithelial monolayers is controlled by the actomyosin cortex. *Nat Phys* 15, 839–847.

Kiehart, D. P., Galbraith, C. G., Edwards, K. A., Rickoll, W. L. and Montague, R. A. (2000). Multiple Forces Contribute to Cell Sheet Morphogenesis for Dorsal Closure in Drosophila. *J Cell Biology* 149, 471–490.

Lee, Y. S. and Carthew, R. W. (2003). Making a better RNAi vector for Drosophila: use of intron spacers. *Methods* 30, 322–329.

Liebl, E. C., Forsthoefel, D. J., Franco, L. S., Sample, S. H., Hess, J. E., Cowger, J. A., Chandler, M. P., Shupert, A. M. and Seeger, M. A. (2000). Dosage-sensitive, reciprocal genetic interactions between the Abl tyrosine kinase and the putative GEF trio reveal trio's role in axon pathfinding. *Neuron* 26, 107–118.

Lin, T. Y., Huang, C. H., Kao, H. H., Liou, G. G., Yeh, S. R., Cheng, C. M., Chen, M. H., Pan, R. L. and Juang, J. L. (2009). Abi plays an opposing role to Abl in Drosophila axonogenesis and synaptogenesis. *Development* 136, 3099–3107.

Longley, R. L. and Ready, D. F. (1995). Integrins and the Development of Three-Dimensional Structure in the Drosophila Compound Eye. *Dev Biol* 171, 415–433.

Mao, Y. and Baum, B. (2015). Tug of war—The influence of opposing physical forces on epithelial cell morphology. *Dev Biol* 401, 92–102.

Mao, Y., Tournier, A. L., Hoppe, A., Kester, L., Thompson, B. J. and Tapon, N. (2013). Differential proliferation rates generate patterns of mechanical tension that orient tissue growth. *Embo J* 32, 2790–2803.

Martin, A. C. and Goldstein, B. (2014). Apical constriction: themes and variations on a cellular mechanism driving morphogenesis. *Development* 141, 1987–1998.

Martin, A. C., Kaschube, M. and Wieschaus, E. F. (2009). Pulsed contractions of an actin–myosin network drive apical constriction. *Nature* 457, 495–499.

Matsuo, T., Takahashi, K., Suzuki, E. and Yamamoto, D. (1999). The Canoe protein is necessary in adherens junctions for development of ommatidial architecture in the Drosophila compound eye. *Cell Tissue Res* 298, 397–404.

Mishra, A. K., Tsachaki, M., Rister, J., Ng, J., Celik, A. and Sprecher, S. G. (2013). Binary Cell Fate Decisions and Fate Transformation in the Drosophila Larval Eye. *Plos Genet* 9, e1004027.

Nagarkar-Jaiswal, S., Lee, P.-T., Campbell, M. E., Chen, K., Anguiano-Zarate, S., Gutierrez, M. C., Busby, T., Lin, W.-W., He, Y., Schulze, K. L., et al. (2015). A library of MiMICs allows tagging of genes and reversible, spatial and temporal knockdown of proteins in Drosophila. *Elife* 4, e05338.

O'Donnell, M. P. and Bashaw, G. J. (2013). Distinct functional domains of the Abelson tyrosine kinase control axon guidance responses to Netrin and Slit to regulate the assembly of neural circuits. *Development* 140, 2724–2733.

Paré, A. C. and Zallen, J. A. (2020). Cellular, molecular, and biophysical control of epithelial cell intercalation. *Curr Top Dev Biol* 136, 167–193.

Pellikka, M., Tanentzapf, G., Pinto, M., Smith, C., McGlade, C. J., Ready, D. F. and Tepass, U. (2002). Crumbs, the Drosophila homologue of human CRB1/RP12, is essential for photoreceptor morphogenesis. *Nature* 416, 143–9.

Perez-Vale, K. Z. and Peifer, M. (2020). Orchestrating morphogenesis: building the body plan by cell shape changes and movements. *Development* 147, dev191049.

Pham, H., Yu, H. and Laski, F. A. (2008). Cofilin/ADF is required for retinal elongation and morphogenesis of the Drosophila rhabdomere. *Dev Biol* 318, 82–91.

Pickup, A. T., Lamka, M. L., Sun, Q., Yip, M. L. R. and Lipshitz, H. D. (2002). Control of photoreceptor cell morphology, planar polarity and epithelial integrity during Drosophila eye development. *Development* 129, 2247–2258.

Popkova, A., Rauzi, M. and Wang, X. (2021). Cellular and Supracellular Planar Polarity: A Multiscale Cue to Elongate the Drosophila Egg Chamber. *Frontiers Cell Dev Biology* 9, 645235.

Raghu, P., Coessens, E., Manifava, M., Georgiev, P., Pettitt, T., Wood, E., GarciaMurillas, I., Okkenhaug, H., Trivedi, D., Zhang, Q., et al. (2009). Rhabdomere biogenesis in Drosophila photoreceptors is acutely sensitive to phosphatidic acid levels. *J Cell Biol* 185, 129–145.

Ready, D. F. (2002). Drosophila compound eye morphogenesis: Blind mechanical engineers? *K. Moses (Ed.) Results and Problems in Cell Differentiation, SpringerVerlag*.

Ready, D. F. and Chang, H. C. (2021). Calcium waves facilitate and coordinate the contraction of endfeet actin stress fibers in Drosophila interommatidial cells.

Development 148,.

Ready, D. F., Hanson, T. E. and Benzer, S. (1976a). Development of the Drosophila retina, a neurocrystalline lattice. *Dev Biol* 53, 217–240.

Ready, D. F., Hanson, T. E. and Benzer, S. (1976b). Development of the Drosophila retina, a neurocrystalline lattice. *Dev Biol* 53, 217–240.

Rebocho, A. B., Southam, P., Kennaway, J. R., Bangham, J. A. and Coen, E. (2017). Generation of shape complexity through tissue conflict resolution. *Elife* 6, e20156.

Roellig, D., Theis, S., Proag, A., Allio, G., Bénazéraf, B., Gros, J. and Suzanne, M. (2022). Force-generating apoptotic cells orchestrate avian neural tube bending. *Dev Cell*.

Rogers, E. M., Allred, S. C. and Peifer, M. (2021). Abelson kinase's intrinsically disordered region plays essential roles in protein function and protein stability. *Cell Commun Signal* 19, 27.

Sherrard, K., Robin, F., Lemaire, P. and Munro, E. (2010). Sequential Activation of Apical and Basolateral Contractility Drives Ascidian Endoderm Invagination. *Curr Biol* 20, 1499–1510.

Shindo, A. (2018). Models of convergent extension during morphogenesis. *Wiley Interdiscip Rev Dev Biology* 7, e293.

Shyer, A. E., Tallinen, T., Nerurkar, N. L., Wei, Z., Gil, E. S., Kaplan, D. L., Tabin, C. J. and Mahadevan, L. (2013). Villification: How the Gut Gets Its Villi. *Science* 342, 212– 218.

Signore, S. J. D., Cilla, R. and Hatini, V. (2018). The WAVE Regulatory Complex and Branched F-Actin Counterbalance Contractile Force to Control Cell Shape and Packing in the Drosophila Eye. *Dev Cell* 44, 471-483.e4.

Silva, S. M. da and Vincent, J.-P. (2007). Oriented cell divisions in the extending germband of Drosophila. *Development* 134, 3049–3054.

Singh, J., Yanfeng, W. A., Grumolato, L., Aaronson, S. A. and Mlodzik, M. (2010). Abelson family kinases regulate Frizzled planar cell polarity signaling via Dsh phosphorylation. *Genes Dev* 24, 2157–2168.

Stooke-Vaughan, G. A. and Campàs, O. (2018). Physical control of tissue morphogenesis across scales. *Curr Opin Genet Dev* 51, 111–119.

Suarez, C. and Kovar, D. R. (2016). Internetwork competition for monomers governs actin cytoskeleton organization. *Nat Rev Mol Cell Bio* 17, 799–810.

Sui, L., Alt, S., Weigert, M., Dye, N., Eaton, S., Jug, F., Myers, E. W., Jülicher, F., Salbreux, G. and Dahmann, C. (2018). Differential lateral and basal tension drive folding of Drosophila wing discs through two distinct mechanisms. *Nat Commun* 9, 4620.

Tamada, M., Farrell, D. L. and Zallen, J. A. (2012). Abl regulates planar polarized junctional dynamics through beta-catenin tyrosine phosphorylation. *Dev Cell* 22, 309–319.

Warga, R. M. and Kimmel, C. B. (1990). Cell movements during epiboly and gastrulation in zebrafish. *Development* 108, 569–580.

Wills, Z., Bateman, J., Korey, C. A., Comer, A. and Vactor, D. V. (1999). The Tyrosine Kinase Abl and Its Substrate Enabled Collaborate with the Receptor Phosphatase Dlar to Control Motor Axon Guidance. *Neuron* 22, 301–312.

Wilson, P. and Keller, R. (1991). Cell rearrangement during gastrulation of Xenopus: direct observation of cultured explants. *Development* 112, 289–300.

Wolff, T. and Ready, D. F. (1993). Pattern Formation in the Drosophila Retina. *Cold Spring Harbor Laboratory Press* 1277–1325.

Wyatt, T. P. J., Fouchard, J., Lisica, A., Khalilgharibi, N., Baum, B., Recho, P., Kabla, A. J. and Charras, G. T. (2020). Actomyosin controls planarity and folding of epithelia in response to compression. *Nat Mater* 19, 109–117.

Xiong, W. and Rebay, I. (2011). Abelson tyrosine kinase is required for Drosophila photoreceptor morphogenesis and retinal epithelial patterning. *Dev Dyn* 240, 1745– 1755.

Xiong, W., Dabbouseh, N. M. and Rebay, I. (2009). Interactions with the abelson tyrosine kinase reveal compartmentalization of eyes absent function between nucleus and cytoplasm. *Dev Cell* 16, 271–279.

Xiong, W., Morillo, S. A. and Rebay, I. (2013). The Abelson tyrosine kinase regulates Notch endocytosis and signaling to maintain neuronal cell fate in Drosophila photoreceptors. *Development* 140, 176–184.

Yang, Q., Roiz, D., Mereu, L., Daube, M. and Hajnal, A. (2017). The Invading Anchor Cell Induces Lateral Membrane Constriction during Vulval Lumen Morphogenesis in C. elegans. *Dev Cell* 42, 271-285.e3.

Yevick, H. G., Miller, P. W., Dunkel, J. and Martin, A. C. (2019). Structural Redundancy in Supracellular Actomyosin Networks Enables Robust Tissue Folding. *Dev Cell* 50, 586-598.e3.

Yu, H. H. and Zallen, J. A. (2020). Abl and Canoe/Afadin mediate mechanotransduction at tricellular junctions. *Science* 370, eaba5528.

Zallen, J. A. and Wieschaus, E. (2004). Patterned Gene Expression Directs Bipolar Planar Polarity in Drosophila. *Dev Cell* 6, 343–355.

Chapter 4. 3D geometrical scaling during Drosophila retinal morphogenesis

Xiao Sun, Seth Donoughe, Saman Tabatabaee, Todd Schoborg, Ed Munro, Ilaria Rebay

ABSTRACT

Bridging cellular behavior and tissue-scale deformation is crucial to understand how organ shape is determined, yet the inherent complexity on both scales presents challenges for 3D characterization. We approached this question using Drosophila compound eye morphogenesis, during which ommatidial units uniformly change their 3D geometry without cell rearrangement, while at tissue scale the epithelium transforms from a thin planar array into a hemispherical organ.

In order to characterize tissue-scale growth patterns, we used microCT to capture retinal 3D geometry at different pupal stages. A major advantage of this approach is that it preserves both tissue geometry and its physical relationship to the growth environment. 3D reconstruction and quantitative analysis revealed a correlation between a discrete transition in the trajectory of eye morphogenesis that occurs around 50% p.d, and transitions in the architecture of ommatidia. The pupal retinal morphogenesis is thus divided into two phases- from 25 to 50% p.d, retinal epithelium forms curvature and establishes the field of optical alignment with defined cytoskeletal network. 50-100% p.d involves the significant tissue growth and elaboration of the cytoskeletal network along the determined orientation to accommodate the functional specialization of the retina.

To understand the cell-based mechanisms that underlie this 3D growth trajectory, we considered each ommatidium as a mesoscale multicellular unit. Each unit is centrally organized by a 3D cytoskeletal network contributed by the different retinal cell types. We used a semi-automated approach to segment the boundaries of each ommatidium, and then characterized their geometrical

arrangement across the tissue. Using a genetic approach, we disrupted the ommatidial organization at an early stage, and found that the initial geometrical arrangement directs the subsequent morphogenetic growth and thus the final tissue morphology. Further, by disrupting cytoskeletal organization at specific planes, we explored how different features of the ommatidial packing influences tissue 3D geometry.

Together, we concluded that the initial geometrical arrangement and the subsequent coordinated growth powered by the 3D cytoskeletal network produce the robust retinal morphology.

INTRODUCTION

Understanding how an organ develops and acquires its functional form is a challenging question that requires the reconstruction of its 3D growth trajectory on multiple scales. Previous studies have performed morphometric analysis on the tissue level, showing that a tissue coordinates its growth along different planes to produce the precise final morphology. In the plant leaf, growth rate is position-dependent across the 2D plane to generate its characteristic shape (Kuchen et al., 2012; reviewed by Coen et al., 2017). Similarly, in 3D avian embryo, axial and paraxial tissues exhibit coordinated growth rates to elongate the body axis (Xiong et al., 2020). In the brain, tangential cortical expansion and relative thickness guides precise brain folding (Tallinen et al., 2016; Mota and Herculano-Houzel, 2015). It remains to be explored how controlled growth is spatially organized in 3D? Are there optimal growth strategies or geometrical arrangements that transform an initial shape to the final form? How can these strategies be plausibly ‘encoded’ in cellular behavior to yield a reproducible shape?

We approach these questions in the context of Drosophila pupal retinal morphogenesis. The Drosophila retinal epithelium offers a unique and tractable model system, as the compound retina comprises ~750 repeating ommatidial units, each with the stereotyped cellular organization. Previous research has revealed an intricate 3D cytoskeletal scaffold spanning the epithelium, which serves as the structural foundation for visual function (Sun et al., 2023). This unique 3D cytoskeletal scaffold also provides a natural coordinate system, allowing for the convenient description of the ommatidial geometrical arrangement across the retina. In specific, each ommatidium is organized around the central cluster of eight photoreceptor neurons, with their photosensitive rhabdomeres defining the longitudinal optical axis of the epithelium. Rhabdomere anchors to the head and feet of the cone cells that are embedded in the center of each ommatidial unit. The photoreceptor apical and basal domain defines the hexagonal lattice that positions the cone cell quartet at the centroid (Ready et al., 1976; Longley and Ready, 1995).

While previous studies have thoroughly described the cellular organization and behaviors within each ommatidium, a quantitative description of the 3D geometrical change of the entire retina is still lacking. Moreover, a critical missing piece to reconstruct the developmental trajectory is that the exact timing at which tissue-scale shape transformation and cellular morphological changes occur, and a clear correlation between these two scales changes is absent. Bridging this knowledge gap will lead to a comprehensive understanding of retinal morphogenesis, and enable the attribution of causal relations between cellular behavior and mechanics to tissue-level morphological changes.

In the first part of the paper, we characterized the retinal 3D geometrical change using X-ray based microCT (Schoborg et al., 2019) at different pupal stages and correlated with the cellular organization within each ommatidium. 3D reconstruction on both scales revealed a correlation

between a discrete transition in the trajectory of eye morphogenesis that occurs around 50% p.d, and transitions in the architecture of ommatidia. The pupal retinal morphogenesis is thus divided into two phases- from 25 to 50% p.d, retinal epithelium forms curvature and establishes the field of optical alignment with defined cytoskeletal network. 50-100% p.d involves the significant tissue growth and elaboration of the cytoskeletal network along the determined orientation to accommodate the functional specialization of the retina. In the second part of the paper, we treat each ommatidium as a unit, and developed a machine-learning based algorithm to analyze different geometrical features of the segmented ommatidial unit. Using a genetic approach to deplete Abl globally or at different planes, we disrupted the ommatidial organization at an early stage, and found that the initial geometrical arrangement directs the subsequent morphogenetic growth and thus determines the final tissue geometry. Together our discoveries reveal a novel tissue-intrinsic property that spatiotemporally controls retinal morphogenesis to achieve a functional final form. We suggest such mechanisms will be at the core of even more complex morphogenetic programs.

RESULTS

Two phases of tissue geometrical change transform an eye disc into a hemispherical organ

Quantitative characterization of the 3D geometrical changes that produce the final form of the Drosophila eye have not been done because the dramatic increase in retinal depth and pigmentation that occurs during the second half of pupal development makes the tissue poorly accessible to light microscopy. To circumvent these challenges, we used X-ray micro-computed tomography (μCT) with 2-3um resolution to characterize tissue-scale retinal growth patterns between 25-100% pupal development (p.d). A major advantage of our approach is that the resulting 3D reconstructions not

only preserve the intrinsic retinal geometry but also reveal its relationship to the surrounding physical environment (Figure 4.1B, D-F).

The packing of ommatidia and the alignment of their optical axes across the retinal epithelium defines an evolving orthogonal coordinate system along which growth is directed (Figure 4.1A). We first asked whether optical axes establishment precedes or is concurrent with tissue growth by tracking surface curvature and volume of 3D reconstructed retinas across nine distinct stages over the final 3 days of pupal development. The measurements revealed two distinct phases of retinal geometrical transformation, the first dedicated to curvature establishment and the second to tissue growth. During the first phase, from early to mid-pupal stage (25- 50% p.d), retinal volume remains constant while curvature increases, orienting the field of optical axes (Figure 4.1D E, G). During the second phase, from 50-100% pd, curvature is maintained while retina deepens and the volume increases (Figure 4.1E-G).

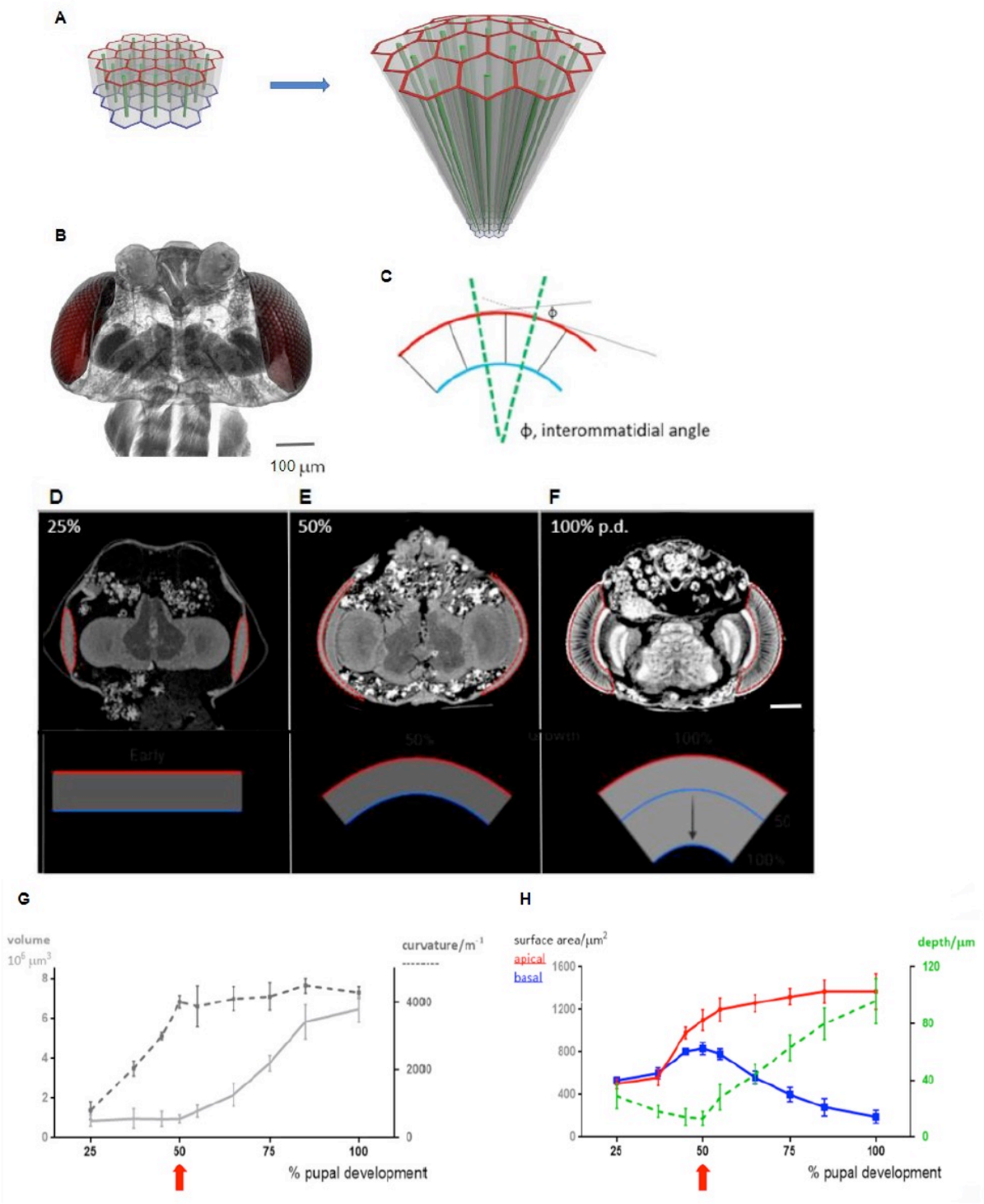

Figure 4.1. microCT to characterize retinal 3D geometrical change during pupal development.

Figure 4.1 continued
(A) Schematic of the compound retinal morphogenesis to establish the field of optical axes. Apical (red), basal (blue) ommatidial boundary, optical axis and structural basis, rhabdomere (green).
(B) 3D reconstruction of the adult Drosophila retina scanned by microCT, with 3um resolution. Retina is segmented in 3D and labeled in red.
(C) Schematic to show tissue curvature is a proxy for interommatidial angle to describe visual acuity.
(D-F) microCT scan reconstructed single plane shows the two phases of geometrical changes. Scale bar = 100μm
(G) Plot of outer surface curvature and tissue volume over time.
(H) Plot of apical, basal, surface area over time.

To understand how growth on different planes is coordinated to generate 3D geometrical change, we measured the outer and inner retinal surface area and epithelial depth along the optical axis from the 3D reconstructed dataset. During the dedicated curving phase, a combined a combined differential growth of apical and basal area two-fold increase in apical surface area and along with two-fold decrease thinning in epithelial depth, along with a more modest increase in basal surface area, allows the retina to stretch and cover half of the head (Figure 4.1D E H). Measurements made during the subsequent growth phase revealed coordinated programs of retinal elongation and basal surface area contraction (Figure 4.1H). At the start of this phase, the high rate of apical surface area expansion that initiated during the curving phase levels off such that by 70% p.d. the final size is established. 50-70% pd also marks the period of maximal rates of tissue deepening and basal area decrease; both basal area constriction and tissue elongation continue until 100% p.d, but at slower rates (Figure 4.1H). The final nearly five-fold increase in tissue depth is consistent with previous measurements (Ready 1995), validating our μCT-based analysis.

Correlation between the discrete transition in retinal geometrical change and the transitions in the architecture of ommatidia

The uCT-based reconstructions revealed two phases of geometrical change on the tissue level (Figure 4.2A). Previous studies showed that on cellular scale, the retinal morphogenesis can be separated into two phases. The first phase involves active cell rearrangements and patterning that establish a network of cell-cell contacts and cytoskeletal domains. The second phase is dominated by the growth and functional specialization of the persisting network of cell-cell contacts and cytoskeletal structure (Longley and Ready, 1995; Ready, 2002) (Figure 4.2B). However, the

correspondence between tissue geometrical change and cellular organizational change has not been examined.

To test whether the tissue geometrical transitions match exactly the timing of the establishment of the 3D cytoskeletal network at the end of patterning phase, we carefully timed pupal development and compared multiple features of pupa selected from close time points before and after the 50% p.d. Pupa show the same sets of features went to either microCT preparation for tissue-level characterization, or sent for confocal microscopy to characterize cellular organization in each ommatidium.

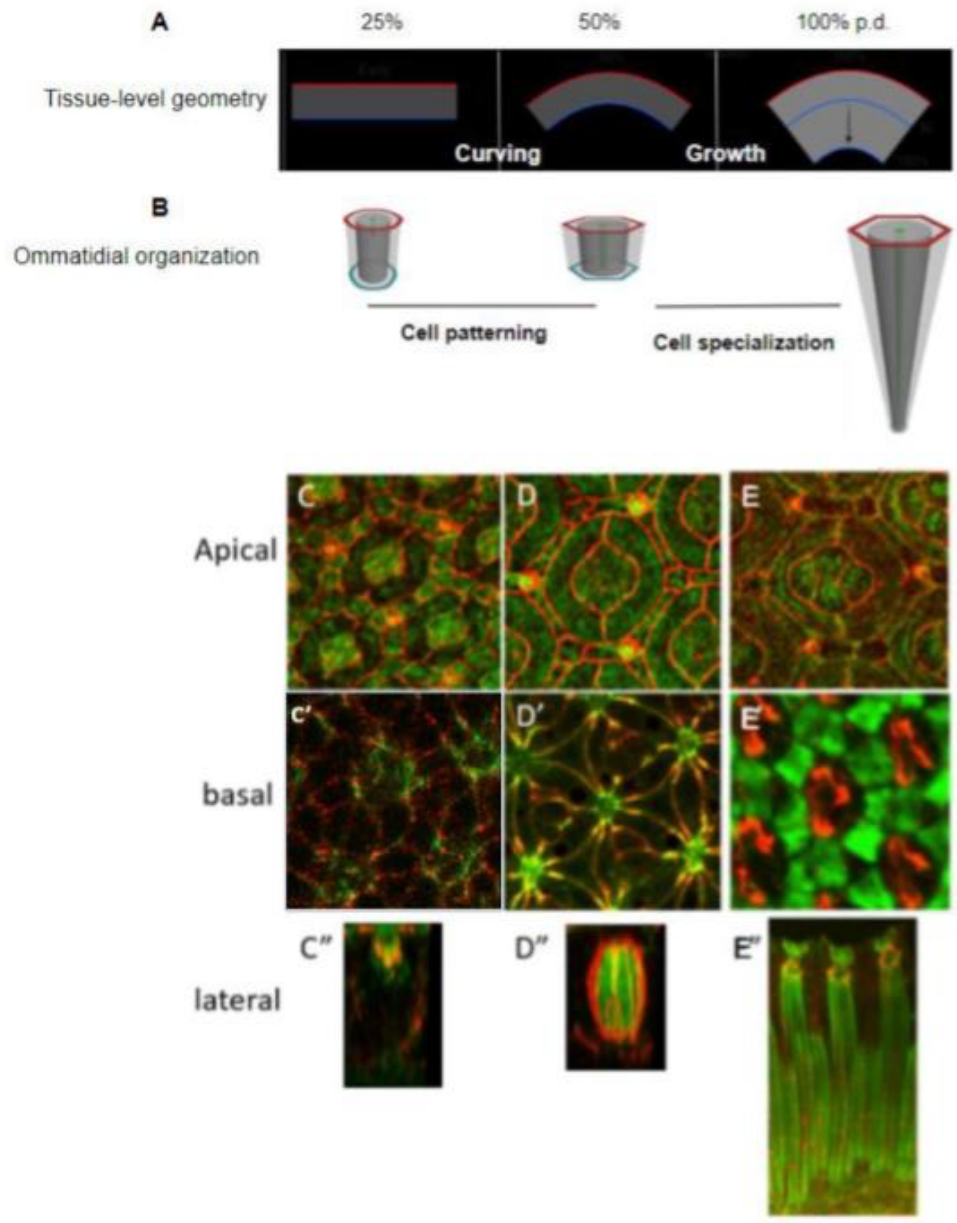

Figure 4.2. Two phases of ommatidial organizational changes matches with the tissue-level geometrical change.

(A) Schematics summarize the tissue-level geometrical change.
(B) Schematics of the establishment and maintenance of the 3D cytoskeletal scaffold. Apical (red), basal (blue) ommatidial boundary, rhabdomere (green). 3D reconstruction and schematic of the 50% p.d. retinal epithelium. Highlight the alignment of rhabdomere along the optical axis and the establishment of the orthogonal organization of the curved retinal epithelium along which the subsequent growth is directed.
(C-E") The 3D reconstruction of individual ommatidium highlights different features during the early patterning phase and later specialization phase. E-cad (red) to label the cell-cell contacts, and F-actin (green) to show the coupled cytoskeletal domain.

Interestingly, we found that there is a correlation between a discrete transition in the trajectory of eye morphogenesis that occurs around 50% p.d. of pupal development, and transitions in the architecture of ommatidia. Cell patterning took place in a relatively relaxed epithelium that retinal cell membrane follows a free curvature determined by junctional contacts (Figure 4.2C C'). At 50% p.d, the chubby cells adopt a defined shape, and the transition between early patterning phase and later specialization phase is marked by the establishment of the 3D cytoskeletal network that bears tension (Figure 4.2D D' D''). In contrast to the first stage where changes in cellular organization are emphasized, the second stage from 50 to 100% p.d., is dominated by the growth and functional specialization of the persisting network of cell-cell contacts and cytoskeletal structures. Two important functional specializations during this stage are the elaboration and expansion of the photoreceptor rhabdomere along the longitudinal axis, and the PC feet specialization that mediates the isotropic contraction of the basal floor (Figure 4.2 E' E").

Together, 3D reconstruction of the tissue-level geometrical change and ommatidial organization suggested that retinal morphogenesis is divided into two phases. An early patterning while curving phase that establishes the field of optical alignment with defined orientation and cytoskeletal organization, and the growth phase, marked by the elaboration of the cytoskeletal network along the determined orientation to accommodate the functional specialization of the compound retina.

Initial ommatidial arrangement determines the subsequent growth pattern and the final geometry

Our tissue and cell-level characterization suggests a coordinated morphogenetic transition at 50% p.d. in which the orientation and structural network of optical alignment and ommatidial packing is determined prior to the elaboration of final morphology. To understand the functional significance of this 3D structural network, we disrupted it by depleting the actin regulator Abl and then examined the subsequent growth pattern. We selected Abl because it localizes to and regulates actin assembly in the relevant domains in both photoreceptors and pigment cells but is not required for cell fate recruitment (Sun et al., 2023).

Indeed, compared to wild type 50% p.d. ommatidia, 3D reconstructions of 50% p.d. *abl* mutant retina reveal a striking disruption of cellular and tissue scale pattern (Figure 4.3A-D). At the cellular level, the rhabdomere bundles no longer connect to both the apical and basal surfaces, making the optical axes of individual ommatidia irregular and difficult to define. Variability in cell packing and apical-basal position within each ommatidium is also evident; for example, cone cells often fail to maintain their apical junctional connections and the photoreceptor clusters similarly collapse basally and later fall out of the retinal epithelium (Figure 4.3B) (Sun et al., 2023). At the apical and basal planes of the retina, variability in IOP number and organization disrupts both ommatidial and tissue scale 2D planar pattern. The resulting heterogeneity in 3D ommatidial shapes precludes regular packing and optical axis orientation (Figure 4.3D).

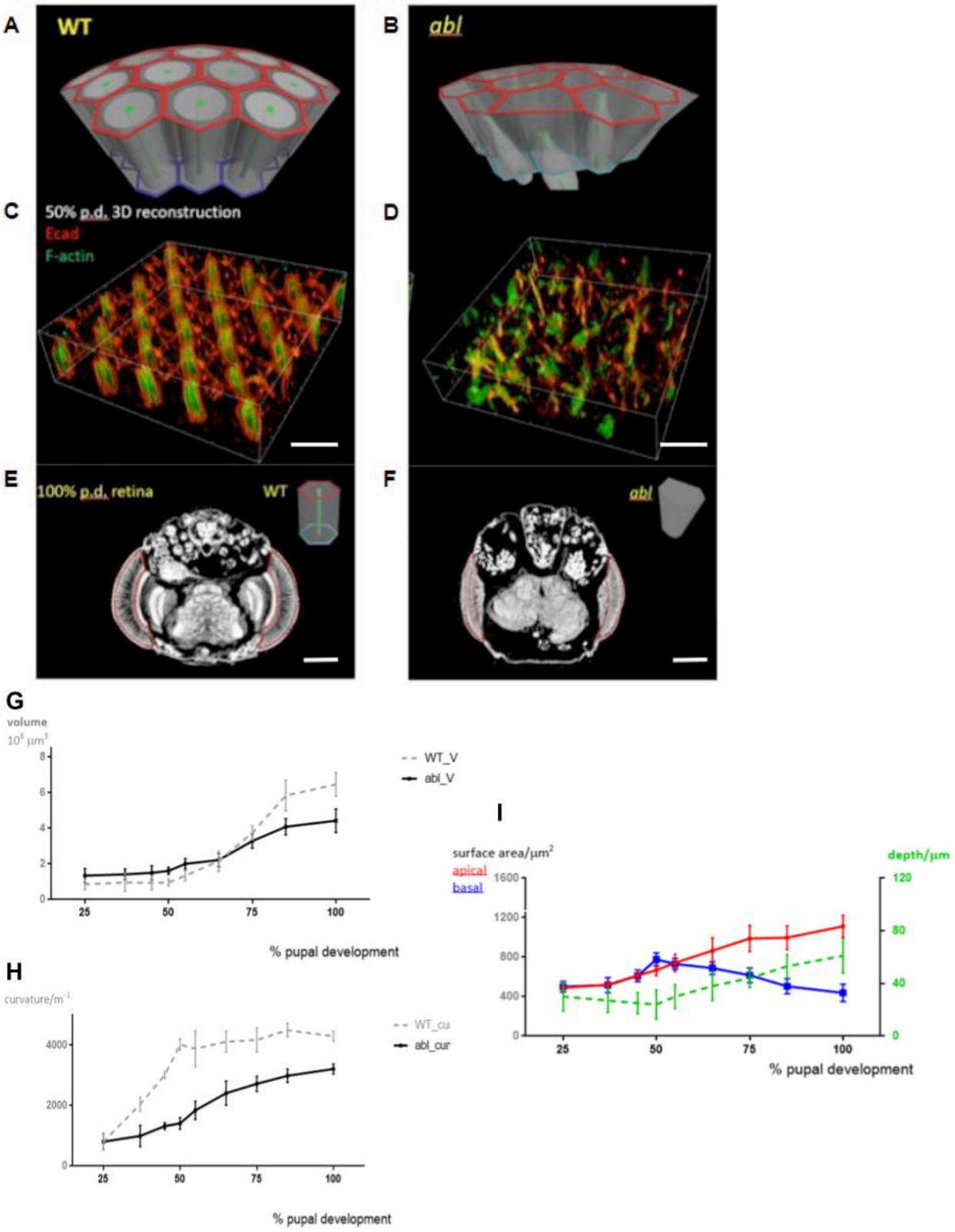

Figure 4.3. Initial ommatidial arrangement determines the subsequent growth pattern and the final geometry

Figure 4.3 continued
(A, B) Schematic of 50% p.d. 3D cytoskeletal scaffold in WT and abl.
(C, D. 3D) reconstructed confocal image of 50% p.d. retinal epithelium. Ecad (red), F-actin (green), scale bar = 10μm
(E, F) Reconstructed microCT single plane of 100% p.d. retina in WT and abl.
(G, H) Plot of WT and abl tissue volume and curvature change over time
(I) Plot of apical, basal surface area and retinal depth over time in abl mutant.

In addition to the failure to establish an organized axial network, loss of *abl* also disrupts the two-phase program of 3D tissue geometrical change. Whereas the wild type morphogenetic program incorporates two discrete phases of curvature establishment and maintenance (Figure 1G), the *abl* mutant retinal epithelium gradually bends as the volume increases (Figure 4.3G H). Despite the loss of a dedicated curvature establishment phase and the relatively constant rate of apical expansion from 37-100% p.d., the transition to coordinated increase in tissue depth and decrease in basal surface area that normally happens at 50% p.d. appeared intact (Figure 4.3I). For those *abl* mutant pupae that eclose, the resulting overall retinal 3D geometry was obviously disrupted relative to that of a wild type adult eye (Figure 4.3E, F). The *abl* mutant phenotypes together suggest that retinal curvature formation and maintenance may require 3D coordination of apical, basal, and lateral growth. In turn, these growth patterns are confined and shaped by the proper organization and mechanical coupling of the cytoskeletal network across all three planes.

Coarse-grained description of ommatidial packing in the compound retina

To examine different geometrical features of ommatidial packing that determines the growth pattern, we developed a semi-automated pipeline that provides a coarse-grained description of the tissue-scale patterning by treating each multicellular ommatidium as one unit.

Unlike segmenting individual cells within a simple epithelium where each cell has defined sides and vertices, the challenge of segmenting a multicellular unit is that the boundaries of each segmented ommatidium are cells with their own size and shape, some of which (PCs) are shared by two or three ommatidia. To solve this problem, we used machine-learning based program Ilastik to train the computer to distinguish the interommatidial space vs. the central photoreceptor cell

cluster, and then used a watershed algorithm to define the ommatidial boundary (Berg et al., 2019). Two measurements provided a readout of the "orderness" of ommatidial patterning: coefficient of variation of neighboring distance (CVND), and area CV. CVND calculates the CV of the centroid connection between all immediate neighbors of each ommatidium, and provides a quantitative metric of local ommatidial patterning. Area CV is the ommatidial area size variation in each retinal image dataset and provides a quantitative metric of global patterning across the entire epithelium. These two different disorder metrics covary with each other, which validate our orderness measurement.

Discussion

Volume conservation as a common strategy in epithelial curving contexts

Quantitative analysis of tissue volume change shows that the retinal epithelium first undergoes the volume preservation phase from 25-50% p.d. In this phase, the retinal epithelium has not yet established the specialized cytoskeletal structures, retinal cells locally rearrange and the epithelium assumes a relatively relaxed state. This phase is comparable to many embryonic epithelial contexts, where volume conservation has been suggested as an effective means for subcellular force-generating machineries to transmit force across depth and produce large changes in cellular or tissue shape. For instance, during ventral furrow formation, the combination of apical constriction and volume conservation alone can cause cell lengthening and transmit force deeper into the tissue, without requiring the specific basal-lateral machinery (Gelbart et al., 2012; He et al., 2014). In the retinal epithelium, the specific force-generating machinery responsible for inducing curving is still unknown. It is likely that the machinery of any one of the apical, basal or lateral planes, combined with the volume conservation, could be sufficient to alter the other two dimensions and induce

curving. Future studies will need to not only characterize the subcellular machinery and dynamics in single cell, but also draw force diagrams for each ommatidium as an entire unit.

Mechanisms that support substantial cell growth remain unknown in the retina

The dedicated curving phase is followed by a substantial growth phase from 50-100% p.d. that results in a fourfold increase in retinal volume. During this stage, the cell-cell contacts are preserved, with no cell rearrangement, proliferation or cell death. Tissue growth is solely contributed by cell growth and structural specialization along each plane. However, cell growth is poorly understood in the retina. Here I will raise three questions regarding the growth control that could be interesting for future exploration in retinal contexts.

First, do different retinal cell types contribute to tissue growth equally? Characterizing cell-type specific growth could be informative to understand what is the major driving force for tissue growth. However, measuring individual cell volume can be tricky because of the non-columnar shape of all retinal cells. The ideal setup is to have a good cell-type specific membrane marker and 3D segment the labeled cells at 50% and 100% p.d.

Second, what drives cell growth? Cell volume is closely coupled to the energetic and metabolic status of the cell. The cell has limited capacity for the synthesis of ribosomes and for translation. Polyploidy or multinucleation, such as in muscle cells and ciliates, could be one way to increase the synthesis capacity. The structural specialization in photoreceptors requires extensive protein synthesis, actin and membrane depositions, however, its polyploidy has never been studied. It

would be interesting to quantify DNA contents, or ribosomal number by high resolution imaging during the dramatic growth phase.

Third, what controls the onset and termination of the growth phase? From my characterization, significant tissue growth starts precisely at the time when the curvature is established and the retina has established the 3D structural contacts. This raises an interesting question of whether the initiation of growth is dependent on timing, mechanics or other factors? This could be an interesting future direction to do comparative studies in different developmental contexts and characterize growth patterns. Specifically, the approach would be to examine if there is a discrete transition between growth and other processes, as observed in the retina. Then, by experimentally controlling one factor (e.g. time) and changing the other factor (mechanics), one could answer the question in different developmental contexts.

REFERENCES

Berg, Stuart, Dominik Kutra, Thorben Kroeger, Christoph N. Straehle, Bernhard X. Kausler, Carsten Haubold, Martin Schiegg et al. "Ilastik: interactive machine learning for (bio) image analysis." Nature methods 16, no. 12 (2019): 1226-1232.

Coen, Enrico, Richard Kennaway, and Christopher Whitewoods. "On genes and form." Development 144, no. 23 (2017): 4203-4213.

Gelbart, Michael A., Bing He, Adam C. Martin, Stephan Y. Thiberge, Eric F. Wieschaus, and Matthias Kaschube. "Volume conservation principle involved in cell lengthening and nucleus movement during tissue morphogenesis." Proceedings of the National Academy of Sciences 109, no. 47 (2012): 19298-19303.

He, Bing, Konstantin Doubrovinski, Oleg Polyakov, and Eric Wieschaus. "Apical constriction drives tissue-scale hydrodynamic flow to mediate cell elongation." Nature 508, no. 7496 (2014): 392-396.

Kuchen, Erika E., Samantha Fox, Pierre Barbier de Reuille, Richard Kennaway, Sandra Bensmihen, Jerome Avondo, Grant M. Calder et al. "Generation of leaf shape through early patterns of growth and tissue polarity." Science 335, no. 6072 (2012): 1092-1096.

Longley Jr, Robert L., and Donald F. Ready. "Integrins and the development of three-dimensional structure in the Drosophila compound eye." Developmental biology 171, no. 2 (1995): 415-433

Mota, Bruno, and Suzana Herculano-Houzel. "Cortical folding scales universally with surface area and thickness, not number of neurons." Science 349, no. 6243 (2015): 74-77.

Ready, Donald F., Thomas E. Hanson, and Seymour Benzer. "Development of the Drosophila retina, a neurocrystalline lattice." Developmental biology 53, no. 2 (1976): 217-240.

Schoborg, Todd A., Samantha L. Smith, Lauren N. Smith, H. Douglas Morris, and Nasser M. Rusan. "Micro-computed tomography as a platform for exploring Drosophila development." Development 146, no. 23 (2019): dev176685.

Sun, Xiao, Jacob Decker, Nicelio Sanchez-Luege, and Ilaria Rebay. "Orthogonal coupling of a 3D cytoskeletal scaffold coordinates cell morphogenesis and maintains tissue organization in the Drosophila pupal retina." bioRxiv (2023): 2023-03.

Tallinen, Tuomas, Jun Young Chung, François Rousseau, Nadine Girard, Julien Lefèvre, and Lakshminarayanan Mahadevan. "On the growth and form of cortical convolutions." Nature Physics 12, no. 6 (2016): 588-593.

Xiong, Fengzhu, Wenzhe Ma, Bertrand Bénazéraf, L. Mahadevan, and Olivier Pourquié. "Mechanical coupling coordinates the co-elongation of axial and paraxial tissues in avian embryos." Developmental Cell 55, no. 3 (2020): 354-366.

Chapter 5. Discussion and outlook.

5.1 Summary

The Drosophila retina has been extensively used as a model system to study cell fate specification during larval stage, and 2D hexagonal patterning during early pupal stage. However, there has been relatively less appreciation attention focused on towards its 3D morphology specifically or on its potential use to establish the pupal retina as a model system to study organ morphogenesis and the functional final form. Although the initial characterization by Don Ready and others considered the 3D integration of various cellular morphogenetic processes, recent studies have shifted the focus to decipher the genetic and signaling control of polarity establishment, subcellular trafficking, and specialization of each individual cell types. This thesis makes two contributes to two assertions. First, it aims to revives the appreciation of the pupal retina as a 3D model system, by reinterpreting and integrating previous molecular and cellular knowledge into a 3D perspective. Second, it updates the framework summarized by Don Ready in 2002 with two new interesting findings.

The first key finding (Chapter 3) involves the 3D reconstruction of the developmental trajectory of the pupal retina. This analysis revealed two distinct phases of retinal geometrical change, which coincide with the known two phases of cellular organization. The first phase is described by a curving process, which reflects the global establishment of the optical axis. The second phase involves dramatic tissue growth and elaboration of the cytoskeletal network along the determined orientation to accommodate the functional specialization of the retina. The establishment of global axes is crucial to the subsequent morphogenesis and thus influences final morphology. The second finding in the thesis (Chapter 4) focuses on the later phase. It revealed a feedback mechanism within a physically coupled network with 3D configuration. This intrinsic feature of the organ

allows matching of developmental progresses between different cell types and to promote robust 3D morphogenesis.

This thesis highlights the importance of considering the 3D integration of pupal retinal morphogenesis and suggests new mechanisms underlying the distinct phases of morphogenesis. However, it also creates raises more questions than it answers. In section 5.2, I will compare the similarity and differences between the retina and other comparable organ contexts to further understand the general rules underlying my two pivotal findings. In section 5.3, as the patterning phase has not been emphasized in this thesis, I will summarize my understanding of the potential factors that drive curving for future explorations.

5.2 Discussion of the key findings and follow-ups

Developmental trajectory – is it possible to maintain curvature during growth?

Based on the developmental reconstruction of the tissue 3D geometrical change, I suggested a model in which the retina first establishes the organizing field which that determines the global orientation and arrangement of optical axes and its structural basis, the rhabdomeres. These determined axes, serve as "mould/template" to further direct growth and specialization along their orientation, and produce the elongated hexagonal arrays. It is important to note that the trajectory, including the maintenance of curvature to "pre-pattern", and proportional elongation and basal contraction, (which might be easily misunderstood), differs significantly from an ancient disproven "preformationism" theory which posits that development only involves proportional size increase from a miniature self. Instead, mechanical feedback mechanisms suggest that the retinal morphogenesis might conform to the self-organization rule with boundary conditions imposed on

it, or a combination of programmed morphogenesis which prescribe the initial conditions, and the subsequent self-organization that relies on local interactions to produce the final order.

When comparing to other model organ formation involving both tissue folding and growth, growth typically results in a change of folding pattern. This is exemplified by brain convolution where the adult folding pattern is significantly more complex than early fetal pattern due to the self-organization of growth-induced local mechanical instabilities. However, the curvature maintenance phase observed in the retina during significant growth presents a unique challenge.

What properties or mechanisms might explain the contrasts of between brain's growth while folding vs. retina's growth but without changing folding maintains? First, I consider propose that the differences in physical properties could lead to the contrasting growth and folding patterns. The brain is a soft tissue that undergoes uneven growth, whereas the pupal-to-adult stage compound retina exhibits almost solid nature, due to the specialized lens system which is the direct extension from the exocuticle, and that the extensive elaboration of the rod-like rhabdomere structures. In addition, external factors such as the exocuticle could serve as physical constraints that also help shape the retina and maintain curvature. Another factor that might also lead to the contrasting pattern is the different scale or size of both tissues, and the relating related factors like uniformity and homogeneity within the different tissue sizes. The Drosophila compound retina can be seen as an infinite small fraction of a bigger organ such as brain. In the brain, due to the connectivity between different small fractions, each part does not have full autonomy and instead influencing influences each other during folding and growing. Whereas in the retina, the uniform arrangement and growth pattern makes it possible to maintain curvature during growing.

Tissue-intrinsic feedback mechanism during patterning and growth

My work extends the idea of 2D superacellular networks to 3D by revealing previously underappreciated feedback between cytoskeletal domains aligned along orthogonal planes. This tissue-intrinsic feedback mechanism facilitates the spatial coordination of diverse cellular morphogenetic events at different sites. Across the retinal epithelium, the spatial coordination is manifested through the matching rate of photoreceptor rhabdomeres expansion and pigment cell mediated basal contraction, as well as the synchrony between different ommatidia to achieve uniform growth pattern. Moreover, this intrinsic feedback mechanism also serves as structure-reinforcement, increasing stress tolerance during drastic tissue morphological changes that tends to break down the junctions. The mechanical status of the a given cell or molecular component can signal and influence the states of other components to further strengthen the cell-cell/ECM contacts. This idea was supported by the evidence of increased deposition of ECM matrix proteins, the secretion of the lens system (apical ECM), as well as the accumulation and elaboration at other contacting sites, such as N-cad between cone cell feet.

Although my work mostly focused on demonstrating the role of the mechanical feedback during the growth phase to coordinate cellular morphogenesis and maintain retinal organization, 50% p.d. 3D reconstruction results show that the feedback mechanism also applies during the patterning phase. Taking LL>Abl, abl^{null} (pigment cell specific restoring normal Abl function in the otherwise mutant background) as an example, restoring normal planar patterning restores rhabdomere remodeling and elongation at 100% p.d.. This suggests that the feedback mechanisms operate during growth phase in a manner explained in Figure 3.7. Intriguingly, the proper pigment cell patterning also facilitates the early photoreceptor involution process as demonstrated by the 50% p.d. 3D reconstruction that shows that proper contacts, both between the rhabdomere and retinal

floor, and between neighboring rhabdomeres, are established. Although the dynamics might differ, both involution and expansion of rhabdomere could be explained by that the proper PC patterning facilitates facilitating the "flow" and material deposition along the central axes. This process is analogous to the crystallization phenomenon, in which crystals first form around the "seed" or nucleation core.

Similar phenomenon phenomena also are observed during Drosophila leg folding, where a transient actomyosin cable forms along the apico-basal axis of the cell, connecting between the cell apex and basal nuclei to produce contractile force (Ambrosini et al., 2019). Additionally, during wing hinge formation, that imaging of Utr-GFP revealed a highly dynamic accumulation and flow of F-actin along the lateral cell membrane and that generates pulsatile dynamics (Sui et al., 2018). These structures were proposed to exert contractile forces along the lateral axes and drive folding. However, how these structures are dynamically formed and whether the lateral machinery associates with other planes is unclear. One possibility is that the transient lateral actomyosin structure are the active remodeling induced by the changes along the apical and basal side or the configuration of the entire cell, in the similar way as what we suggested of the interplay between orthogonally oriented rhabdomere and basal floor in the multicellular unit. It would be interesting to explore in the retina as well as other epithelial contexts, if the configuration facilitates the communication between cellular machinery along different axes of the cells. On the subcellular level, to explore how the wildtype rhabdomeres are formed and elongated and if there is are differences in the timescale and subcellular machinery of material deposition during each process in normal situation. It will also be interesting to compare the dynamics and machinery in PC-specific restore rescue conditions that where the processes are solely generated through the feedback from PC contraction. To characterize the dynamics, one way is to sparsely label the

cytoskeletal component (because it is too abundant at sites) or the vesicles, and perform live imaging in both WT and PC rescue conditions. On the tissue scale, it would be interesting to explore how these processes affect the general tissue forms such as thinning, and curving during the involution phase, and elongation dynamics during expansion phase.

5.3 Curving

In general, tissue shape is determined by a combination of cellular mechanics that generate mechanical forces and the physical properties which reflects how tissue responds to the forces. Early pupal retina is subjected to both internal and external forces, and retina shows gradual increase of tissue stiffness over time. These three factors collectively contribute to the curving process. Although the source of forces and change of tissue properties has not been extensively studied in the retina, I will summarize what we can learn from other numerous comparable examples and summarize my own preliminary observations to suggest potential mechanisms that contribute to the curving process. Future mechanical measurement and quantitative analysis are needed to explore these hypotheses.

5.3.1 Internal forces

Differential growth of apical and basal surfaces

Differential growth is a common mechanism to induce tissue curvature. For example, differential growth of grey and white matter induces cortical convolution (Tallinen et al., 2014). Within monolayer epithelium, apical contraction and basal expansion induces ventral furrow formation

(Sweeton et al., 1991). Different growth rate of epithelial cell layer and its enveloping ECM induces wing doming (Stefan et al., 2023).

In the early pupal retina, the apical and basal surface starts around the same area size, with slight larger basal area than apical in some cases or slight earlier time points. As the retinal epithelium expands to cover half of the head, apical expansion is significantly faster than basal expansion. The differential expansion rate of apical relative to basal surface might be one source that led to curving of the retinal epithelium. However, retina is different from the examples listed above in terms of growth pattern. Each compositing ommatidium shows similar morphogenetic progress and thus generate a uniform pattern throughout the retinal epithelium.

Lateral thinning

Interestingly, retinal epithelium thinning from ~30 to 15 μcm during the curving process. However, whether lateral thinning suggests a contraction process, and the machinery that controls the lateral contraction is unclear. One possibility is that the tissue thinning is a merely passive result of the expanding surface area while keeping the volume constant. Another intriguing possibility is that the rhabdomere involution drives the lateral contraction, in a way similar to the transient actomyosin cables drive Drosophila leg and wing hinge folding (Gracia et al., 2019; Sui et al., 2018). Although the rhabdomere involution is to elaborate and extend the photoreceptor apical domain from the initial “adherens junctions spots”, the involution process could also "expel" the existing membrane outwards to the baso-lateral side of the photoreceptor, and thus shorten the distance between the apical and basal surface and pulling the basal floor towards the extending rhabdomeres. It would be interesting to use live imaging to characterize the involution dynamics, and focus on the relationship of the involuting length, tissue depth and baso-lateral membrane outward movement. Next, to test in the Crumbs or Bazooka mutant where rhabdomere involution

process is disrupted (Izaddoost et al., 2002; Nam et al., 2007), whether the tissue still undergoes contraction.

5.3.2 External forces

Hydrostatic pressure

From pre-pupa to ~50% p.d. pupal stage, one of the major changes in physical environment is the increase in hydrostatic pressure which inflates the early pupa. It has been extensively studied that increase in the hydrostatic pressure plays significant role to shape epithelial tissue, including imaginal discs such as legs, wings, and sac-like appendages (Waddlngton, 1942; Fortier et al., 2003; Zarek and Stanley; 1986). Don Ready in his book also mentioned "The tension stretching the epithelium appears to arise largely in the increasing hydrostatic pressure which inflates the pupa". Although lacking direct evidence in the specific eye context, it is almost beyond question the fluid environment that pushing the wispy epithelium against the pupal hypoderm boundary is the major contribution to its shape.

Two of my own anecdotal observations support this conclusion. First, by poking a tiny hole of early pupa from 20% to 50% p.d. (at almost the same relative position at the dorsal side of the right eye with controlled forces), and observing the fluid with fat body pumping out, I can develop a sense of the pressure inside the pupa, as well as the tissue "texture" or physical property of the outer membrane as I poke it. The result is consistent, pressure increases from 20% to 50% p.d, and seems not much difference or slightly decreases from 50% to 60% p.d. Second, by poking a hole on the dorsal side in the center of the head at ~20% p.d, and observe the side of pupal head that reflects the eye boundary at later stage (from 40-50% p.d.), the curvature is significantly lower compared to normal development. In addition, the size of the head and the eye are both evidently

smaller. Future quantitative characterization of hydrostatic pressure change during pupal stage will be informative, when combining the quantitative measurement of tension at different planes in 3D, to build a quantitative model that recapitulate the curving process.

REFERENCES

Ambrosini, Arnaud, Mégane Rayer, Bruno Monier, and Magali Suzanne. "Mechanical function of the nucleus in force generation during epithelial morphogenesis." Developmental cell 50, no. 2 (2019): 197-211.

Fortier, Tina M., Priya P. Vasa, and Craig T. Woodard. "Orphan nuclear receptor βFTZ-F1 is required for muscle-driven morphogenetic events at the prepupal–pupal transition in Drosophila melanogaster." Developmental biology 257, no. 1 (2003): 153-165.

Gracia, Mélanie, Sophie Theis, Amsha Proag, Guillaume Gay, Corinne Benassayag, and Magali Suzanne. "Mechanical impact of epithelial− mesenchymal transition on epithelial morphogenesis in Drosophila." Nature communications 10, no. 1 (2019): 2951.

Harmansa, Stefan, Alexander Erlich, Christophe Eloy, Giuseppe Zurlo, and Thomas Lecuit. "Growth anisotropy of the extracellular matrix shapes a developing organ." Nature Communications 14, no. 1 (2023): 1220.

Izaddoost, Shayan, Sang-Chul Nam, Manzoor A. Bhat, Hugo J. Bellen, and Kwang-Wook Choi. "Drosophila Crumbs is a positional cue in photoreceptor adherens junctions and rhabdomeres." Nature 416, no. 6877 (2002): 178-183.

Nam, Sang-Chul, Bibhash Mukhopadhyay, and Kwang-Wook Choi. "Antagonistic functions of Par-1 kinase and protein phosphatase 2A are required for localization of Bazooka and photoreceptor morphogenesis in Drosophila." Developmental biology 306, no. 2 (2007): 624-635.

Ready, Donald F. "Drosophila compound eye morphogenesis: blind mechanical engineers?." Drosophila Eye Development (2002): 191-204.

Sui, Liyuan, Silvanus Alt, Martin Weigert, Natalie Dye, Suzanne Eaton, Florian Jug, Eugene W. Myers, Frank Jülicher, Guillaume Salbreux, and Christian Dahmann. "Differential lateral and basal tension drive folding of Drosophila wing discs through two distinct mechanisms." Nature communications 9, no. 1 (2018): 4620.

Sweeton, D. A. R. I., S. U. K. I. Parks, Michael Costa, and E. R. I. C. Wieschaus. "Gastrulation in Drosophila: the formation of the ventral furrow and posterior midgut invaginations." Development 112, no. 3 (1991): 775-789.

Tallinen, Tuomas, Jun Young Chung, François Rousseau, Nadine Girard, Julien Lefèvre, and Lakshminarayanan Mahadevan. "On the growth and form of cortical convolutions." Nature Physics 12, no. 6 (2016): 588-593.

Tallinen, Tuomas, Jun Young Chung, John S. Biggins, and L. Mahadevan. "Gyrification from constrained cortical expansion." Proceedings of the National Academy of Sciences 111, no. 35 (2014): 12667-12672.

Waddlngton, C. H. "The Pupal Contraction as an Epigenetic Crisis in Drosophila." In Proceedings of the Zoological Society of London, vol. 111, no. 3-4, pp. 181-188. Oxford, UK: Blackwell Publishing Ltd, 1942.